STUDY OF CAPACITIVE AND PIEZORESISTIVE FUNCTIONAL SILICONE ELASTOMERIC NANOCOMPOSITES FOR MECHANICAL SENSING APPLICATIONS

力学センサ用静電容量及びピエゾ抵抗特性を有するシリコーンエラストマーナノコンポジットに関する研究

CHEN GUO

郭　辰

Supervisor: Prof. Masayoshi Fuji

A Dissertation Submitted in Partial Fulfillment of the Requirements for the Degree of Doctor of Philosophy in Engineering in the Department of Frontier Materials

NAGOYA INSTITUTE OF TECHNOLOGY

SEPTEMBER 2017

© Copyright by CHEN GUO 2017
All Rights Reserved

ABSTRACT

Mechanical Sensor is a significant device to convert different types of exterior mechanical stimulus, such as force, pressure, impact, vibration, and acceleration, to usable electrical signals. The demand for diverse types of sensors with smart property and low cost is growing rapidly as the development and widespread of many novel technologies. However, despite their various shapes and functionalities, traditional mechanical sensors are relatively expensive, limited by their fixed shapes, and sometimes even too fragile to measure the mechanical stimulus. Thus the demand of a variety of flexible mechanical sensors, which are cheap, sensitive, which can be applied to a flat or curving surface with large areas, is expanding fast. Such a flexible mechanical sensor has the ability of not only measuring an external mechanical stimulus, but also providing a protection to the inner device or apparatus. To develop a flexible mechanical sensor, silicone elastomer was utilized as a substrate, which is a special type of elastomer which possesses a lot of advantages, such as an extremely good flexibility, a very wide temperature tolerance range, an excellent insulation and an unparalleled excellent biocompatibility. Different types of particle-like functional additional materials can be integrated into the elastomer to provide their special functionalities, widen the areas of use, and overcome some drawbacks of the silicone elastomer matrix. This thesis aims to investigate the ability of different types of silicone elastomeric functional nanocomposites, including ferroelectric particles and conductive particles incorporated silicone elastomeric nanocomposites, to be applied as mechanical sensors, in other words, the ability of convert a mechanical stimulus to an electrical signal, with the efficiency and sensitivity as high as possible. This thesis includes 6 chapters as below:

Chapter 1 is a general introduction to the background of the research of this thesis. The basic introduction, the advantages and disadvantages of silicone elastomer were introduced. Then a brief introduction to the polymeric functional nanocomposites was

made. Their characteristics and many related previous works were emphasized. As the mainstays of this thesis, the dielectric property, dielectric polymeric composites, electrically conductivity as well as electrically conductive nanocomposites was introduced in detail. Finally the object of the work was illustrated.

In Chapter 2, the extra-high dielectric properties of $BaTiO_3$, as well as its drawbacks were introduced. The potential of incorporate $BaTiO_3$ particles in an elastomer matrix to obtain a high mechanical sensing ability was demonstrated. A low dispersity, caused by the effects of incompatibility accompanied with the gravity during the curing procedure of silicone elastomer, was proved to be able to reduce the dielectric constant of the composites obviously. However, it is difficult to distribute $BaTiO_3$ nanoparticles into the silicone substrate due to the poor surface affinities between these two materials. The dielectric behaviors were found to be weakened by the incompatibility. To improve the dispersity of $BaTiO_3$ particles, a novel silicone coupling agent was used to modify the surface of particles. TG and FTIR results show that coupling agent was successfully coated on the surface. Raw $BaTiO_3$ particles and $BaTiO_3$ particles modified by silicone coupling agents were incorporated in the silicone elastomer to fabricate $BaTiO_3$/silicone membranes. Particle size distribution measurement and SEM observation show that $BaTiO_3$ particles get higher compatibility with silicone, dispersity of $BaTiO_3$ particles and the dielectric properties of $BaTiO_3$/silicone membranes were both improved by the surface modification.

In Chapter 3, the capacitive features of $BaTiO_3$/silicone nanocomposites were theoretically analyzed. To take advantage of the excellent insulation features as well as the excellent dielectric property, surface treated ferroelectric $BaTiO_3$ nanoparticles were added into the silicone elastomer to fabricate a flexible nanocomposite with a high dielectric constant. A measuring system containing the silicone coupling agent modified BT/silicone elastomeric membranes was assembled, connecting with a LCR meter and a Multimeter. Continuously increasing stresses and periodic varying stress (vibrations) were applied to the membranes, respectively. The changing capacities

(equivalent to the generated currents) were evaluated by the LCR meter, while the generated instantaneous current was measured by the Multimeter. Clear and sensitive signals were obtained from both of the measurements even without a poling process during the fabrication or measurement. This type of materials is expected to have the applications in mechanical sensors due to its rapid response of instantaneous electric signals, simple structures and low costs.

In Chapter 4, in order to predict and elucidate the mechanisms of the factors and variation procedures of the resistance of flexible conductive nanocomposites, 3 types of theoretic piezoresistive models were introduced from different prospects. Each model was built considering both the solid and foamed conductive nanocomposite. A piezoresistive model was deduced based on the percolation threshold of conductive elastomeric nanocomposites, which is simple but can only be used for the calculation of the resistance variation in a conductive nanocomposite with a volume fraction near its percolation threshold. Another type of piezoresistive model was deduced based on the tunnel conductive theory for elastomeric nanocomposites, which is able to explain the resistance of flexible conductive nanocomposites with a wide range of volume fraction and with spherical conductive particles. To broaden the applicable scope of the model for a variety of particle shapes, a piezoresistive model based on the tunnel conductive theory for elastomeric nanocomposites considering the distribution, aspect ratio, and orientation of each fiber-like conductive particle was developed. Although with a high accuracy, its complexity reduced the practicality.

In Chapter 5, multi-walled carbon nanotubes (MWCNTs), with a high electrical conductivity and large relative surface areas, were integrated in the silicone elastomer to provide a high conductivity as well as a piezoresistive property. To raise the sensitivity and improve the piezoresistivity of the nanocomposite, a foaming procedure was introduced to reduce the viscoelasticity of the silicone elastomer. A series of conductive foamed nanocomposites were fabricated with different types of foaming agents to obtain a diverse porous structure. The porous structures of the foams, the

distribution and orientation status of the multi-walled carbon nanotubes in the silicone matrix were observed/analyzed using laser microscope and SEM with/without a compression load. The influences of the porous structure and porosity on the foam were studied. It was found that a different porosity and different voids structure affected the density, elastic modulus, resistivity as well as piezoresistive property significantly. This type of piezoresistive active nanocomposite was proved to have an obvious potentiality for utilizations in a mechanical sensor, such as a tactile sensor or an impact sensor. Applications of MWCNT/silicone elastomeric nanocomposites for mechanical sensing were investigated deeply. A mechanical sensing system was assembled with a piezoresistive MWCNT/silicone sponge-like sheet. It was found to have the ability of detecting not only a wide range of tactile pressure, but also a mechanically impact by measuring the variation of the resistive through a Multimeter.

In Chapter 6, a general conclusion of this work was made. It was concluded that a relatively precise and sensitive mechanical sensor can be easily developed from different prospects. It was found that a system containing a BT/silicone membrane and a Multimeter is appropriate for detection of a short-time mechanical stimulus, like an instantaneous impact or a vibration with a short period; a system containing a BT/silicone membrane and a LCR meter is able to measure a constant pressure; while a small pressure can be detected with a system containing MWCNT/silicone foamed nanocomposites. The directions for the future research were also mentioned, such as investigating the temperature dependent conductive property of MWCNT/silicone nanocomposites; enhancing the capacitive and piezoresistive property of the silicone elastomeric nanocomposites; expanding the versatility of the silicone elastomeric nanocomposite; and conducting the research of some practical applications using silicone elastomeric nanocomposites.

TABLE OF CONTENTS

LIST OF FIGURES

LIST OF TABLES

Chapter1 General Introduction

1.1 Introduction to Silicone Elastomer

Elastomer is a vague definition of a wide range of polymeric materials. Elastomers are amorphous polymers with glass transition temperatures below room temperature, which exhibit elastomeric behaviors such as viscoelasticity, very weak inter-molecular forces and generally low Young's modulus accompanied with high failure strain compared to other materials [1-6]. "Rubber" and "elastomer" can be used interchangeably, the latter often refers to synthetically produced elastomeric polymers. An elastomer can be crosslinked or not. A crosslinked elastomer, or thermoset elastomer, has covalent bonds between the different polymer chains, joining them all into a single networked molecule, which prevents the plastic deformation caused by the slippage of molecular chains. An elastomer without chemical covalent bonds usually has physically crosslinks such as hydrogen bonds and Van der Waals forces between their polymer chains, defined as thermoplastic elastomer (TPE) that can be produced with a simple casting molding method and can be recycled. The backbones of the polymer chains in a common elastomer are usually made up of carbon-carbon or carbon-oxygen bonds, the flexibility of the elastomer is related to the saturation levels of the carbon-carbon bonds and the sizes or the cis/trans structures of the side chains.

Silicone, which has a scientific name of polysiloxane, is a series of polymeric materials made up of repeating units of a siloxane with an inorganic backbone of alternating silicon atoms and oxygen atoms, frequently combined with organic side chains of carbon and hydrogen [7-10]. The chemical structures of the silicone backbones are similar with the structures of quarts, giving it a superb heat-resistant ability [11,12]. A longer bond length and a larger bond angle of silicon-oxygen-silicon bond in silicone lead to an easier

configuration variation, which brings a highly flexible behavior. By varying the molecular weight, side groups, and crosslinking structures, silicone can be synthesized with a wide variety of properties and compositions. They can vary in consistency from oil to gel/grease to rubber/elastomer to rigid plastic/resin. The most common silicone is linear polydimethylsiloxane (PDMS), a type of silicone oil. Another large group of silicone materials is based on silicone resins, which are formed by branched and cage-like oligosiloxanes. Silicone elastomer possesses a lot of advantages, such as a low thermal conductivity, a low chemical reactivity, an extreme flexibility, a very wide temperature tolerance range, an excellent insulation, an unparalleled good biocompatibility and low toxicity, a low level of combustible components , the ability to repel water, resistance to oxygen, ozone, and ultraviolet (UV) light, and a high gas permeability. All types of silicones are known to be good insulation which can act as good dielectric substrates [13]. Due to their advantages, silicone elastomers have been widely utilized both industrially and daily, such as electrical, electronics, household/cookware, automobile, aeroplane, office machines, medicine/dentistry, personal care, textiles/paper, automotive etc.

However, there are also some disadvantages in silicone elastomers, such as a poor abrasion, a poor petroleum resistance, and relatively low tear strength. Many of them could be overcome by the nanocomposite process. Different types of particle-like functional additional materials can be integrated in the elastomer to provide their special functionalities, widen the areas of use and overcome some drawbacks of the silicone elastomer matrix. Such a nanocomposite with functional particles randomly dispersed in the silicone matrix has an obvious advantage that easy to be fabricated, remaining the functional activity of the particles.

1.2 Polymeric Functional Nanocomposites

Polymers have replaced a large part of conventional metals/inorganic materials in a variety of applications because of its ease of processing, productivity, and cost reduction. Nanocomposite is a multiphase composite where one of the phases has one, two or three dimensions within nano-scale or having nano-scale repeat distances between the different phases. Polymers are extremely suitable for being used as the substrates of nanocomposites. In many applications, the properties of polymers are modified by particles/fibers to enhance the mechanical properties [14-21]. S. R. White et al [22] reported a structural polymeric material with the ability to autonomically heal cracks. The material incorporates a microencapsulated healing agent that is released upon crack intrusion. Polymerization of the healing agent can be triggered by contact with the embedded catalyst to bond the crack faces. Their fracture experiments yielded 75% in toughness.

On the other side, functional nanocomposites that are made up of functional particles and polymer matrix will obtain both the functionality of the particles and the flexibility, processability of the polymer. K. Rezwan et al [23] have combined biodegradable polymers and bioactive ceramics in a variety of composite materoials for tissue engineering scaffolds. The impact of each component on biodegradability and bioactivity of the scaffolds are discussed using in vitro and in vivo assessments. The main target is to design and fabricate reproducible bioactive and bioresorbable robotic 3D scaffolds of tailored porosity and pore structure. But it was found that the mechanical integrity of the artificial composite scaffolds is still lower than that of cancellous or cortical bone. Robert b. Grubbs [24] introduced the use of functional block copolymers for the localization of metal species on the nanometer scale through block copolymer phase segregation, for

instance, the use of alkyne-functional block copolymers for the preparation of cobalt-containing materials offers a great measure of promise, especially in combination with established methods for spatial control at large scales. However, the understanding of multiple interactions and intergrade it within devices over length scales from the nanometer top the meter still remains as a question. In Zsolt Varga' study, the magnetic elastomer was prepared by dispersing carbonyl iron particles randomly into dimethylpolysiloxane (PDMS) [25]. It was found that the elastic modulus of this magneto elastomer could be increased by an external magnetic field which is called as temporary reinforcement. Anisotropic samples were prepared by varying the spatial distribution of the magnetic particles in the elastic matrix to enhance the magnetic reinforcement effect. It was found that much larger increase in modulus can be exhibited by the uniaxial field structures than the one with randomly dispersed particles. The most significant temporary reinforcement effect was found if the applied field, the particle alignment, and the mechanical stress are all parallel with each other.

1.3 Dielectric Properties and Applications of Dielectrics/Polymer Nanocomposites

As the pioneer of the researcher for dielectric/polymer composite, R.E. Newnham has studied a lot of piezoelectric smart composite materials for a wide variety of engineering applications, firstly established the notation for the connectivity of functional composites [26,27]. This notation describes the number of dimensions that each phase is physically in contact with itself. The first number in the notation denotes the physical connectivity of the active phase and the second number refers to that of the passive phase. Composites with 0-3 connectivity consist of functional particles randomly dispersed in a 3D polymer

matrix. The primary advantage of a composite with 0-3 connectivity is that it is easy to fabricate, especially to make a thin membrane from it, while remaining the functional activity of the particles [28]. Their research group studied fired 0-3 piezoelectric composites for biomedical ultrasonic imaging applications, consisting of pellets of Lead Zirconate Titanate (PZT) ceramic powders and backfilled with a series of epoxy resins. It was found that composite made out of PZT-Spurr epoxy and fired at 900°C gave the best performance and the best efficiency as an underwater sensor [29]. A poly (dimethylsiloxane)-titania nanocomposites was prepared using heat-treated titania as fillers by Suryakanta Nayak et al [30], dielectric and mechanical properties of the composites were measured, it was found that both the dielectric constant and the loss factor of the composites was increased dramatically with the addition of the titanium dioxide filler, whereas resistivity was decreased. Both electrical and mechanical properties were affected by heat treatment of titania particles. It was known that heat treatment decreased the moisture content and also affected the concentration of Ti^{3+} in TiO^{2}, which in turn affects electrical properties of the system. It was confirmed that presence of surface hydroxyl groups enhances the dielectric constant of the composites. Federico carpi et al [31] firstly reported the embedding of highly dielectric ceramic inclusions in a rubber medium as a method to improve the electromechanical material for dielectric elastomer actuation. In comparison with pure silicone, a decreased elastic modulus, as well as an increased dielectric constant was exhibited. The utilization of this composite as an elastomeric dielectric for planar actuators enabled a reduction of the driving electrical fields. Especially the strain and stress were more than 8 and 4 times higher than the corresponding values that generated with the pure silicone matrix for the analogous electrical stimuli. A novel polymer composite was developed by Jiawen Xu et

al [32], using self-passivated aluminum particles as the filler. The nanoscale insulating oxide layer of which allows the composites to have a high dielectric constant as a percolation system, while confines the electrons within the aluminum particle, which helps to keep a low loss of the composites. A high dielectric constant with low dissipation factor was obtained from an aluminum/epoxy composite. The thickness of the alumina insulating layer is found to have a negative relation with the particle size. It was found that the polymer matrix can significantly change the dielectric properties of the composites. Functional nanocomposites consist of a dielectric active ceramics phase incorporated with a polymer matrix have found use in a variety of applications for sensors and actuators.

1.4 Electrically Conductivity and Applications of CNT/Polymeric Nanocomposites

Electrically conductive polymeric composites have been widely studied for many decades. Unlike the inherently electrically conductive polymers whose conductivity is originated from the conjugate double bonds inside the polymer chains, the conductivity of the conductive polymeric composites depends on the conductive fillers. The polymer matrix could be in resin, elastomer, fabric or even gel-like forms. The conductive fillers could be spherical/fiber/flake shaped metal or carbon materials. Among many of the conductive fillers, carbon nanotube (CNT) is a type of cylindrical-like carbon nanomaterial with many unusual properties such as extraordinary thermal conductivity, mechanical and electrical properties which are valuable in many structural and functional applications [33-37]. Especially the multi-walled carbon nanotube (MWCNT) has a relatively low cost and many special behaviors [38-40]. The carbon nanotube has metallic

conductivity or semiconducting behavior along its tubular axis. In theory, an armchair type carbon nanotube can carry an electric current density about 1000 times greater than that of copper [41]. Thus CNTs have been investigated as the conductivity enhancing fillers in polymeric nanocomposites. CNT/polymer conductive nanocomposites have many unique electrical and mechanical properties, such as piezoresistivity, electromagnetic interference (EMI) shielding effect and highly flexibility, which are appropriate for applications as smart functional materials. J. O. Aguilar et al. studied the influence of CNT clustering on the electrical properties of polymer composite films by comparing the composites with CNTs uniformly dispersed and with those agglomerated in clusters at micro-scale. They found that films with micrometer-size agglomerations have a slightly lower percolation threshold and a higher conductivity than those with uniformly dispersed CNTs, which can be explained that the increased density of CNT-to-CNT junctions favors the formation of the conductive networks [42]. Some previous works have been conducted for the implementation of carbon nanotubes in advanced bio-sensing applications [43-49]. M. L. Yola et al. developed a novel imprinted electrochemical biosensor based on Fe@AuNPs and f-MWCNTs for direct determination of cefixime (CEF) in human plasma, which showed high sensitivity and selectivity towards CEF and offers the advantages of simplicity and efficiency in target detection from biological samples [43]; their groups also reported the synthesis and application of NiO-multiwall carbon nanotube nanocomposite (NiO/MWCNTs) and 1-butyl-3-methylimidazolium tetrafluoroborate ([Bmim]BF4) in the carbon paste matrix as high sensitive sensors for voltammetric determination of vitamin C in the presence of vitamin B9 in food and drug samples [44]. Al-Saleh et al. analyzed the EMI shielding mechanisms of MWCNT/polypropylene composite plates experimentally and

theoretically, found that the absorption is the major shielding mechanism and the reflection is the secondary shielding mechanism. A negative influence on the overall EMI shielding effectiveness brought by multiple-reflection was shown by the theoretical analysis. They believed that a multi-surface shield such as conductive polymer composites might drastically enhance the overall EMI shielding effectiveness if multiple-reflection can be minimized [50]. Polymeric conductive nanocomposites provide obvious piezoresistive behaviors, having applications in many special fields due to their high flexibility, which can be easily produced with large sizes and very low costs. Piezoresistive effect is a change in the electrical resistivity of a semiconductor-like material when a mechanical strain is applied. In contrast to the piezoelectric effect, the piezoresistive effect causes a change only in electrical resistance, but not in electrical potential. Benefited from the piezoresistivity, stretchable devices for converting mechanical energy to electrical energy, such as mechanical sensors and wearable electronic devices could be developed [51].

As rapidly growing of the health care industry, the demand for the flexible tactile sensors with high reliability and large areas are needed. To meet this demand, a variety of tactile sensors have been developed and studied, such as a discrete semiconductor type tactile sensor [52], a conductive pigment touch sensor [53], a photo reflector type tactile sensor [54], or a fluid-filled micro-vibration sensor [45]. However, these sensors ether have complicated structures, or are not robust enough to be practically utilized, compared to the simple, low-costed piezoresistivity based flexible tactile sensor [55]. However, there still exist many drawbacks for the piezoresistivity based tactile sensors needed to be overcome, such as a relative low repeatability brought with by the viscoelasticity of the polymer substrates.

1.5 Object of the Thesis

Living in a world full of all kinds of information, it is important to detect, collect, analyze, and distribute tons of information. Mechanical Sensor is a significant device to convert different types of exterior mechanical stimulus, such as force, pressure, impact, vibration, and acceleration, to usable electrical signals. The demand for diverse types of sensors with smart property and low cost is growing rapidly as the widespread of small gadgets like smartphones or tablets, development of many novel technologies such as robots, drones, electric vehicles (EV), artificial intelligence (AI), virtual reality (VR), bionics and biotechnology etc. However, despite their various shapes and functionalities, traditional mechanical sensors are relatively expensive, limited by their fixed shapes, and sometimes even too fragile to measure the mechanical stimulus. Thus the demand of a variety of flexible mechanical sensors, which are cheap, sensitive, which can be applied to a flat or curving surface with large areas, is expanding fast. Such a flexible mechanical sensor has the ability of not only measuring an external mechanical stimulus, but also providing a protection to the inner device or apparatus.

This thesis aims to investigate the ability of different types of silicone elastomeric functional nanocomposites to be applied as mechanical sensors, in other words, the ability of convert a mechanical stimulus to an electrical signal, with the efficiency and sensitivity as high as possible.

1.6 Thesis Organization

The thesis consists of following 6 Chapters.

Chapter 1 is a general introduction to this thesis. The background of the research and

the object of the work have been explained in detail.

In Chapter 2, the potential of incorporate $BaTiO_3$ particles in an elastomer matrix to obtain a high mechanical sensing ability was demonstrated. However, it is difficult to distribute $BaTiO_3$ nanoparticles into the silicone substrate due to the poor surface affinities between these two materials. This was found to have weakened the dielectric behaviors. To improve the dispersity of $BaTiO_3$ particles, a novel silicone coupling agent was used to modify the surface of particles. TG and FTIR results show that coupling agent was successfully coated on the surface. Raw $BaTiO_3$ particles and $BaTiO_3$ particles modified by silicone coupling agents were incorporated in the silicone elastomer to fabricate $BaTiO_3$/silicone membranes. Particle size distribution measurement and SEM observation show that $BaTiO_3$ particles get higher compatibility with silicone, dispersity of $BaTiO_3$ particles and the dielectric properties of $BaTiO_3$/silicone membranes were both improved by the surface modification.

In Chapter 3, to take advantage of the excellent insulation features as well as the excellent dielectric property, surface treated ferroelectric $BaTiO_3$ nanoparticles were added into the silicone elastomer to fabricate a flexible nanocomposite with a high dielectric constant. A measuring system containing modified $BaTiO_3$/silicone membrane was assembled. An obvious and variable capacitance was obtained due to the high dielectric constant of the membrane. In addition, corresponding current generated from the capacitance variation has been detected form the system, confirming its possibility for mechanical sensing application. The application of silicone elastomeric nanocomposites for mechanical sensing was realized by a mechanical sensing system assembling with a capacitive $BaTiO_3$/silicone membrane. It is able to detect an external mechanically impact, or a vibration by measuring the variation of the capacitance through a LCR

meter/Multimeter mounted in the system with a high precision and a short response time.

In Chapter 4, 3 types of theoretic piezoresistive models for the conductive particles reinforced elastomeric nanocomposites were introduced from different prospects. Each model was built considering both the solid and foamed conductive nanocomposite. These piezoresistive models were deduced based on the percolation threshold and the tunnel conductive theory of conductive elastomeric nanocomposites, the situations both considering and ignoring the spherical/fiber-like shapes of the conductive particles were discussed in detail. Although the overall trend of the resistance changes matched, notable separations were found between the theoretical values and the measured values, which are thought to be caused by the viscoelasticity of the silicone matrix.

In Chapter 5, multi-walled carbon nanotubes (MWCNTs), with a high electrical conductivity and large relative surface areas, were integrated in the silicone elastomer to provide a high conductivity as well as a piezoresistive property. To raise the sensitivity and improve the piezoresistivity of the nanocomposite, a foaming procedure was introduced to reduce the viscoelasticity of the silicone elastomer. A series of conductive foamed nanocomposites were fabricated with different types of foaming agents to obtain a diverse porous structure. The porous structures of the foams, the distribution and orientation status of the multi-walled carbon nanotubes in the silicone matrix were observed/analyzed using laser microscope and SEM with/without a compression load. The influences of the porous structure and porosity on the foam were studied. It was found that a different porosity and different voids structure affected the density, elastic modulus, resistivity as well as piezoresistive property significantly. This type of piezoresistive active nanocomposite was proved to have an obvious potentiality for utilizations in a mechanical sensor, such as a tactile sensor or an impact sensor.

Applications of MWCNT/silicone elastomeric nanocomposites for mechanical sensing were investigated deeply. A mechanical sensing system was assembled with a piezoresistive MWCNT/silicone sponge-like sheet. It is able to detect not only a wide range of tactile pressure, but also a mechanically impact by measuring the variation of the resistive through a Multimeter.

In Chapter 6, a general conclusion of this work was made.

References

[1] Jo, B. H., Van Lerberghe, L. M., Motsegood, K. M., & Beebe, D. J. (2000). Three-dimensional micro-channel fabrication in polydimethylsiloxane (PDMS) elastomer. Journal of microelectromechanical systems, 9(1), 76-81.

[2] Pearson, R. A., & Yee, A. F. (1986). Toughening mechanisms in elastomer-modified epoxies. Journal of materials science, 21(7), 2475-2488.

[3] Carlson, J. D., & Jolly, M. R. (2000). MR fluid, foam and elastomer devices. Mechatronics, 10(4), 555-569.

[4] Wang, Y., Ameer, G. A., Sheppard, B. J., & Langer, R. (2002). A tough biodegradable elastomer. Nature biotechnology, 20(6), 602-606.

[5] Carpi, F., Bauer, S., & De Rossi, D. (2010). Stretching dielectric elastomer performance. Science, 330(6012), 1759-1761.

[6] Camacho-Lopez, M., Finkelmann, H., Palffy-Muhoray, P., & Shelley, M. (2004). Fast liquid-crystal elastomer swims into the dark. Nature materials, 3(5), 307-310.

[7] LeBaron, P. C., & Pinnavaia, T. J. (2001). Clay nanolayer reinforcement of a silicone elastomer. Chemistry of Materials, 13(10), 3760-3765.

[8] Gallone, G., Carpi, F., De Rossi, D., Levita, G., & Marchetti, A. (2007). Dielectric

constant enhancement in a silicone elastomer filled with lead magnesium niobate–lead titanate. Materials Science and Engineering: C, 27(1), 110-116.

[9] Khoo, M., & Liu, C. (2001). Micro magnetic silicone elastomer membrane actuator. Sensors and Actuators A: Physical, 89(3), 259-266.

[10] Holland, R., Dugdale, T. M., Wetherbee, R., Brennan, A. B., Finlay, J. A., Callow, J. A., & Callow, M. E. (2004). Adhesion and motility of fouling diatoms on a silicone elastomer. Biofouling, 20(6), 323-329.

[11] Nayak, S., Rahaman, M., Pandey, A. K., Setua, D. K., Chaki, T. K., & Khastgir, D. (2013). Development of poly (dimethylsiloxane)–titania nanocomposites with controlled dielectric properties: Effect of heat treatment of titania on electrical properties. Journal of Applied Polymer Science, 127(1), 784-796.

[12] Liou, J. W., & Chiou, B. S. (1998). Dielectric tunability of barium strontium titanate/silicone-rubber composite. Journal of Physics: Condensed Matter, 10(12), 2773.

[13] Farzaneh, M., Baker, T., Bernstorf, A., Burnham, J. T., Carreira, T., Cherney, E., & de Tourreil, C. (2005). Selection of station insulators with respect to ice and snow-part I: technical context and environmental exposure. IEEE Transactions on Power Delivery, 20(1), 264-270.

[14] Jordan, J., Jacob, K. I., Tannenbaum, R., Sharaf, M. A., & Jasiuk, I. (2005). Experimental trends in polymer nanocomposites—a review. Materials science and engineering: A, 393(1), 1-11.

[15] Ray, S. S., & Okamoto, M. (2003). Polymer/layered silicate nanocomposites: a review from preparation to processing. Progress in polymer science, 28(11), 1539-1641.

[16] Moniruzzaman, M., & Winey, K. I. (2006). Polymer nanocomposites containing carbon nanotubes. Macromolecules, 39(16), 5194-5205.

[17] Manias, E., Touny, A., Wu, L., Strawhecker, K., Lu, B., & Chung, T. C. (2001). Polypropylene/montmorillonite nanocomposites. Review of the synthetic routes and materials properties. Chemistry of Materials, 13(10), 3516-3523.

[18] Kim, H., Abdala, A. A., & Macosko, C. W. (2010). Graphene/polymer nanocomposites. Macromolecules, 43(16), 6515-6530.

[19] Ramanathan, T., Abdala, A. A., Stankovich, S., Dikin, D. A., Herrera-Alonso, M., Piner, R. D., ... & Nguyen, S. T. (2008). Functionalized graphene sheets for polymer nanocomposites. Nature nanotechnology, 3(6), 327-331.

[20] Ma, P. C., Siddiqui, N. A., Marom, G., & Kim, J. K. (2010). Dispersion and functionalization of carbon nanotubes for polymer-based nanocomposites: a review. Composites Part A: Applied Science and Manufacturing, 41(10), 1345-1367.

[21] Pavlidou, S., & Papaspyrides, C. D. (2008). A review on polymer–layered silicate nanocomposites. Progress in polymer science, 33(12), 1119-1198.

[22] White, Scott R., N. R. Sottos, P. H. Geubelle, J. S. Moore, M_R Kessler, S. R. Sriram, E. N. Brown, and S. Viswanathan. "Autonomic healing of polymer composites." Nature 409, no. 6822 (2001): 794-797.

[23] Saheb, D. Nabi, and Jyoti P. Jog. "Natural fiber polymer composites: a review." Advances in polymer technology 18, no. 4 (1999): 351-363.

[24] Grubbs, Robert B. "Hybrid metal–polymer composites from functional block copolymers." Journal of Polymer Science Part A: Polymer Chemistry 43, no. 19 (2005): 4323-4336.

[25] Varga, Z., Filipcsei, G., & Zrínyi, M. (2006). Magnetic field sensitive functional

elastomers with tuneable elastic modulus. Polymer, 47(1), 227-233.

[26] Newnham, R. E., Skinner, D. P., & Cross, L. E. (1978). Connectivity and piezoelectric-pyroelectric composites. Materials Research Bulletin, 13(5), 525-536.

[27] Newnham, R. E., & Ruschau, G. R. (1993). Electromechanical properties of smart materials. Journal of Intelligent Material Systems and Structures, 4(3), 289-294.

[28] Tressler, J. F., Alkoy, S., Dogan, A., & Newnham, R. E. (1999). Functional composites for sensors, actuators and transducers. Composites Part A: Applied Science and Manufacturing, 30(4), 477-482.

[29] Madhavan, C., Gururaja, T. R., Srinivasan, T. T., Xu, Q. C., & Newnam, R. E. (1987, October). Fired 0-3 piezoelectric composite materials for biomedical ultrasonic imaging applications. In IEEE 1987 Ultrasonics Symposium (pp. 645-650). IEEE.

[30] Nayak, S., Rahaman, M., Pandey, A. K., Setua, D. K., Chaki, T. K., & Khastgir, D. (2013). Development of poly (dimethylsiloxane)–titania nanocomposites with controlled dielectric properties: Effect of heat treatment of titania on electrical properties. Journal of Applied Polymer Science, 127(1), 784-796.

[31] Carpi, F., & Rossi, D. D. (2005). Improvement of electromechanical actuating performances of a silicone dielectric elastomer by dispersion of titanium dioxide powder. IEEE Transactions on Dielectrics and Electrical Insulation, 12(4), 835-843.

[32] Xu, J., & Wong, C. P. (2004). In Advanced Packaging Materials: Processes, Properties, and Interfaces, 2004. Proceedings, 9th International Symposium on (pp. 158-170). IEEE.

[33] George, R., Kashyap, K. T., Rahul, R., & Yamdagni, S. (2005). Strengthening in carbon nanotube/aluminium (CNT/Al) composites. Scripta Materialia, 53(10),

1159-1163.

[34] Kim, J. A., Seong, D. G., Kang, T. J., & Youn, J. R. (2006). Effects of surface modification on rheological and mechanical properties of CNT/epoxy composites. Carbon, 44(10), 1898-1905.

[35] Curtin, W. A., & Sheldon, B. W. (2004). CNT-reinforced ceramics and metals. Materials Today, 7(11), 44-49.

[36] Peng, S., Cho, K., Qi, P., & Dai, H. (2004). Ab initio study of CNT NO 2 gas sensor. Chemical Physics Letters, 387(4), 271-276.

[37] Saleh, T. A., & Gupta, V. K. (2012). Column with CNT/magnesium oxide composite for lead (II) removal from water. Environmental Science and Pollution Research, 19(4), 1224-1228.

[38] Su, Y. S., & Manthiram, A. (2012). A new approach to improve cycle performance of rechargeable lithium–sulfur batteries by inserting a free-standing MWCNT interlayer. Chemical Communications, 48(70), 8817-8819.

[39] Antunes, E. F., Lobo, A. O., Corat, E. J., Trava-Airoldi, V. J., Martin, A. A., & Veríssimo, C. (2006). Comparative study of first-and second-order Raman spectra of MWCNT at visible and infrared laser excitation. Carbon, 44(11), 2202-2211.

[40] Kota, A. K., Cipriano, B. H., Duesterberg, M. K., Gershon, A. L., Powell, D., Raghavan, S. R., & Bruck, H. A. (2007). Electrical and rheological percolation in polystyrene/MWCNT nanocomposites. Macromolecules, 40(20), 7400-7406.

[41] Hong, S., & Myung, S. (2007). Nanotube Electronics: A flexible approach to mobility. Nature Nanotechnology, 2(4), 207.

[42] Aguilar, J. O., Bautista-Quijano, J. R., & Avilés, F. (2010). Influence of carbon nanotube clustering on the electrical conductivity of polymer composite films.

Express Polym. Lett, 4, 292-299.

[43] Yola, M. L., Eren, T., & Atar, N. (2014). Molecularly imprinted electrochemical biosensor based on Fe@ Au nanoparticles involved in 2-aminoethanethiol functionalized multi-walled carbon nanotubes for sensitive determination of cefexime in human plasma. Biosensors and Bioelectronics, 60, 277-285.

[44] Khaleghi, F., Arab, Z., Gupta, V. K., Ganjali, M. R., Norouzi, P., Atar, N., & Yola, M. L. (2016). Fabrication of novel electrochemical sensor for determination of vitamin C in the presence of vitamin B9 in food and pharmaceutical samples. Journal of Molecular Liquids, 221, 666-672.

[45] Fishel, J. A., Santos, V. J., & Loeb, G. E. (2008, October). A robust micro-vibration sensor for biomimetic fingertips. In Biomedical Robotics and Biomechatronics, 2008. BioRob 2008. 2nd IEEE RAS & EMBS International Conference on (pp. 659-663). IEEE.

[46] Wei, C., Dai, L., Roy, A., & Tolle, T. B. (2006). Multifunctional chemical vapor sensors of aligned carbon nanotube and polymer composites. Journal of the American Chemical Society, 128(5), 1412-1413.

[47] Yola, M. L., & Atar, N. (2014). A novel voltammetric sensor based on gold nanoparticles involved in p-aminothiophenol functionalized multi-walled carbon nanotubes: application to the simultaneous determination of quercetin and rutin. Electrochimica Acta, 119, 24-31.

[48] Karimi-Maleh, H., Tahernejad-Javazmi, F., Atar, N., Yola, M. L., Gupta, V. K., & Ensafi, A. A. (2015). A novel DNA biosensor based on a pencil graphite electrode modified with polypyrrole/functionalized multiwalled carbon nanotubes for determination of 6-mercaptopurine anticancer drug. Industrial & Engineering

Chemistry Research, 54(14), 3634-3639.

[49] Ertan, B., Eren, T., Ermiş, İ., Saral, H., Atar, N., & Yola, M. L. (2016). Sensitive analysis of simazine based on platinum nanoparticles on polyoxometalate/multi-walled carbon nanotubes. Journal of colloid and interface science, 470, 14-21.

[50] Hennings, D., & Rosenstein, G. (1984). Temperature-Stable Dielectrics Based on Chemically Inhomogeneous BaTiO3. Journal of the American Ceramic Society, 67(4), 249-254.

[51] Noh, J. S. (2016). Conductive elastomers for stretchable electronics, sensors and energy harvesters. Polymers, 8(4), 123.

[52] Mukai, T. (2004, October). Soft areal tactile sensors with embedded semiconductor pressure sensors in a structured elastic body. In Sensors, 2004. Proceedings of IEEE (pp. 1518-1521). IEEE.

[53] Koehly, R., Curtil, D., & Wanderley, M. M. (2006, June). Paper FSRs and latex/fabric traction sensors: methods for the development of home-made touch sensors. In Proceedings of the 2006 conference on New interfaces for musical expression (pp. 230-233). IRCAM—Centre Pompidou.

[54] Ohmura, Y., Kuniyoshi, Y., & Nagakubo, A. (2006, May). Conformable and scalable tactile sensor skin for curved surfaces. In Robotics and Automation, 2006. ICRA 2006. Proceedings 2006 IEEE International Conference on (pp. 1348-1353). IEEE.

[55] Shimojo, M., Namiki, A., Ishikawa, M., Makino, R., & Mabuchi, K. (2004). A tactile sensor sheet using pressure conductive rubber with electrical-wires stitched method. IEEE Sensors journal, 4(5), 589-596.

Chapter2 Dielectric Properties of $BaTiO_3$/silicone Elastomeric Nanocomposites

2.1 Introduction

Among many types of dielectrics, $BaTiO_3$ (which has an abbreviation of BT) has a relatively high dielectric constant. BT is a type of significant ceramic dielectric material with ferroelectric properties under its curie point of 123°C, which is widely used for ceramic capacitors [1]. It is difficult to measure the dielectric constant of powder material directly, therefore the evaluation of connection between grain sizes of BT particles with its dielectric constant, which is often called “size effect”. According to the study of S. Wada [2], a new powder dielectric measurement method was developed by combining measurement of a suspension and calculation with a finite element method. Using this method, the dielectric constants of BT particles with different sizes were estimated [3]. The result indicated that the dielectric constants of BT particles with a size of 70nm has a highest value of about 15000, and decreased sharply with decreasing of the particle size. The dielectric constants would also decrease with an increasing particle sizes larger than 70nm, and would reach a constant of about 3300 with sizes over 300nm.

Although having such a high dielectric constant, BT still has some drawbacks such as a low breakdown strength, brittleness, and processing difficulty. On the other hand, despite with a low dielectric constant, organic polymers have many advantages such as a low dielectric loss, a high electric breakdown strength, a low elastic modulus and good processability [4,5]. Those problems could be overcome by integrating the BT particles in a flexible elastomer to fabricate a dielectric elastomeric nanocomposite, combining the advantages of both, which might bring a lot of potential novel applications. For instance,

a dielectric elastomer actuator can be made by sandwiching membrane of dielectric nanocomposites in between two compliant electrodes, after loading a voltage on the compliant electrodes, compression in the thickness direction and stretching in area direction of the elastomer membrane will occur due to the Coulombic force [6-11]. On the contrary, a mechanical sensor can be assembled by such a dielectric elastomer, which is able to detect the external tactile pressure or mechanical impact by measuring the capacitance change [12-17].

2.2 Significance of Dispersity of $BaTiO_3$ particles in $BaTiO_3$/Silicone Nanocomposite for Dielectric Constant Enhancement

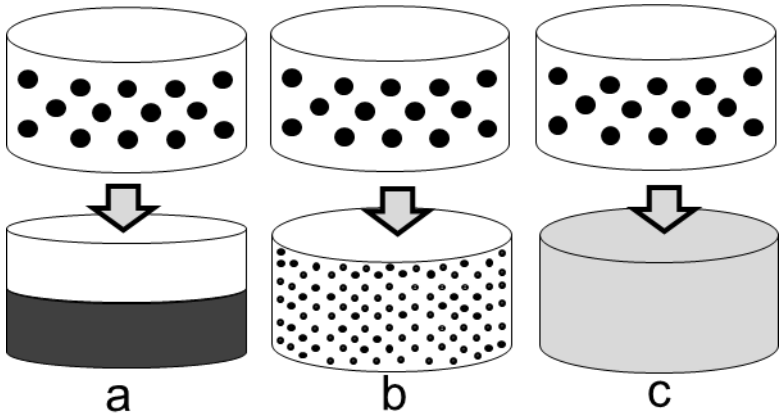

Fig.2.1 Theoretic models of BT/silicone nanocomposites membrane

a: the most serious agglomeration/sedimentation, absolutely divided by two parts

b: the middle state between a and c

c: dispersed very well, absolutely becomes one part

Theoretic dielectric constant of a BT/silicone nanocomposite can be derived from the

calculation of the capacitance of the nanocomposite. As shown in Fig. 2.1, dispersion status of BT particles in silicone elastomer can be classified as 3 situations. During the experiment, BT particles were dispersed into uncured silicone elastomer and always affected by gravity until curing. The density of silicone elastomer is 0.93g/cm^3, the density of BT particles is about 6.02g/cm^3, which is much bigger. Therefore during the curing procedure, BT particles always tend to sediment to the bottom and agglomerate together. In Fig. 2.1, part a shows the situation of the most severe agglomeration and sedimentation, with all the BT particles precipitated to the bottom, finally the membrane is absolutely divided into two parts: silicone elastomer part at upper side and BT particles part at bottom side. Part c shows the most well dispersed situation, in which all the BT particles are dispersed well that every single particle are separated apart and uniformly distributed into the silicone monomers. Part a and part c show the ideal situations with extreme statuses. Part b is a normal status between situation a and c, as an example that easy to understand, all of the BT particles are divided by a large amounts of units, each unit contains several BT particles and every unit is relative uniformly distributed into the silicone monomers. The size of each unit is not sure and varies as the amount of BT particles in one unit changing.

The dielectric constant of vacuum is ε_0. Set the area of membrane as A, the thickness of the membrane as d, the volume fraction of BT particles in membrane as x. Assume that for every membrane is sandwiched by a pair of parallel electrodes with areas of A with no gaps. Then set dielectric constant of silicone elastomer, BT particles and the whole membrane as ε_e, ε_f, ε, respectively. Capacitance of the entire membrane can be calculated as follows:

$$C = \frac{\varepsilon_0 \varepsilon A}{d} \quad (2\text{-}1)$$

For the situation a in Fig. 2.1, capacitance of the silicone part and the BT part can be calculated respectively. The capacitance of the membrane is reversely proportional to the capacitance of the silicone part and the BT part, thus the capacitance of the membrane can also be calculated as:

$$C = \frac{1}{\frac{x}{C_e}+\frac{1-x}{C_f}} = \frac{C_e C_f}{xC_f+(1-x)C_e} = \frac{\frac{\varepsilon_0^2 A^2 \varepsilon_e \varepsilon_f}{d^2}}{\frac{\varepsilon_0 A[x\varepsilon_f+(1-x)\varepsilon_e]}{d}} = \frac{\varepsilon_0 A \varepsilon_e \varepsilon_f}{d[x\varepsilon_e+(1-x)\varepsilon_f]} \quad (2\text{-}2)$$

Compare Eq. (2-2) with Eq. (2-1), we can get the dielectric of the membrane as:

$$\varepsilon = \frac{\varepsilon_e \varepsilon_f}{x\varepsilon_e+(1-x)\varepsilon_f} \quad (2\text{-}3)$$

For situation c in Fig. 2.1, the Lenchtenecker' logarithmic law [18] can be used to calculate dielectric constant of the membrane because of its well dispersity:

$$\log\varepsilon = (1-x)\log\varepsilon_e + x\log\varepsilon_f \quad (2\text{-}4)$$

From Eq. (2-4), we can get the dielectric constant:

$$\varepsilon = \varepsilon_e^{(1-x)}\varepsilon_f^x \quad (2\text{-}5)$$

The dielectric constant of BT particles with sizes around 300~500nm can be estimated as about 2000 [3]. According to the previous result, the silicone elastomer has a dielectric constant of about 8. By substituting ε_e=8 and ε_f=2000 into Eq. (2-3) and Eq. (2-5), the theoretic dielectric constant of the membrane in situation a and c in Fig. 2.1 can be calculated.

Table 2.1 Theoretical dielectric constant of membrane in situation a and c

volume fraction	10%	20%	30%	40%	50%
ε in situation a	8.9	10.0	11.4	13.3	15.9
ε in situation c	13.9	24.1	42.0	72.8	126.6

As shown in Table 2.1. It is confirmed from the calculated results that during the wide volume fraction range from 10% to 50%, the well dispersed BT/silicone membrane has a higher dielectric constant than the agglomerated/sedimented one. BT/silicone membranes, in reality, should have a dielectric constant value between situation a and situation c in Fig. 2.1. The dielectric constant of the nanocomposite membrane can be enhanced by improving the dispersity status of the BT particles, making it close to situation c in Fig. 2.1. However, because of the relative poor compatibility between inorganic dielectric particles and organic silicone elastomer, sedimentation of particles is difficult to avoid, leading to higher dielectric loss and producing much pores that might reduce the dielectric constant [5]. Obviously, it is of great significance to improve the compatibility between inorganic dielectric particles and elastomers, overcoming the influence from gravity. Many previous works shows that surface modification with coupling agents is a good method to improving the compatibility. Shu-Hui Xie, Bao-Ku Zhu and their coworkers [19] synthesized polyimide/barium titanate composites through a colloidal process, finding that the BT particles in the size of 100 nm were dispersed homogeneously in the polyimide matrix without aggregation. Dang Zhi-Min and his coworkers [20] fund the increased dielectric constant in the PVDF matrix composites with BT treated by 1.0wt% silane coupling agent KH550. Their group also found that [21] an appropriate silane coupling agent can be used to improve the interaction between BT and epoxy resin, getting high dielectric permittivity barium titanate/epoxy resin composites. L. Ramajo and their research group [22] studied the influence of silane coupling agents on the micro structure and dielectric behavior of epoxy/BT composites, finding that their composites presented good dielectric properties and a strong dependence with the silane concentration.

In the study, in order to improve the dispersity of BT particles and avoid sedimentation, a new type of silicone coupling agent was used to modify the surface of particles with a novel super-critical method. Then raw BT particles and modified BT particles were incorporated in the silicone elastomer to fabricate the BT/silicone membranes. Dispersity of BT particles, dielectric properties and piezoelectric properties of BT/silicone membranes were evaluated. The utilization of BT/silicone functional nanocomposites for a variety of mechanical sensing applications has been studied.

2.3 Experimental Section

2.3.1 Materials

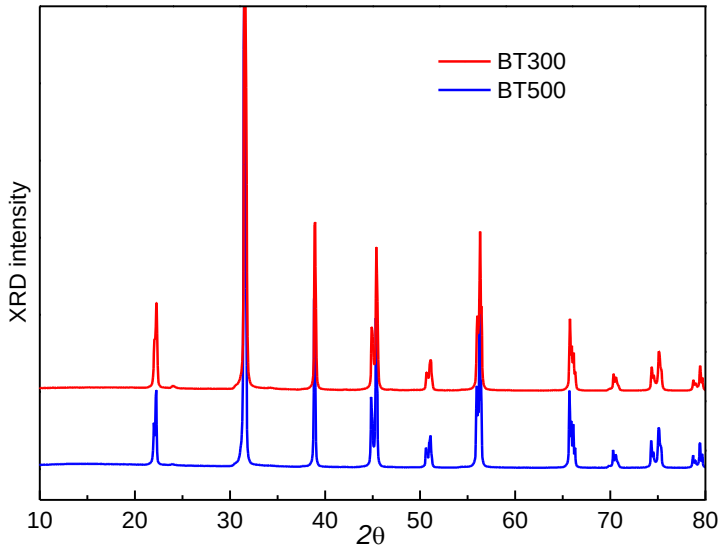

Fig.2.2 XRD patterns of BT300 and BT500 particles

BT particles with sizes of 300nm and 500nm (BT300 and BT500, with average crystallite sizes of 42.4nm and 53.4nm, respectively) were provided by KCM

Corporation, Japan. The XRD patterns of BT300 and BT500 particles are shown in the Fig. 2.2. It can be known from the XRD patterns that both the BT300 and BT500 are polycrystalline particles, the crystal structures of which are tetragonal, with a c/a ratio of about 1.011. Two-component RTV silicone elastomer KE-103 (containing a main component and a crosslinker), silicone coupling agent triethoxysilylethyl polydimethylsiloxyethyl dimethicone, silicone oil KF-96-6CS (a low viscosity dimethylsiloxane silicone oil) were supplied by Shin-Etsu Chemical Co. Ltd., Japan; hydrogen peroxide aqueous (30%) was provided by Tokyo Chemical Industry Co. Ltd., Japan; ethanol, acetone and other reagents were obtained from Wako Pure Chemical Industries, Ltd., Japan.

2.3.2 Surface Modifications of $BaTiO_3$ Using Silicone Coupling Agent

In this thesis, BT is an abbreviation of BT, while BT300 and BT500 are abbreviations of BT particles with sizes of 300nm and 500nm, respectively. Before modifying, surface of BT particles were activated by creating hydroxyl groups to the surface using hydrogen peroxide aqueous, according to Shinn-Jen Chang' work [23]. On the surface of BT particles, the amount of active groups, such as amino groups or hydroxyl groups, is too little to be used for modification. To solve the problem, hydroxyl groups were introduced to the surface using hydrogen peroxide to activate the surface, according to Shinn-Jen Chang' work. When using boiling hydrogen peroxide to treat the BT particles, H_2O_2 can decompose and hydroperoxyl radical (·OH) will generated on the surface. Then the ·OH will react with H_2O_2 to form hydroperoxyl radical ($\cdot O_2H$) or further react with produced $\cdot O_2H$ to form water and oxygen. Due to the highly acidic property of $\cdot O_2H$, hydroxyl groups can be easily produced by reaction between $\cdot O_2H$ and the oxygen ions on the

surface of BT particles. In addition, the $O_2^{-}\cdot$ radical can continuously react with water to yield hydroxyl anions into the aqueous, reducing the pH scale. The reaction procedures are shown in Fig. 2.2, the last equation in which shows the overall reaction.

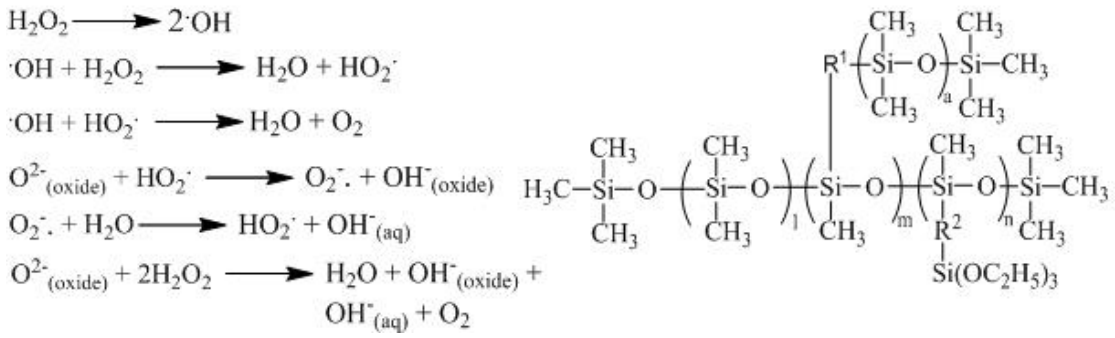

Fig.2.3 The structure of silicone coupling agent and the coupling agent modification reaction

Fig. 2.3 shows the structure of silicone coupling agent. It is an oligomeric polysiloxane that has the similar structure with silicone elastomer. It contains silicon-ethoxyl groups which can easily hydrolysis when contacting with moisture in the air. Predetermined ratio of BT particles and silicone coupling agent were dispersed into hexane, put in an autoclave and heated to 234.5ºC, 3.01MPa, a condition which hexane will become to supercritical status. During the modification, -OH groups on the surface of BT particles and Si-OH groups from silicone coupling agent could get a well contact and obtain a high reacting activity due to the excellent dissolving capacity of supercritical hexane.

Table 2.2 The addition amount of coupling agent

Modified BT300 (BT500)	BT300-0 (BT500-0)	BT300-1 (BT500-1)	BT300-3 (BT500-3)	BT300-5 (BT500-5)
Activated BT300 (BT500)	35g	35g	35g	35g
Coupling agent	0	1g	3g	5g
m (coupling agent) / m (BT particles)	0	2.86%	8.57%	14.29%

In the experiment, 40g of BT300 (or BT500) particles and 200mL of hydrogen peroxide aqueous (30%) were added into a round bottom flask and the mixture was stirred at boiling point (106ºC) for 5h with refluxing, then the particles was washed by deionized water several times. Finally the surface activated BT particles were obtained after drying under vacuum at 60ºC for 12h. After surface activation, BT particles were surface modified by silicone coupling agent through a treatment in super-critical status. 35g of activated BT300 (BT500) particles, predetermined amount of silicone coupling agent triethoxysilylethyl polydimethylsiloxyethyl dimethicone and 80mL hexane were added into tubular bottle and mixed. Coupling agent was added according to Table 2.2. Then the mixture was set into autoclave and heated to supercritical status (234.5ºC, 3.01MPa) for 1h. The modified particles were obtained after cooling to room temperature, being washed by acetone several times and dried under vacuum at 60ºC for 12h.

2.3.3 Preparation of $BaTiO_3$/Silicone Nanocomposites

Table 2.3 The formula of BT300/silicone composites

BT / silicone membrane	Membrane of pure silicone	M300-0-20	M300-1-20	M300-3-20	M300-5-20	M300-0-40	M300-1-40	M300-3-40	M300-5-40
BT300-0		6.02g				12.04g			
BT300-1			6.02g				12.04g		
BT300-3				6.02g				12.04g	
BT300-5					6.02g				12.04g
Silicone	4.85g	3.88g	3.88g	3.88g	3.88g	2.91g	2.91g	2.91g	2.91g
Volume fraction	0	20%				40%			

Table 2.4 The formula of BT500/silicone composites

BT / silicone membrane	Membrane of pure silicone	M500-0-20	M500-1-20	M500-3-20	M500-5-20	M500-0-40	M500-1-40	M500-3-40	M500-5-40
BT500-0		6.02g				12.04g			
BT500-1			6.02g				12.04g		
BT500-3				6.02g				12.04g	
BT500-5					6.02g				12.04g
Silicone	4.85g	3.88g	3.88g	3.88g	3.88g	2.91g	2.91g	2.91g	2.91g
Volume fraction	0	20%				40%			

The required amounts of raw and modified BT300 or BT500 particles were mixed with the main component of silicone elastomer together according to Table 2.3 and Table 2.4,

with a high-shearing blender. The crosslinker was then added to the mixture and absolutely dispersed. The ratio of m(main component):m(crosslinker) was controlled to 100:5. Finally, the BT/silicone nanocomposites membrane was obtained by pouring the mixture into PTFE mold and making it cure at room temperature for 72h.

2.3.4 Characterizations

Trace of chemical groups on the surface of BT particles was detected by fourier-transform infrared spectrum (FTIR) using a JASCO FT/IR-6200 Fourier Transform Infrared Spectrometer. Thermogravimetric analysis (TG) was conducted with a heating rate of 10ºC/min in air atmosphere using a Rigaku Thermo plus TG 8120. Scanning electron microscopy (SEM) images were obtained under an accelerating voltage of 15kV with a JEOL JSM-7600F Field Emission Scanning Electron Microscope. Particle size distribution was measured by a MALVERN nano series particle size measuring instrument. Dielectric constant and dielectric loss (tanδ) were measured by a NF ZM 2371 LCR meter. Mechanical properties were measured by SHIMADZU AGS-G Autograph. Current in the measuring system was measured by a KEITHLEY 2000 Multimeter.

2.4 Results and Discussion

2.4.1 Evaluation of the Surface Modification

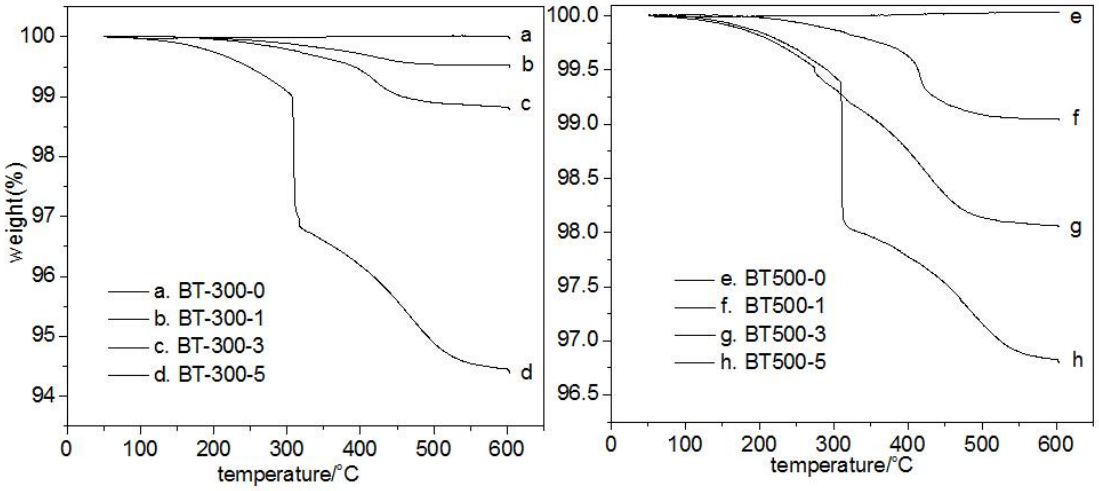

Fig.2.4 TG results of raw BT particles and silicone coupling agent modified BT particles

To estimate the amounts of covered coupling agent on the BT surface, TG measurement for raw BT particles and silicone coupling agent modified BT particles was conducted. The results are shown in Fig. 2.4. TG was measured in pure atmosphere. All samples were heated from room temperature to 600ºC to make sure all of the coupling agent on the surface can absolutely react with O_2. Organic side groups containing -CH_3 and -R would be burned out and the Si-O backbones will absorb O_2 and remain as a status of SiO_2. Therefore the mass loss equals to the lost weight of side groups, -CH_3 and –R, minus the obtained weight of absorbed oxygen atoms. It can be seen from Fig. 2.4 that: (1) When all the BT particles heated to 600ºC, the weight loss of raw/modified BT particles is decided by the modification ratio of silicone coupling agent. For BT300 particles, weight loss increases from almost 0 to 5.6% as the modification ratio increasing from 0 to 14.29%Wt. For BT500 particles, weight loss increases from almost 0 to 3.2% as the modification ratio increasing from 0 to 14.29%Wt. The raw BT particles have only a tiny weight loss that might be due to the measuring error. In contrast, silicone coupling agents modified BT particles have large weight losses. This result confirmed the truth that silicone

coupling agent has been successfully coated on the surface of BT particles. (2) Dramatic mass losses appeared when the BT-300-5 and BT-500-5 particles heated to about 300ºC. It is considered that a BT particle could obtain a 3-layer structure during surface modification, containing an inorganic BT particle core, a chemical bonded coupling agent middle layer and a physical attached coupling agent outer layer. At about 300ºC, the outer layer is beginning to burn and generated SiO_2 is fume-like that is difficult to deposit as a layer. The inner layer of coupling agent is also beginning to burn, but generated SiO_2 is easy to deposit as a layer due to the Si-O-Metal chemical bond between BT particles and silicone coupling agent. So it could be proved that a modification ratio of 14.29%Wt is fully enough for the need of the BT particles surface; BT-300-5 and BT-500-5 have thick physical attached coupling agent layer coated on the surface, leading to obvious weight losses at around 300ºC; for BT-300-3 and BT-500-3 particles, the modification ratio of 8.57%Wt is no more than the need of the BT particles surface, so there is only a thin coupling agent layer physically attached on the surface, without dramatic weight loss to be observed at around 300ºC. (3) Even with a same coupling agent modification ratio, weight loss of modified BT-300 particles is higher than that of modified BT-500 particles. This is because the BT-300 particle has a slightly larger specific surface area of 3.81m^2/g, compared to that of BT-500 particles of about 2.28 m^2/g.

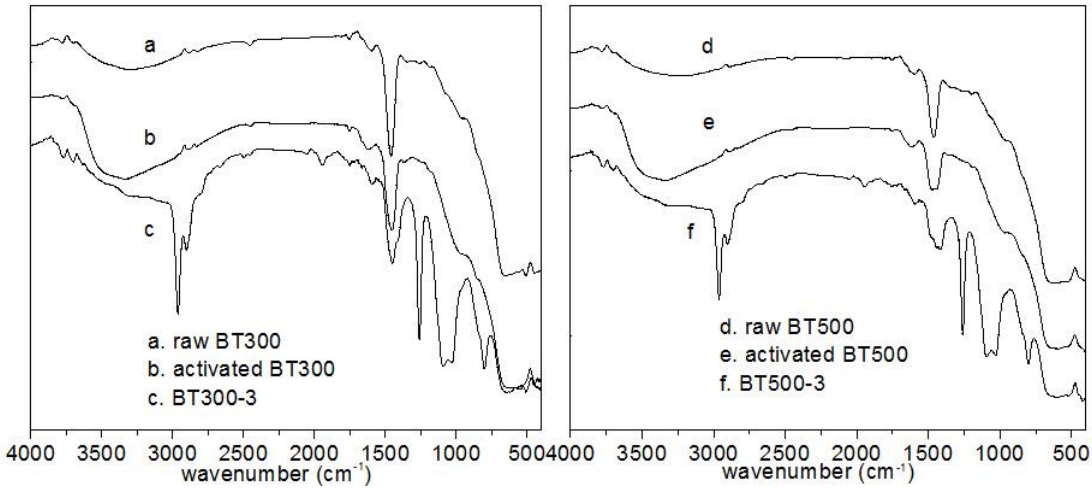

Fig.2.5 The FTIR spectra of raw/activated/modified of BT particles

Fig. 2.5 shows the FTIR spectra of raw/activated/modified of BT particles. Hydroxyl groups generated on the surface of BT particles after H_2O_2 activation can be detected by FTIR spectra. As shown in Fig. 2.5, absorption peak at around 525~550cm^{-1} can be found, representing for the vibration of Ti-O bond in BT [24]. For both the BT-300 and BT-500 particles, absorption bands at 3100~3700cm^{-1} (-OH) become larger after activation, which is the strong evidence that large amount of hydroxyl groups have generated on the surface [25]. It could also be found from the spectra that after surface modification, many strong and narrow peaks appeared. Peaks at about 2950cm^{-1}, 1000cm^{-1}~1150cm^{-1}, and 1260~1320cm^{-1} show the evidence of C-H bonds, Si-O bonds, and CH_3-Si bonds, respectively [4,5,23,26]. These peaks clearly confirm that the silicone coupling agent has been coated on the of BT surface.

2.4.2 Evaluation of the Dispersity of $BaTiO_3$ Particles With/Without Surface Modification

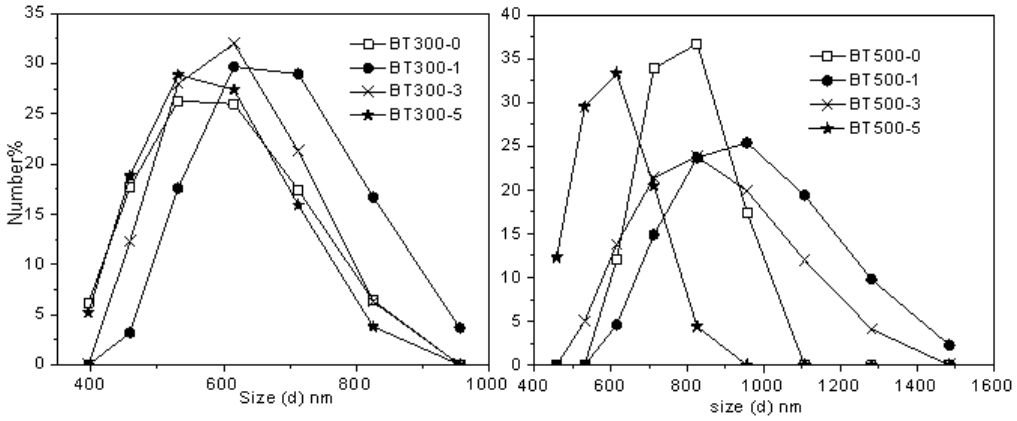

Fig.2.6 The particle size distribution of BT300 and BT500 particles in silicone oil

Table 2.5 Average sizes of BT particles

Particles	Average size (d, nm)	Particles	Average size (d, nm)
BT300-0	582.1	BT500-0	784.3
BT300-1	670.6	BT500-1	946.9
BT300-3	605.7	BT500-3	835.6
BT300-5	573.5	BT500-5	600.3

Fig. 2.6 shows the results of particle size distribution measurement. Dimethylsiloxane silicone oil KF-96-6CS, with no chemically reactive activity, was used to substitute the silicone matrix KE-103 because of their similar physical property. BT300 and BT500 particles were added into silicone oil and dispersed sufficiently by ultrasonic homogenizer for 10 min. Then the size distribution (particle diameter) of BT particles was measured by MALVERN nano series particle size measuring instrument, using a non-contact backward light scattering method. The calculated average BT particle sizes were listed in Table 2.5. The left side and right side of Fig. 2.6 show the size distribution of BT300 and BT500 particles, respectively. It can be found from the figure that the sizes

of raw or modified BT300 particles are ranging from about 570~670nm while the sizes of raw or modified BT500 particles are ranging from about 600~950nm. Compared to their average SEM particle sizes of 300nm and 500nm, non-contact backward light scattering sizes are bigger and distributed wider. It is considered that a BT particle in silicone oil dispersion is being affected by force originated from Brownian motion of silicone molecules and cohesive force between BT particles. These forces are competing continuously, forming an equilibrium status. The force originated from Brownian motion of silicone molecules tends to prevent the agglomeration of BT particles and separate the BT particles in an agglomeration apart from each other; cohesive force between BT particles tends to pull them into and maintain the shape of an agglomeration. Although the non-contact backward light scattering sizes are bigger and distributed wider, these sizes are not bigger than twice of the SEM sizes, confirming the existence of a strong Brownian motion caused well-dispersed status.

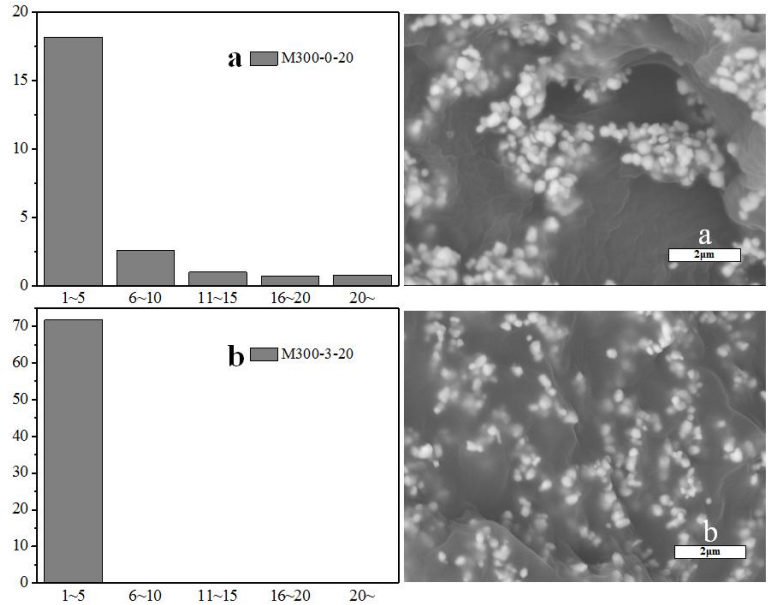

Fig.2.7 Dispersity statistics and SEM images of cross section of BT/silicone nanocomposites membrane

a. SEM of M300-0-20 b. SEM of M300-3-20

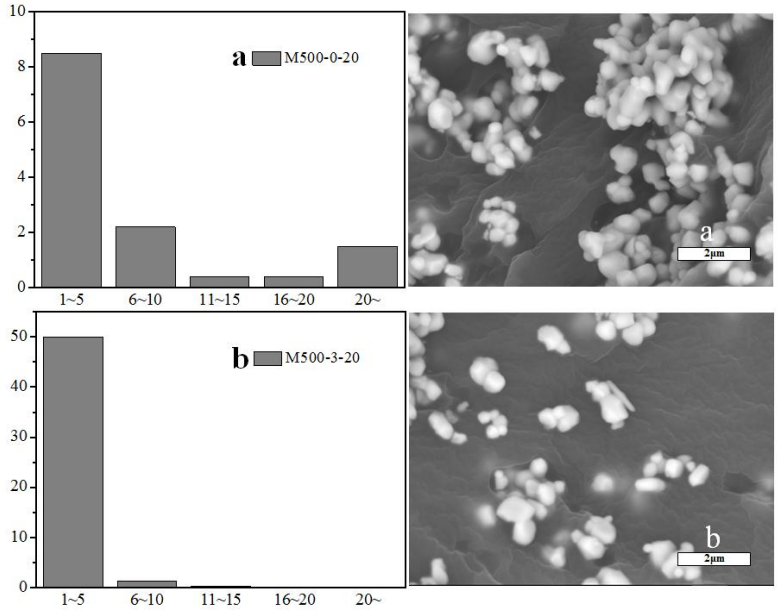

Fig.2.8 Dispersity statistics and SEM images of cross section of BT/silicone nanocomposites membrane

a. SEM of M500-0-20 b. SEM of M500-3-20

SEM images from cross sections along the horizontal direction of BT/silicone membranes, as well as the statistics for dispersions of BT particles in silicone elastomer based on SEM observations are showed in Fig. 2.7 and Fig. 2.8. BT/silicone membranes with volume fraction of 20% were used. Cross sections of samples were obtained by breaking them immediately after soaking in liquid nitrogen. Backscattered electron images were selected purposely to observe the dispersing situations in deeper places of the nanocomposites. Several SEM photos were taken for raw BT/silicone membrane (M300-0-20, M500-0-20) and BT/silicone membrane with BT modification ratios of 8.57% (M300-3-20, M500-3-20). For every membrane, the SEM image is shown in the right parts of the figures, the amount of BT particles and amount of their agglomerates in the visual field were counted. In each membrane, for per 100 single particles, the amounts of agglomerates with 1~5 particles, 6~10 particles, 11~15 particles, 16~20 particles and

more than 20 particles are shown in the left parts of the figures. Part a in the figures shows the situation of raw BT/silicone membrane while part b shows the situation of surface modified BT/silicone membrane. In the part a of the figures, agglomerates of large amounts of BT300/BT500 particles and some voids can be clearly observed. BT particles without surface modification are relatively hydrophilic while silicone elastomer is relatively hydrophobic, which could lead to the relatively weak compatibility and a large contact angle between them. Although fabricating of the samples was carried out at vacuum environment, due to the high viscosity of BT/silicone mixture and large contact angle between BT particles and silicone monomer, it is almost impossible to eliminating all the bubbles or making the silicone monomer penetrate into all the gaps between of BT particles, which would cause agglomerates/sediments in cured nanocomposites. Besides, statistics of dispersing situations in the left parts of the figures show that many agglomerates consist of more than 5 particles exist. Agglomerates consist of less than 5 particles are less, proving the low dispersity of the raw BT/silicone nanocomposites. From Part b of the figures, BT particles seem to have been dispersed much better than from the part a. Even there are still agglomerates in the substrates, their sizes are much smaller and distributed within a wider area. More BT particles are found to be single. Besides, statistics of dispersing situations in left b parts of the figures show that agglomerates consist of more than 5 particles rarely exist. In contrast, agglomerates consist of less than 5 particles become the major formations. Observation of SEM images proves that surface modification by silicone coupling agent can obviously improve their dispersity in the silicone elastomer.

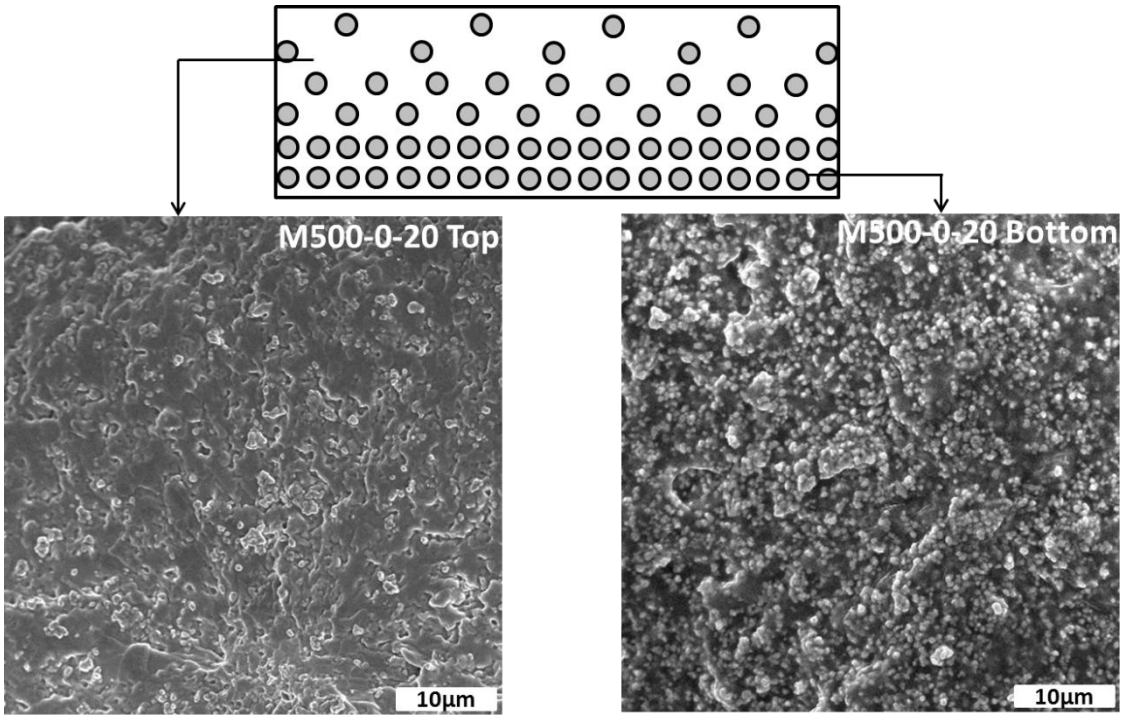

Fig.2.9 SEM images of the cross sections from the upper surface and inferior surface of M500-0-20

SEM images of cross sections along the vertical direction of the samples were also taken to illustrate influence of the gravity on the distribution status of BT particles within the silicone substrate. Each BT/silicone membrane has a thickness around 1mm, which is too huge compared to that of the BT particles sizes of about 300~500nm. Therefore it is impossible to exhibit the BT particle distribution status within one SEM photo. The SEM images of the cross sections in vertical direction from the upper surface and inferior surface of unmodified BT500/silicone with a volume fraction of 20% are shown in the left and right parts of Fig. 2.9, respectively. Obviously, the density of the BT500 particles from the upper surface could be found much lower than that from inferior surface, indicating that the sedimentation promotion by the gravity during the curing process.

2.4.3 Dielectric Properties of the $BaTiO_3$/Silicone Membranes

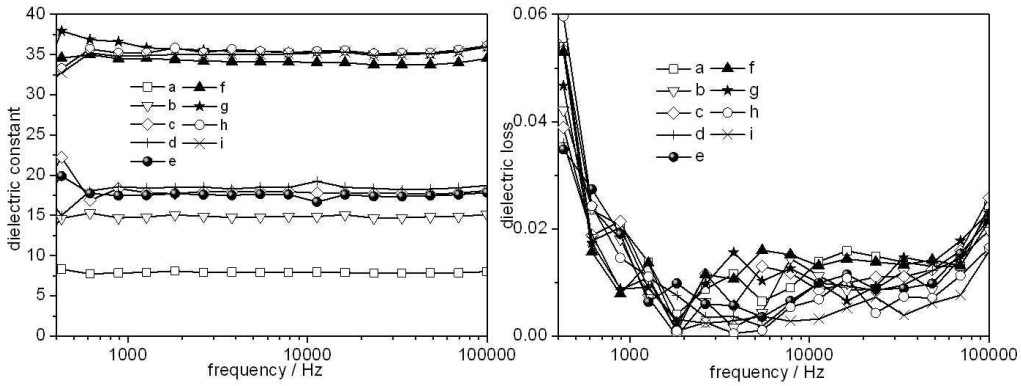

Fig.2. 10 Dielectric constant and dielectric loss (tanδ) of BT300/silicone membranes at different frequencies

a. Pure silicone b. M300-0-20 c. M300-1-20 d. M300-3-20 e. M300-5-20

f. M300-0-40 g. M300-1-40 h. M300-3-40 i. M300-5-40

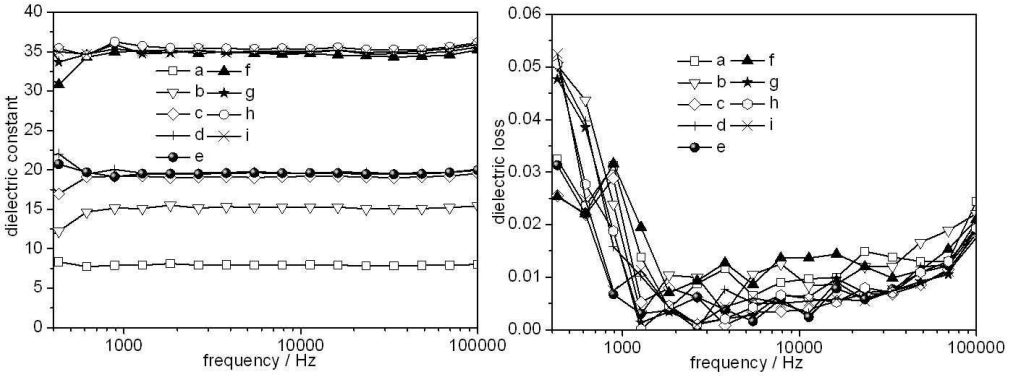

Fig.2. 11 Dielectric constant and dielectric loss (tanδ) of BT500/silicone membranes at different frequencies

a. Pure silicone b. M500-0-20 c. M500-1-20 d. M500-3-20 e. M500-5-20

f. M500-0-40 g. M500-1-40 h. M500-3-40 i. M500-5-40

Dielectric properties of BT/silicone membranes were measured by LCR meter.

Dielectric constants of BT/silicone nanocomposite membranes with different volume fractions at frequency from 400Hz to 100kHz are shown in Fig. 2.10 and Fig. 2.11. It can be known that for every membrane with a same volume fraction but different modification ratios, from low frequency to high frequency, there is no apparent variation observed from the dielectric constant-frequency curves, because the whole dielectric properties were measured at a low frequency area. Obviously, dielectric constant considerably improves as increasing of the volume fraction of BT particles. At frequency of 10 kHz, dielectric constant of pure silicone membrane is about 8, and that is about 35 for the raw BT-300/silicone membrane with volume fracture of 40%. It can also be found that the dielectric constant was raised up slightly after surface modification by silicone coupling agent. For example, at frequency of 10 kHz, for BT300/silicone membrane with volume fraction of 20%, the dielectric constant varies from 15, 18, 18.5 to 17.5, as modification mass ratio increasing from 0, 2.86%, 8.57% to 14.29%, respectively. An obvious dielectric constant enhancement could be found between the unmodified and modified BT300/silicone composites. It is considered that with this volume fraction, a lot of space left for the BT300 particles to agglomerate and sediment during the curing procedure, leaving an obvious layered membrane structure. The modified BT300 particles have much higher surface compatibility with the silicone mixture, so this sedimentation could be reduced obviously, leading to slightly higher dielectric constants. Comparatively, for BT-300/silicone membrane with volume fraction of 40%, dielectric constants are 34, 34, 35.5 to 35, for membranes with modification mass ratios of 0, 2.86%, 8.57% and 14.29%, respectively. No obvious difference of dielectric constants could be found from the unmodified and modified BT300/silicone composites. It is considered that with such a volume fraction as high as 40%, the space would be absolutely

occupied by the BT300 particles, thus there is no enough space for the particles to sediment. Therefore the influence from the gravity could be ignored. BT-500/silicone membranes show the similar variation and have almost the same dielectric values with the BT300/silicone membranes.

The right side of figures shows dielectric losses of BT/silicone membranes with different volume fractions at frequency from 400Hz to 100kHz. It can be found that the dielectric losses of all kinds of nanocomposites membranes have similar variation trends. For both BT300/silicone and BT500/silicone nanocomposites, at a frequency below 1000Hz, the dielectric losses are very unstable and have relative high values from about 0.03 to 0.06; when the frequency becoming higher, from about 1000Hz to 50kHz, the dielectric losses become stable and decrease to about 0~0.02; at a frequency higher than about 50kHz, the dielectric losses increase slightly to about 0.01~0.03. The origin of dielectric loss of nanocomposites may be due to the factors [3] as follows: (1) Direct current conduct (DC conduct); (2) Space charge migration (interfacial polarization contribution) and (3) Dipole loss caused by movement of molecular dipoles. The reason for the variation of dielectric loss is considered as that, at a low frequency, electrons are easy to accumulated at the two sides of the electrodes, so the space charge can maintain a high level, making the direct current be easier to occur, leading to a higher dielectric loss; if the frequency is improved to a rather high level near the frequency of vibration of dipoles, the dielectric loss caused by dipole loss can become higher. This can explain why the dielectric loss at middle frequency range has the lowest value and seems stable. It is also believed that the dielectric loss may decrease after surface modification by silicone coupling agent because if most of BT particles are coated by coupling agent layers with excellent insulation property, conductivity through BT particles could be significantly

reduced, while accumulation and migration of electric charge within the nanocomposites could also be restricted.

2.5 Conclusion

Silicone coupling agent was used to modify the surface of BT particles. The TG, FTIR results show that coupling agent was successfully coated on the surface of BT particles. BT/silicone nanocomposites membranes were fabricated using raw BT particles and BT particles modified by silicone coupling agent. The particle size distribution measurement and SEM observation show that BT particles can get higher compatibility with silicone. Their dispersity in silicone substrate was considerably improved after surface modification. Dielectric properties were evaluated by a LCR meter, the results show dielectric constant of nanocomposites membranes with a lower volume fraction was increased after the dispersion status of BT particles improved by surface modification using silicone coupling agent. Theoretical calculation from extreme cases proves that sedimentation of BT fillers in vertical direction can seriously reduce the dielectric constant of nanocomposites membranes and dielectric constant can be raised by improving the dispersion and preventing the sedimentation of BT particles. Although significantly lower than theoretic values, the dielectric properties of BT/Silicone nanocomposites show the expectation of being applied in mechanical sensors due to its simple structures and low costs.

References

[1] D. Hennings, G. Rosenstein, Temperature-Stable Dielectrics Based on Chemically Inhomogeneous $BaTiO_3$, J. Am. Ceram. Soc. 67 (1984) 249–254.

doi:10.1111/j.1151-2916.1984.tb18841.x.

[2] Wada, S., Hoshina, T., Yasuno, H., Nam, S. M., Kakemoto, H., & Tsurumi, T. (2003). Preparation of nm-sized BaTiO3 crystallites by the 2-step thermal decomposition of barium titanyl oxalate and their dielectric properties. In Key Engineering Materials (Vol. 248, pp. 19-22). Trans Tech Publications.

[3] Wada, S., Yasuno, H., Hoshina, T., Nam, S. M., Kakemoto, H., & Tsurumi, T. (2003). Preparation of nm-sized barium titanate fine particles and their powder dielectric properties. Japanese journal of applied physics, 42(9S), 6188.

[4] K. Yang, X. Huang, Y. Huang, Fluoro-polymer@ BaTiO3 Hybrid Nanoparticles prepared via RAFT polymerization: Toward Ferroelectric Polymer Nanocomposites with High Dielectric Constant and, Chem. 25 (2013) 2327–2338.

[5] L. Xie, X. Huang, Y. Huang, K. Yang, P. Jiang, Core@Double-Shell Structured $BaTiO_3$–Polymer Nanocomposites with High Dielectric Constant and Low Dielectric Loss for Energy Storage Application, J. Phys. Chem. C. 117 (2013) 22525–22537. doi:10.1021/jp407340n.

[6] Y. Liu, L. Liu, Z. Zhang, J. Leng, Dielectric elastomer film actuators: characterization, experiment and analysis, Smart Mater. Struct. 18 (2009) 095024. doi:10.1088/0964-1726/18/9/095024.

[7] F. Carpi, D.D. Rossi, Improvement of electromechanical actuating performances of a silicone dielectric elastomer by dispersion of titanium dioxide powder, Dielectr. Electr. Insul. IEEE Trans. 12 (2005) 835–843. doi:10.1109/TDEI.2005.1511110.

[8] F. Carpi, G. Gallone, F. Galantini, D. De Rossi, Silicone–Poly(hexylthiophene) Blends as Elastomers with Enhanced Electromechanical Transduction Properties, Adv. Funct. Mater. 18 (2008) 235–241. doi:10.1002/adfm.200700757.

[9] B. Kussmaul, S. Risse, G. Kofod, R. Waché, M. Wegener, D.N. McCarthy, et al., Enhancement Of Dielectric Permittivity And Electromechanical Response In Silicone Elastomers: Molecular Grafting Of Organic Dipoles To The Macromolecular Network, Adv. Funct. Mater. 21 (2011) 4589–4594. doi:10.1002/adfm.201100884.

[10] A. O'Halloran, F. O'Malley, P. McHugh, A review on dielectric elastomer actuators, technology, applications, and challenges, J. Appl. Phys. 104 (2008) 1–10. doi:10.1063/1.2981642.

[11] P. Brochu, Q. Pei, Advances in Dielectric Elastomers for Actuators and Artificial Muscles, Macromol. Rapid Commun. 31 (2010) 10–36. doi:10.1002/marc.200900425.

[12] Jung, K., Kim, K. J., & Choi, H. R. (2008). A self-sensing dielectric elastomer actuator. Sensors and Actuators A: Physical, 143(2), 343-351.

[13] Kornbluh, R. D., Pelrine, R., Pei, Q., Heydt, R., Stanford, S., Oh, S., & Eckerle, J. (2002, July). Electroelastomers: applications of dielectric elastomer transducers for actuation, generation, and smart structures. In SPIE's 9th Annual International Symposium on Smart Structures and Materials (pp. 254-270). International Society for Optics and Photonics.

[14] Mannsfeld, S. C., Tee, B. C., Stoltenberg, R. M., Chen, C. V. H., Barman, S., Muir, B. V., & Bao, Z. (2010). Highly sensitive flexible pressure sensors with microstructured rubber dielectric layers. Nature materials, 9(10), 859-864.

[15] O'Brien, B., Thode, J., Anderson, I., Calius, E., Haemmerle, E., & Xie, S. (2007, April). Integrated extension sensor based on resistance and voltage measurement for a dielectric elastomer. In The 14th International Symposium on: Smart Structures and Materials & Nondestructive Evaluation and Health Monitoring (pp. 652415-652415). International Society for Optics and Photonics.

[16] Goulbourne, N. C., Son, S., & Fox, J. W. (2007, April). Self-sensing McKibben actuators using dielectric elastomer sensors. In The 14th International Symposium on: Smart Structures and Materials & Nondestructive Evaluation and Health Monitoring (pp. 652414-652414). International Society for Optics and Photonics.

[17] Rosenthal, M., Bonwit, N., Duncheon, C., & Heim, J. (2007, April). Applications of dielectric elastomer EPAM sensors. In The 14th International Symposium on: Smart Structures and Materials & Nondestructive Evaluation and Health Monitoring (pp. 65241F-65241F). International Society for Optics and Photonics.

[18] R. Sengupta, S. Chakraborty, S. Bandyopadhyay, S. Dasgupta, R. Mukhopadhyay, K. Auddy, et al., A Short Review on Rubber / Clay Nanocomposites With Emphasis on Mechanical Properties, Engineering. 47 (2007) 21–25. doi:10.1002/pen.

[19] Shu-Hui Xie, Bao-Ku Zhu, Xiu-Zhen Wei, Zhi-Kang Xu, You-Yi Xu, Polyimide/$BaTiO_3$ composites with controllable dielectric properties, Composites Part A: Applied Science and Manufacturing. 36 (2005) 1152-1157.

[20] Dang, Zhi-Min, Wang Hai-Yan, Xu Hai-Ping, Influence of silane coupling agent on morphology and dielectric property in $BaTiO_3$, polyvinylidene fluoride composites. Applied Physics Letters. 89 (2006) 112902.

[21] Zhi-min Dang, Yan-Fei Yu, Hai-Ping Xu, Jinbo Bai, Study on microstructure and dielectric property of the $BaTiO_3$/epoxy resin composites, Composites Science and Technology. 68 (2008) 171-177.

[22] L. Ramajo, M.S. Castro, M.M. Reboredo, Effect of silane as coupling agent on the dielectric properties of $BaTiO_3$-epoxy composites, Composites Part A: Applied Science and Manufacturing. 38 (2007) 1852-1859.

[23] S.J. Chang, W.S. Liao, C.J. Ciou, J.T. Lee, C.C. Li, An efficient approach to derive

hydroxyl groups on the surface of barium titanate nanoparticles to improve its chemical modification ability, J. Colloid Interface Sci. 329 (2009) 300–305. doi:10.1016/j.jcis.2008.10.011.

[24] X. Jin, D. Sun, M. Zhang, Y. Zhu, J. Qian, Investigation on FTIR spectra of barium calcium titanate ceramics, J. Electroceramics. 22 (2009) 285–290. doi:10.1007/s10832-007-9402-1.

[25] T. Kondo, The assignment of IR absorption bands due to free hydroxyl groups in cellulose, Cellulose. 4 (1997) 281–292. doi:10.1023/A:1018448109214.

[26] Y. Hasegawa, K. Okamura, Synthesis of continuous silicon carbide fibre - Part 4 The structure of polycarbosilane as the precursor, J. Mater. Sci. 21 (1986) 321–328. doi:10.1007/BF01144739.

Chapter3 Capacitive Features of $BaTiO_3$/Silicone Elastomeric Nanocomposites for Mechanical Sensing

3.1 Introduction

For a dielectric ceramic material with a pre-poling treatment, an obvious potential difference will be generated under a uniaxial pressure due to its piezoelectric behavior [1-6]. Many types of tactile sensors have been developed and applied based on the piezoelectricity. However, just as many traditional mechanical sensors, these are relatively expensive, limited by their fixed shapes, and sometimes even too fragile. Application of dielectrics/polymer nanocomposites for mechanical sensing is a crucial solution to this problem. Unlike the piezoelectric material, it is the variation of capacitance of the dielectrics/polymer nanocomposites but not the generated potential difference that can be utilized as a mechanical sensor [7-13]. Obviously, to enhance the variation of capacitance, a dielectric/polymer nanocomposite with a higher dielectric constant and a lower elastic modulus is preferable.

3.2 Theory Analysis of Capacitive Features of the $BaTiO_3$/Silicone Elastomeric Nanocomposites

Silicone elastomer has a Poisson's ratio of about ν=0.48 [14]. For the BT/silicone membrane, if set strain in thickness direction as -s, strain in horizontal direction will become νs. So area for cross section will become $(1+\nu s)^2$ times, volume will becomes $(1-s)(1+0.48s)^2$ times as before. At the same time, set original thickness as d, original area as A. After loading a pressure on the membrane, its thickness will shrink to d' and area will stretch to A'.

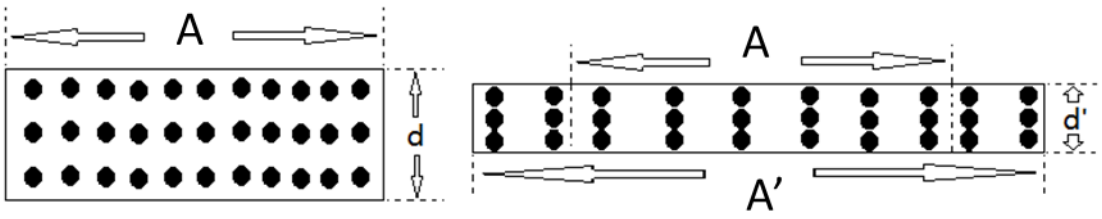

Fig. 3.1 Image of the thickness variation of BT/silicone membrane

As it shows in Fig. 3.1, for the effective area sandwiched by electrodes, volume before pressing is V=Ad and becomes to V'=A'd' after pressing, while the effective volume becomes to Ad'. Here d'=(1-s)d, A'=$(1+\nu s)^2$A=$(1+0.48s)^2$A, V'=(1-s)$(1+0.48s)^2$V. BT particles dispersed in silicone are always moving with the deforming of silicone substrates. Here set the number of BT particles in the original effective area as n and set the average volume of one single particle as V_0, the volume fraction at original state will be nV_0/Ad. After deformation, number of BT particles in the effective area will be nA/A'. Movements of BT particles caused by compression of membrane are considered uniform, therefore the volume fraction of BT particles in the effective area can be calculated by $\frac{nV_0A/A'}{Ad'} = \frac{nV_0}{A'd'}$. Thus volume fraction after deformation is Ad/A'd'=V/V'=1/[(1-s)$(1+0.48s)^2$] times of the volume fraction before deformation. For example, when the membrane is pressed to half of its thickness, namely, when the strain s is 0.5, the volume fraction will become about 1.3 times of the original state. Variations of the dielectric constants of BT/silicone membranes can be calculated here. According to the Eq. (2-5), variations of the dielectric constants is $\left({}^{\varepsilon_2}/_{\varepsilon_1}\right) = \frac{\varepsilon_e^{(1-1.3x)}\varepsilon_f^{1.3x}}{\varepsilon_e^{(1-x)}\varepsilon_f^{x}} = \left(\frac{\varepsilon_f}{\varepsilon_e}\right)^{0.3x}$. Therefore for the BT/silicone membrane with a volume fraction of 40%, the dielectric constant will become 1.94 times of before after pressing the membrane to half of its

thickness.

For the measured circuit, capacitance C can be calculated by equation $C = \frac{\varepsilon_0 \varepsilon_r A}{d - vt}$ and the instantaneous current i can be calculated by Eq. (3-1) in the compression stage;

$$i = \frac{dQ}{dt} = \frac{d(CU)}{dt} = U\frac{dC}{dt} = \varepsilon_0 AU\frac{d(\frac{\varepsilon_r}{d-vt})}{dt} = (\frac{\varepsilon_0 AU}{d-vt})\frac{d\varepsilon_r}{dt} + \frac{\varepsilon_0 \varepsilon_r vAU}{(d-vt)^2} \quad (3\text{-}1)$$

the capacitance C can be calculated by equation $C = \frac{\varepsilon_0 \varepsilon_r A}{0.5d + vt}$ and the instantaneous current i can be calculated by Eq. (3-2) in the returning stage.

$$i = \frac{dQ}{dt} = \frac{d(CU)}{dt} = U\frac{dC}{dt} = \varepsilon_0 AU\frac{d\left(\frac{\varepsilon_r}{0.5d+vt}\right)}{dt} = \left(\frac{\varepsilon_0 AU}{0.5d+vt}\right)\frac{d\varepsilon_r}{dt} - \frac{\varepsilon_0 \varepsilon_r vAU}{(0.5d+vt)^2} \quad (3\text{-}2)$$

Here take the BT/silicone membrane mentioned in Chapter 2 (M300-3-40 and M500-3-40) as samples. If the applied voltage U is 5V, the electrodes area is 1cm^2, for the M300-3-40, the thickness d is 3.01mm, its dielectric constant ε_r is 35, the theoretically calculated average current will range from 0 to 1.519 nano Ampere; for M500-3-40, the thickness d is 2.21mm, its dielectric constant ε_r is 35, the theoretically calculated average current will range from 0 to 2.818 nano Ampere. These calculated results show the similar scales with experimental data.

3.3 Experimental Section

3.3.1 Materials

In the experiment, BT300/silicone membrane (M300-3-40) with a thickness of 3.01mm and BT500/silicone membrane (M500-3-40) with a thickness of 2.21mm were used.

3.3.2 Capacitance Measurement

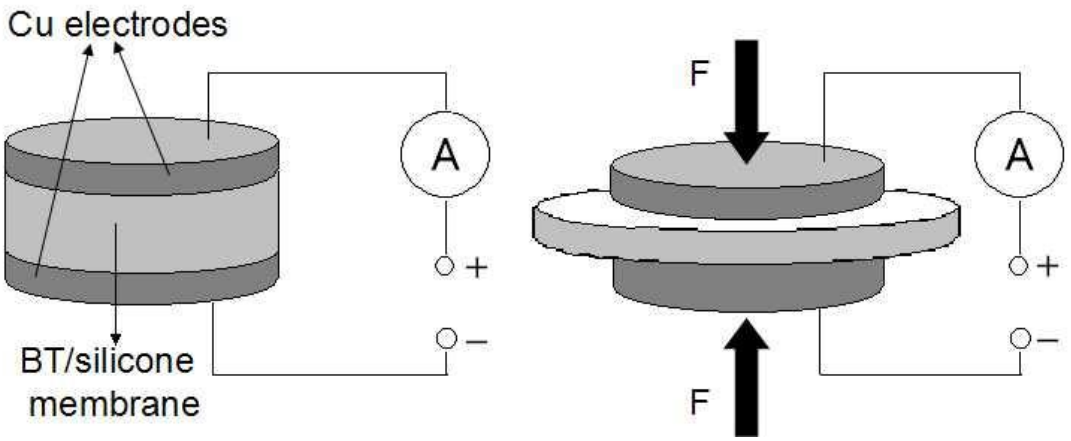

Fig. 3.2 A measuring system for BT/silicone membranes

As shows in Fig. 3.2, measuring system including a pair of copper electrodes and a BT/silicone membrane sandwiched between the electrodes pairs, acting as a simple parallel plate capacitor. In order to prevent the complex calculation caused by a varying surface area, conductive paint was not used. A constant voltage of 5V was loaded by a DC power, which is in the safety range and can be easily obtained. The membrane with electrodes was set on a metal plate, a periodically stress was loaded on the membrane by a metal cylinder. A Multimeter was mounted into the circuit to test the instantaneous current, while a LCR meter was also mounted to measure the varying capacitance of the capacitor. During the measurement, the cylinder fell down with a constant speed of 1000 mm/min, compressing the membrane until its thickness becoming the half; then the cylinder rose up immediately with the same speed until returning to the original position. This procedure was repeated periodically. It is noteworthy that because the BT particles are randomly distributed within the silicone elastomeric substrate and would not be compressed by the applied pressure directly, there will be no intrinsic charge generated between the surfaces of the membrane. The electrodes in the system need to be charged

by an external power supply with a constant voltage. It is the changing capacitance originated from the applied pressure that leads to a charge-discharge recycle, as well as an instantaneous current which could be detected by the Multimeter. Furthermore, in order to prevent a short circuit and simplify the calculation, the area of the membrane was made always bigger than that of the electrodes.

3.4 Results and Discussion

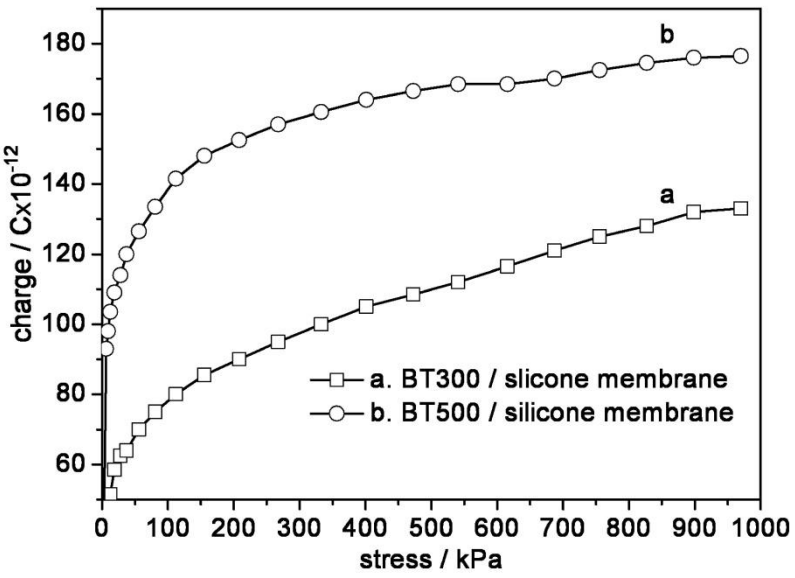

Fig. 3.3 Charge vs. Stress for BT/silicone membranes

Fig. 3.3 shows the charge vs. stress of the measuring system containing these membranes. Variation of charge was considered to be originated from the capacitance change caused by the changing thickness of the membrane, which acts as the dielectrics in capacitor. The varying capacitance was measured by the LCR meter during the compressing and returning procedures, the charged were obtained by multiplying the

capacitances by the applied voltage of 5V. It can be found that charges of the capacitor made by BT/membrane were raised during compressing procedure and reduced during stretching procedure. Due to the small thickness of membrane, compressive elasticity increased quickly as the increasing of compressive stress, making the variation of thickness be nonlinear, that is, the charge grows quickly at first and soon loses its growing speed. It can be found that BT500/silicone membrane has a better performance.

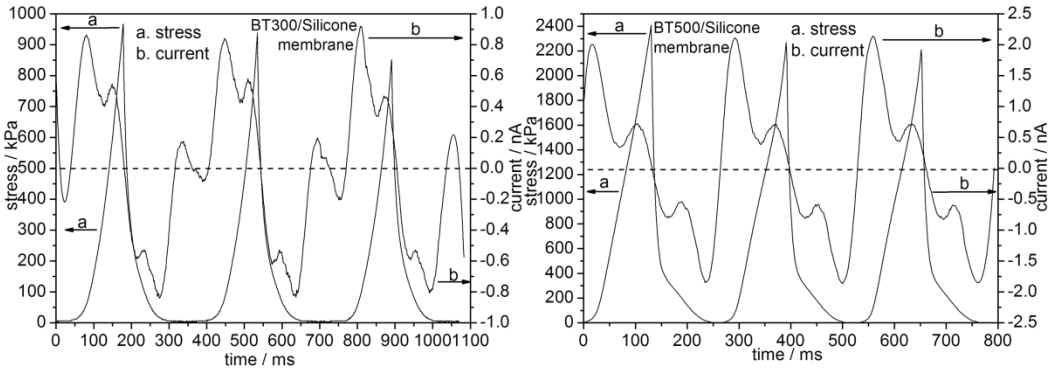

Fig. 3.4 Periodic variation of stress and current of measuring system containing BT/silicone membranes

Fig. 3.4 shows the periodic variation of current occurs in measuring system, about 3 cycles was shown. The oscillation periods of current generated by the periodically transforming stresses are about 250 ms and 350 ms for the measuring system containing BT300/silicone membrane and BT500/silicone membrane, respectively. For the system containing BT300/silicone membrane, stress increases from 0 to about 900 kPa and returns to 0 with a sharp peak. It can be found that from cycle 1 to cycle 3, the max stress becomes smaller, which is considered be related to the stress relaxation of silicone elastomer. At first half period, current increases from 0 to about 0.9 nano Ampere

immediately and soon decreases to 0; at the next half period, the current changes to the opposite direction, then, like the first half period, increases from 0 to about 0.8 nano Ampere immediately and soon decreases to 0. The variation of current within a half period does not show a linear trend, a curve with 2 obvious peaks was exhibited. The reason of which is considered as a non-linear changing of capacitance with 3 stages for each half period. For example, for the first half period of compression, the BT concentration was enhanced rapidly in the first stage, leading to a rapidly growing capacitance; this enhancement could be reduced obviously by the Poisson's deformation and resulted in a slowly growing capacitance during the second stage; in the third stage, the membrane was compressed to a very low thickness, leading to a rapidly growing capacitance again with a constant compressing speed. The rapidly changes of capacitance in the first and third stage resulted in 2 peaks of current from each half period. A similar variation trend of current was shown in measuring system with the BT500/silicone membrane, but the values of max stress and max current become about twice as large as the BT300/silicone membrane. The better performance of current/stress properties for BT500/silicone membrane should be because of the smaller thickness of the BT500/silicone membrane and the differences of dielectric constant and elastic modulus between the BT300/silicone membrane and the BT500/silicone membrane. This measuring system is expected to have some applications in mechanical sensors, benefitied from its rapid response of instantaneous electric signals and simple structures.

3.5 Conclusion

A mechanical sensing system consisting of the silicone coupling agent modified BT/silicone elastomeric membranes (prepared in Chapter2) was assembled, connecting

with a LCR meter and a Multimeter. Continuously increasing stresses and periodic varying stress (vibrations) were applied to the membranes, respectively. The changing capacities (equivalent to the generated currents) were evaluated by the LCR meter, while the generated instantaneous current was measured by the Multimeter. Clear and sensitive signals were obtained from both of the measurements even without a poling process during the fabrication or measurement. This type of materials is expected to have the applications in mechanical sensors due to its rapid response of instantaneous electric signals, simple structures and low costs. Theoretic calculation shows the similar results. It is believed that the gaps between real values and theoretic values were caused by ignorance of the changing time of pressing direction, the variation for Young's modulus, effect of BT particles on the Poisson's ratio of silicone elastomer and resistance of measuring system.

References

[1] Su, J., Harrison, J. S., Clair, T. S., Bar-Cohen, Y., & Leary, S. (1999). Electrostrictive Grafr Elastomers and Applications. In MRS Proceedings (Vol. 600, p. 131). Cambridge University Press.

[2] Khastgir, D., & Adachi, K. (1999). Piezoelectric and dielectric properties of siloxane elastomers filled with bariumtitanate. Journal of Polymer Science Part B: Polymer Physics, 37(21), 3065-3070.

[3] Brochu, P., & Pei, Q. (2010). Advances in dielectric elastomers for actuators and artificial muscles. Macromolecular rapid communications, 31(1), 10-36.

[4] Silva, M. P., Costa, C. M., Sencadas, V., Paleo, A. J., & Lanceros-Méndez, S. (2011). Degradation of the dielectric and piezoelectric response of β-poly (vinylidene fluoride)

after temperature annealing. Journal of Polymer Research, 18(6), 1451-1457.

[5] Galantini, F., Gallone, G., & Carpi, F. (2012). Effects of Corona treatment on electrical and mechanical properties of a porous dielectric elastomer. IEEE Transactions on Dielectrics and Electrical Insulation, 19(4).

[6] Vu-Cong, T., Jean-Mistral, C., & Sylvestre, A. (2013). Electrets substituting external bias voltage in dielectric elastomer generators: application to human motion. Smart materials and structures, 22(2), 025012.

[7] Keplinger, C., Kaltenbrunner, M., Arnold, N., & Bauer, S. (2008). Capacitive extensometry for transient strain analysis of dielectric elastomer actuators. Applied Physics Letters, 92(19), 192903.

[8] Koh, S. J. A., Keplinger, C., Li, T., Bauer, S., & Suo, Z. (2011). Dielectric elastomer generators: How much energy can be converted?. IEEE/ASME Transactions on mechatronics, 16(1), 33-41.

[9] McKay, T., O'Brien, B., Calius, E., & Anderson, I. (2010). Self-priming dielectric elastomer generators. Smart Materials and Structures, 19(5), 055025.

[10] Chiba, S., Waki, M., Wada, T., Hirakawa, Y., Masuda, K., & Ikoma, T. (2013). Consistent ocean wave energy harvesting using electroactive polymer (dielectric elastomer) artificial muscle generators. Applied Energy, 104, 497-502.

[11] Laflamme, S., Kollosche, M., Connor, J. J., & Kofod, G. (2012). Soft capacitive sensor for structural health monitoring of large‐scale systems. Structural Control and Health Monitoring, 19(1), 70-81.

[12] Hu, W., Niu, X., Zhao, R., & Pei, Q. (2013). Elastomeric transparent capacitive sensors based on an interpenetrating composite of silver nanowires and polyurethane. Applied Physics Letters, 102(8), 38.

[13] Gisby, T. A., Calius, E. P., Xie, S., & Anderson, I. A. (2008, March). An adaptive control method for dielectric elastomer devices. In The 15th International Symposium on: Smart Structures and Materials & Nondestructive Evaluation and Health Monitoring (pp. 69271C-69271C). International Society for Optics and Photonics.

[14] N. Bowden, S. Brittain, A. Evans, Spontaneous formation of ordered structures in thin films of metals supported on an elastomeric polymer, Nature. 393 (1998) 146–149. doi:10.1038/30193.

Chapter4 A Brief Introduction to Several Piezoresistive Models for Conductive Elastomeric Nanocomposites

4.1 Introduction

Various theoretical electrically conductive models and piezoresistive models have been developed in many previous works [1-3]. In M. Taya' work, an analytical modeling was developed to study the piezoresistive behavior of a conductive short fiber reinforced elastomer composite, the reorientation distributions of the conductive short fibers due to stretching strain were computed by using a fiber reorientation model. It was found that the threshold fiber volume fraction increases as the applied strain increases [4]. An analytical model of the effective electrical conductivity of carbon nanotube composites was developed by Fei Deng et al., which takes account of not only the CNT concentration and percolation, but also CNT conductivity anisotropy, aspect ratio and non-straightness [5].

4.2 A Piezoresistive Model Based on the Percolation Threshold of Conductive Elastomeric Nanocomposites

Conductivity of the conductor-insulator nanocomposites is usually described by a percolation model:

$$\sigma_c = \sigma_f (f - f^*)^t \quad (4\text{-}1)$$

Here $f > f^*$, σ_f is the conductivity of the fillers, f is the volume fraction of the fillers, f^* is the percolating threshold, above which a percolation network is just established through the nanocomposites, t is the critical conductivity exponent [6-9]. At a volume fraction close to the percolating threshold, a small change in the volume fraction will lead to a large change in the conductivity.

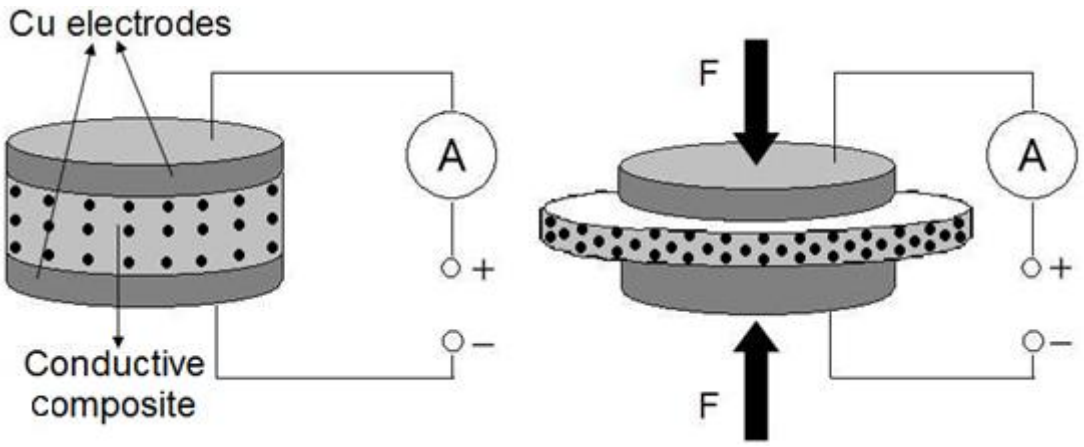

Fig. 4.1 A schematic description of the piezoresistivity calculation according to the percolation model

As it shows in the Fig. 4.1, imagine that a cylinder-shape conductive nanocomposite homogeneously filled with sphere-like conductive fillers is sandwiched by a pair of copper electrodes. The electrodes and the cylinder-shape conductive nanocomposite have the same area of A. Suppose that the elastic modulus of the nanocomposite is a constant value of E. Poisson's ratio of the nanocomposite is υ. If load a uniaxial force of F on the nanocomposite, it will be compressed along the vertical direction and extend along the horizontal direction. The vertical strain is set as *s*. It is considered that the temporary content of the fillers will change with the variation of the volume due to the horizontal and vertical deformation under the uniaxial force. The temporary volume fraction will change from f_0 to

$$f_1 = f_0/(1-\varepsilon)(1+\upsilon\varepsilon)^2 \quad (4\text{-}2)$$

If the conductivity before and under the external uniaxial force is σ_{c0} and σ_{c1}, respectively, the changing rate of the conductivity will be

$$\frac{\sigma_{c1}}{\sigma_{c0}} = \left[\frac{\frac{f_0}{(1-\varepsilon)(1+\upsilon\varepsilon)^2} - f^*}{f_0 - f^*}\right]^t \quad (4\text{-}3)$$

Compared to the resistance R_0 before compressing, the resistance under pressure will become to

$$R_1 = R_0\left[\frac{f_0 - f^*(1-\varepsilon)(1+\upsilon\varepsilon)^2}{(f_0 - f^*)(1-\varepsilon)(1+\upsilon\varepsilon)^2}\right]^{-t} \quad (4\text{-}4)$$

This function can only be used for the calculation of the resistance variation in a conductive nanocomposite with a volume fraction near its percolation threshold. A much more widely used resistive model is desirable.

4.3 A Piezoresistive Model Based on the Tunnel Conductive Theory for Elastomeric Nanocomposites with Spherical Conductive Particles

In the works of Xiang-wu Zhang [10,11], the total resistance in conductive nanocomposites is considered to be a function of both the resistance through each conducting particle and the polymer matrix. The resistivity of the matrix is assumed to be constant everywhere, the resistance of the conductive paths perpendicular to the current flow was neglected. Then the number of the conductive particles between electrodes, the number of the conducting paths and the average distance between the adjacent particles become the main factors, the resistance for the conductive nanocomposites can be described as

$$R = \frac{M}{N}\left[\frac{8\pi hs}{3A\gamma e^2}\exp(\gamma s)\right] \quad (4\text{-}5)$$

where

$$\gamma = \frac{4\pi}{h}\sqrt{2m\varphi} \quad (4\text{-}6)$$

s is the average minimum distance between two adjacent conductive particles, *A* is the

effective cross-sectional area of one electrically conducting path, h is Plank' constant, e and m are the electron charge and electron mass, φ is the tunneling potential barrier height, N is the number of conducting paths in the nanocomposite and M is the number of conductive particles forming one conducting path. If the initial average minimum distance between two adjacent conductive particles and the initial resistance is assumed as s_0 and R_0, respectively, the relative resistance of the conductive nanocomposites when a stress is applied can be described as

$$\frac{R}{R_0} = \frac{s}{s_0}\exp[\gamma(s - s_0)] \quad (4\text{-}7)$$

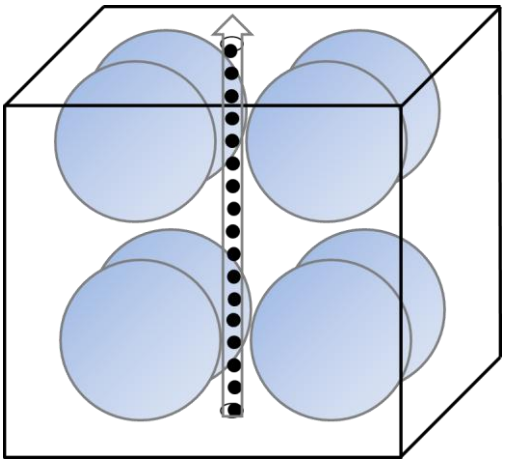

Fig. 4.2 An image of an electrically conductive path in a cubic space of the conductive foamed nanocomposite

Considering the situation of the conductive foamed nanocomposite, the compression would become much more complex because of the influence of the porous structure on the elastic modulus. In this thesis, a cubic space in the conductive foam with a length of L was illustrated in the Fig. 4.2. Both voids and conductive particles were assumed as spherical shapes and to be distributed in the polymer matrix with absolute homogeneities.

The voltage was loaded to the nanocomposite, making the current flow through the vertical direction. The current was thought homogeneously distributed in the space without being blocked by the voids through the vertical direction. One of the conducting paths was shown in the Fig. 4.2, which was thought to keep being perpendicular to the horizontal plane. If a uniaxial pressure is loaded on the conductive foam through the vertical direction, the cubic space will be compressed, the average distance between the conductive particles will be shortened and the resistance of the conductive foam through the vertical direction will be reduced. However, the influence of the voids on the compressing procedure is extremely complex, making it difficult to calculate the piezoresistive property of the conductive foam.

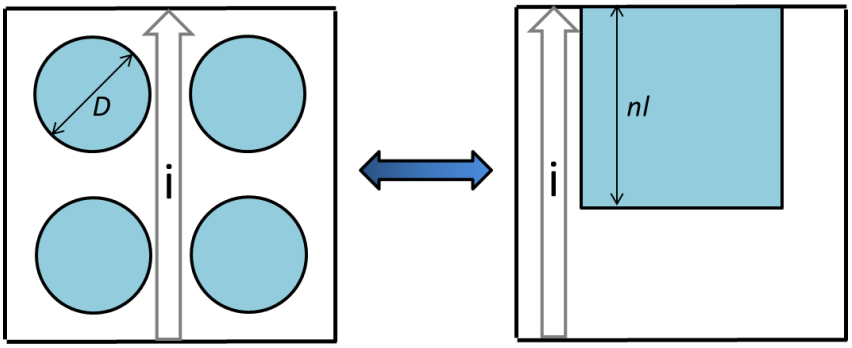

Fig. 4.3 The flow chart of simplification of the piezoresistance analysis of a cubic space in the conductive foamed nanocomposite

In order to simplify the calculation procedures, several assumptions were made for the voids: the spherical voids with an average diameter *D* were treated as cubic shapes with an average length of *l* and could maintain a constant average volume. As shown in the Fig. 4.3, the vertical plane from the Fig. 4.3 was illustrated. One electrically conductive path through the vertical direction was shown in the Fig. 4.3. Therefore

$$\frac{\pi}{6}D^3 = l^3 \quad (4\text{-}8)$$

$$l = \left(\frac{\pi}{6}\right)^{1/3} D \quad (4\text{-}9)$$

the effect of the pressure of confined gas in the voids and the atmospheric pressure on the compressing procedure was neglected; the number of conductive particles within one conductive path in the cubic space was expressed as *n*. These cubic-like voids in this cubic space were assumed to be combined together as a big cubic-like void, which has a length of *nl*. This big void was thought to be able to move freely within the cubic space without affecting the calculation of the piezoresistive property due to its cubic shape. Assume that it was moved to the top of the cubic space, dividing the space into a "hollow" part at the top and a "solid" part inferior. The length of the big cubic-like void is

$$nl = \sqrt[3]{\frac{(1-\rho_r)L^3}{l^3}} \cdot l = (1-\rho_r)^{\frac{1}{3}} \cdot L = kL \quad (4\text{-}10)$$

Thus the ratio of the length of the big cubic void versus the length of the entire cubic space can be calculated as

$$k = \frac{nl}{L} = (1-\rho_r)^{1/3} \quad (4\text{-}11)$$

Here ρ_r is the relative density of the conductive foam (the density of the conductive foam divided by the density of the unfoamed conductive nanocomposites with the same volume fraction of conductive particles). *l* is the length of a single void before combination, L is the length of the big void after combination, respectively.

When an external force was loaded on the cubic space though the vertical direction, the compressive strain of the upper "hollow" part s_h and the compressive strain of the inferior "solid" part s_s were different because of the different force areas. Considering this difference and neglecting the compression of the conductive particles, the average inter-particle distance *s* in the conductive foam can be calculated as

$$s = s_0[1 - \varepsilon_h - \varepsilon_s] = s_0\left[1 - \left(1 - k + \frac{k}{1-k^2}\right)\frac{\sigma}{E}\right] \quad (4\text{-}12)$$

In which σ is the applied uniaxial stress, E is the elastic modulus of the unfoamed conductive nanocomposites with the same volume fraction of conductive particles. The average inter-particle distance can be calculated as

$$s_0 = d\left[\left(\frac{\pi}{6}\right)^{1/3}\left(\frac{f}{\rho_r}\right)^{-1/3} - 1\right] \quad (4\text{-}13)$$

In which d is the average particle diameter, f is the volume fraction of the conductive particle in the conductive foam, f/ρ_r is thought as the "real" volume fraction in the polymer matrix. Then substitute the Eq. (4-12) and Eq. (4-13) into the Eq. (4-7), the relative resistance of the conductive foam when a stress is applied can be calculated as

$$\frac{R}{R_0} = \left[1 - \left(1 - k + \frac{k}{1-k^2}\right)\frac{\sigma}{E}\right]\exp\left[-\frac{\sigma\gamma s_0}{E}\left(1 - k + \frac{k}{1-k^2}\right)\right] \quad (4\text{-}14)$$

The piezoresistive property can be simply estimated with the Eq. (4-14). This piezoresistive model can be used to predict the effect of the porosity of the conductive foam on its piezoresistance effectively. However there are some drawbacks in this model which would reduce the accuracy of the prediction: Pores in the conductive foam were considered as cubic shapes, which have a different compression mode with the spherical one. Furthermore, the average pore diameter was neglected due to the combination of the pores; the competition between the pressures of the gas confined in the pores and the atmospheric pressure was neglected, which in fact brings some effect on the compressing procedures; the electrically conductive particles were assumed to be spherical. In fact, many fiber-like or sheet-like conductive particles were found to have lower percolation thresholds and be much more effective in conductivity enhancing compared to the spherical particles.

4.4 A Piezoresistive Model Based on the Tunnel Conductive Theory for Elastomeric Nanocomposites with Fiber-like Conductive Particles

In the study, piezoresistive models for fiber-like conductive fillers/polymeric solid nanocomposites and for fiber-like fillers/polymeric foam were both developed. Those models were designed to reflect the effects of both the displacement and orientation of the fiber-like fillers precisely, although leading to some extremely complex calculation and thereby reduce the practicability. The Eq. (4-14) accompanied with Eq. (4-11) and Eq. (4-13) was used to calculate the piezoresistive variations of the MWCNT/silicone conductive foams and the results were used to compare to the measured values.

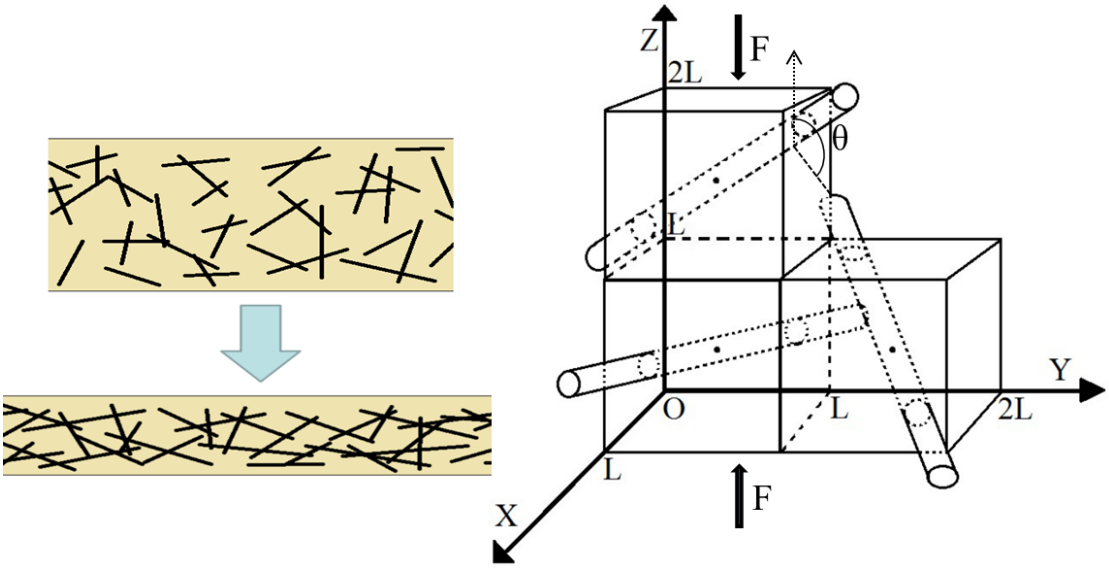

Fig. 4.4 A brief image of the compressing procedure of unfoamed MWCNT/silicone elastomers by external pressure

Many types of fiber-like carbon fillers such as carbon nanofiber (CNT) are found useful to confer conductivity and piezoresistivity [12-15]. There are more opportunities for the formation of the conductive paths in the fiber-like particles filled nanocomposites.

The distributions and orientations of the fiber-like fillers always change with the deformation of the substrates, leading to a unique alteration of conductivity. Many previous works focused on the piezoresistivity brought by fiber-like particles [16-18].

According to the Eq. (4-7), if a pressure is loaded on the nanocomposite, the average minimum distance between adjacent MWCNTs will be changed from s_0 to s_1, the resistance will become from R_0 to

$$R_1 = \frac{s_1 A_0 R_0}{s_0 A_1} \exp\left[\frac{4\pi}{h}\sqrt{2m\varphi}(s_1 - s_0)\right] \quad (4\text{-}15)$$

As shown in Fig. 4.4, the MWCNTs dispersed in the substrates are described as ideal cylinders with the same length and the same radius of l and r. The continuous substrate is described as divided cube-like rooms which all have a same edge length of L, so the average minimum distance between adjacent MWCNTs s ranges randomly from 0 to L. The MWCNTs are thought to be distributed in the substrate absolutely homogeneously, whose centers absolutely coincide with the centers of the cubes. When the nanocomposite deforms under the uniaxial pressure from the vertical direction, the edge length L is assumed to vary with the deformation. θ is the angle between the shortest connecting line of two adjacent fibers and the uniaxial pressure direction, which ranges from 0 to π randomly. s is the compressing strain of the nanocomposite, so

$$\frac{s_1}{s_0} = 1 - \varepsilon(\cos^2\theta - \upsilon\sin^2\theta) \quad (4\text{-}16)$$

Substitute it into the Eq. (4-7), the resistance of the nanocomposite under a pressure can be randomly calculated as

$$R_1 = \frac{A_0 R_0}{A_1}[1 - \varepsilon(\cos^2\theta - \upsilon\sin^2\theta)] \exp\left[\frac{4\pi\varepsilon s_0}{h}\sqrt{2m\varphi}(\upsilon\sin^2\theta - \cos^2\theta)\right] \approx$$

$$R_0 \exp\left[\frac{4\pi\varepsilon s_0}{h}\sqrt{2m\varphi}(\upsilon\sin^2\theta - \cos^2\theta)\right] \quad (4\text{-}17)$$

If the relationship between θ and s is neglected, the average resistance of nanocomposite

under a pressure can be calculated by

$$\overline{R_1} \approx \frac{R_0}{\pi L}\int_0^{\pi}\int_0^{L} \exp\left[\frac{4\pi\varepsilon s_0}{h}\sqrt{2m\varphi}(\upsilon \sin^2\theta - \cos^2\theta)\right] ds_0 d\theta$$

$$= \frac{R_0}{\pi L}\int_0^{\pi}\left\{\frac{h\exp\left[\frac{4\pi\varepsilon L}{h}\sqrt{2m\varphi}(\upsilon \sin^2\theta - \cos^2\theta)\right] - h}{4\pi\varepsilon\sqrt{2m\varphi}(\upsilon \sin^2\theta - \cos^2\theta)}\right\} d\theta \quad (4\text{-}18)$$

The effective volume fraction of MWCNTs can be thought as

$$f = \frac{\pi l^3}{48L^3} \quad (4\text{-}19)$$

Therefore the average resistance of nanocomposite under pressure can be described as

$$\overline{R_1} \approx R_0\left(\frac{48f}{\pi^4 l^3}\right)^{\frac{1}{3}}\int_0^{\pi}\left\{\frac{h\exp\left[\frac{4\varepsilon}{h}\left(\frac{\pi^4 l^3}{48f}\right)^{\frac{1}{3}}\sqrt{2m\varphi}(\upsilon \sin^2\theta - \cos^2\theta)\right] - h}{4\pi\varepsilon\sqrt{2m\varphi}(\upsilon \sin^2\theta - \cos^2\theta)}\right\} d\theta \quad (4\text{-}20)$$

In the experiment, novel highly sensitive piezoresistive foams with excellent elasticity were fabricated by adding a new type of thermally expandable microbeads, which leads to a cell-filled flexible structure. Effects of MWCNT and the foaming agent on the piezoresistivity were investigated. The deformation of the cross section caused by a uniaxial pressure was observed originally and its effect on the piezoresistivity was discussed in detail.

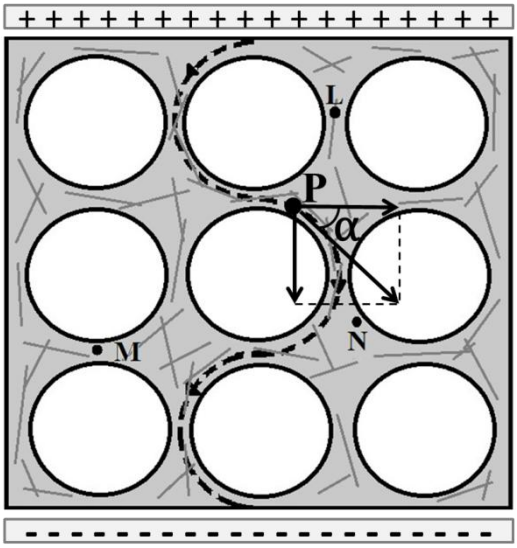

Fig. 4.5 A brief image of the piezoresistive mechanism for microbeads cells filled conductive nanocomposites

The mechanism for the microbeads loaded MWCNT/silicone elastomeric nanocomposite was also discussed. As it shows in the Fig. 4.5, the electric conductive paths are confined in the matrix area between the insulated cells. According to the SEM observation result, the cells were slightly being compressed when the foams were under a uniaxial pressure. In order to simplify the piezoresistive model, some assumptions are made: The cells always keep perfect sphere-like shapes when under a pressure; the current passes through the foam matrix along the edges of these cells; the Poisson's deformation of the substrate area with cells only in its horizontal direction, such as the point L in the Fig. 4.5, would be absolutely blocked by the adjacent cells; the Poisson's deformation would not be affected in the substrate area with cells only in its vertical direction, like the point M; the Poisson's deformation of the other areas, such like the point N, would be partially affected. Based on these assumptions, the Eq. (4-5) and Eq. (4-7) can be used to describe the piezoresistive phenomenon of the cell introduced foams,

in which the conductive paths become to longer semicircle. As in the Fig. 4.5, for the point P in the conductive path from A to B, if the angle between the conductive direction and the horizontal direction is set as α, the ratio of the average minimum distance between adjacent MWCNTs in the foam before and after compression will be

$$\frac{s_1}{s_0} = 1 - \int_0^{\pi} \varepsilon(\cos^2\theta \cdot \sin\alpha - v\sin^2\theta \cdot \cos a)\, d\alpha = 1 - 2\varepsilon\cos^2\theta \quad (4\text{-}21)$$

Substitute it into the Eq. (4-7), use the same method in Eq. (4-16) ~ Eq. (4-20), the average resistance of the foam under a pressure can be easily calculated as

$$\overline{R_1} = R_0\left(\frac{48f}{\pi^4 l^3}\right)^{\frac{1}{3}} \int_0^{\pi} \left\{ (1 - 2\varepsilon\cos^2\theta) \cdot \frac{h\exp\left[\frac{4\varepsilon}{h}\left(\frac{\pi^4 l^3}{48f}\right)^{\frac{1}{3}}\sqrt{2m\varphi}\left(v\sin^2\theta - \cos^2\theta\right)\right] - h}{4\pi\varepsilon\sqrt{2m\varphi}\left(v\sin^2\theta - \cos^2\theta\right)} \right\} d\theta \quad (4\text{-}22)$$

The theoretical values calculated by Eq. (4-20) and Eq. (4-22) were used to compare with the experimental results in Chapter 5, relatively well-fit results were obtained.

4.5 Conclusion

In order to predict and elucidate the mechanisms of the factors and variation procedures of the resistance of flexible conductive nanocomposites, 3 types of theoretic piezoresistive models were introduced from different prospects. Each model was built considering both the solid and foamed conductive nanocomposite. A piezoresistive model was deduced based on the percolation threshold of conductive elastomeric nanocomposites, which is simple but can only be used for the calculation of the resistance variation in a conductive nanocomposite with a volume fraction near its percolation threshold. Another type of piezoresistive model was deduced based on the tunnel conductive theory for elastomeric nanocomposites, which is able to explain the resistance of flexible conductive nanocomposites with a wide range of volume fraction and with spherical conductive particles. To broaden the applicable scope of the model

for a variety of particle shapes, a piezoresistive model based on the tunnel conductive theory for elastomeric nanocomposites considering the distribution, aspect ratio, and orientation of each fiber-like conductive particle was developed. Although with a high accuracy, its complexity reduced the practicality. There is still much works need to do to assure the practicality and precision at the same time.

References

[1] Kim, W. J., Taya, M., & Nguyen, M. N. (2009). Electrical and thermal conductivities of a silver flake/thermosetting polymer matrix composite. Mechanics of Materials, 41(10), 1116-1124.

[2] Seidel, G. D., & Lagoudas, D. C. (2009). A micromechanics model for the electrical conductivity of nanotube-polymer nanocomposites. Journal of Composite Materials, 43(9), 917-941.

[3] Carmona, F., Canet, R., & Delhaes, P. (1987). Piezoresistivity of heterogeneous solids. Journal of Applied Physics, 61(7), 2550-2557.

[4] Taya, M., Kim, W. J., & Ono, K. (1998). Piezoresistivity of a short fiber/elastomer matrix composite. Mechanics of materials, 28(1), 53-59.

[5] Deng, F., & Zheng, Q. S. (2008). An analytical model of effective electrical conductivity of carbon nanotube composites. Applied Physics Letters, 92(7), 071902.

[6] Dunn, M. L., & Taya, M. (1993, November). An analysis of piezoelectric composite materials containing ellipsoidal inhomogeneities. In Proceedings of the Royal Society of London A: Mathematical, Physical and Engineering Sciences (Vol. 443, No. 1918, pp. 265-287). The Royal Society.

[7] Li, C., Thostenson, E. T., & Chou, T. W. (2007). Dominant role of tunneling resistance

in the electrical conductivity of carbon nanotube–based composites. Applied Physics Letters, 91(22), 223114.

[8] Zhan, Y., Lavorgna, M., Buonocore, G., & Xia, H. (2012). Enhancing electrical conductivity of rubber composites by constructing interconnected network of self-assembled graphene with latex mixing. Journal of Materials Chemistry, 22(21), 10464-10468.

[9] Huang, Y., Xiang, B., Ming, X., Fu, X., & Ge, Y. (2008, June). Conductive mechanism research based on pressure-sensitive conductive composite material for flexible tactile sensing. In Information and Automation, 2008. ICIA 2008. International Conference on (pp. 1614-1619). IEEE.

[10] Zhang, X. W., Pan, Y., Zheng, Q., & Yi, X. S. (2000). Time dependence of piezoresistance for the conductor-filled polymer composites. Journal of Polymer Science part B: polymer physics, 38(21), 2739-2749.

[11] Zhang, X. W., Pan, Y., Zheng, Q., & Yi, X. S. (2001). Piezoresistance of conductor filled insulator composites. Polymer international, 50(2), 229-236.

[12] Byrne, M. T., & Gun'ko, Y. K. (2010). Recent advances in research on carbon nanotube–polymer composites. Advanced Materials, 22(15), 1672-1688.

[13] Hao, X., Gai, G., Yang, Y., Zhang, Y., & Nan, C. W. (2008). Development of the conductive polymer matrix composite with low concentration of the conductive filler. Materials Chemistry and Physics, 109(1), 15-19.

[14] Finegan, I. C., & Tibbetts, G. G. (2001). Electrical conductivity of vapor-grown carbon fiber/thermoplastic composites. Journal of Materials Research, 16(06), 1668-1674.

[15] Zhang, C., Wang, L., Wang, J., & Ma, C. A. (2008). Self-assembly and conductive

network formation of vapor-grown carbon fiber in a poly (vinylidene fluoride) melt. Carbon, 46(15), 2053-2058.

[16] Li, C., Thostenson, E. T., & Chou, T. W. (2007). Dominant role of tunneling resistance in the electrical conductivity of carbon nanotube–based composites. Applied Physics Letters, 91(22), 223114.

[17] Li, J., Ma, P. C., Chow, W. S., To, C. K., Tang, B. Z., & Kim, J. K. (2007). Correlations between percolation threshold, dispersion state, and aspect ratio of carbon nanotubes. Advanced Functional Materials, 17(16), 3207-3215.

[18] Seidel, G. D., & Lagoudas, D. C. (2009). A micromechanics model for the electrical conductivity of nanotube-polymer nanocomposites. Journal of Composite Materials, 43(9), 917-941.

Chapter5 Multi-walled Carbon Nanotubes/Silicone Elastomeric Conductive Nanocomposites and Their Piezoresistive Behaviors

5.1 Introduction

Nowadays, the demand for a device with tactile sensors is growing very fast as the developing of the artificial intelligent [1-5]. Not only the high accuracy, but also the low cost and the eco-friendly fabrication of the tactile sensors are needed by the industry and our daily lives. Tactile sensors made by electroactive conductive polymer nanocomposites (ECPCs) are low-cost, easy to process and can bring many unique electrical and mechanical properties [6]. Unlike the expensive, processing-difficult intrinsic conductive polymers, just by dispersing conductive particles into a polymer substrate, a conductive nanocomposite with a wide rage and a diverse conductivity can be obtained [7-16].

A material exhibits piezoresistivity as its electrical resistance depends upon external deformation, which is optimal to be utilized in mechanical sensors [17]. Many types of conductive fillers are expected to be used to obtain the piezoresistive property, such as metallic particles, carbon black, carbon fibers, CNT or graphene. As the substrates, a wide range of polymers can be used, from hard resins like epoxy, to soft elastomers, such as nature rubber or silicone rubber. Electrically conductive epoxy/clay/vapor grown carbon fiber hybrids were made and the effects of highly exfoliated clay layers on electrical properties of the hybrids were studied by Masaya Kotaki's research group [18]. Based on the piezoresistivities of these nanocomposites, mechanical sensors can be simply assembled. A low volume resistivity was achieved with a low content, effective dispersed MWCNT, of which conductive network was enhanced by highly exfoliated clay layers. Two types of stretchable and flexible strain sensors in terms of high

measurable strain and high sensitivity with good durability were fabricated by sandwiching conductive films between natural rubbers in Sreenivasulu Tadakaluru' work, in which MWCNT or graphite flakes were randomly distributed. A method to linearize the exponential response curves from the sensors was also introduced [19]. In Ning Hu' works [20], a strain sensor has been fabricated from a polymer nanocomposite with multi-walled carbon nanotube fillers. The piezoresistivity of this strain sensor has been investigated based on a 3D statistical resistor network model with the tunneling effect between the neighboring carbon nanotubes, accompanied with a fiber reorientation model. The tunneling effect is considered to be the principle mechanism of the sensor under small strains, according to the well agreement between the numerical results and the experimental measurements.

5.2 The Significance of a Foaming Treatment

Among the common polymers, silicone is a type of elastomer with numerous good properties such as a highly flexibility, a widely temperature resistance, an eco-friendly feature and a relatively high dielectric constant, which acts as an excellent matrix for tactile sensors or actuators [21]. However, silicone elastomer also brings some demerits, like its low tear strength and a relative high density. As a polymer, its viscoelasticity that is not negligible is also a disadvantage for the applications in tactile sensors. To overcome these demerits, adding the reinforcing agent, such as white carbon black (SiO_2), is a common industrial method. The overall strength can be improved and the viscoelasticity can be reduced, but the flexibility will decrease due to the reinforcement, which limits the applications as a piezoresistive material. In comparison, foaming is an ideal method to overcome these disadvantages [22-27]. The flexibility can be significantly improved by

the foaming procedure. The viscoelasticity could be reduced drastically as a shift of the deforming configuration. Another obvious advantage of foaming is a weight/cost reduction. Some previous works focused on exhibiting the possibility of the piezoresistive foaming materials. K. A. Klicker et al. explored the effect of porosity on the hydrostatic piezoelectric sensitivity of 3-1 connectivity in a foamed polyurethane matrix [25]. It was found that hydrostatic sensitivity increases rapidly with the increasing of porosity of the nanocomposites, the piezoelectric coefficient under hydrostatic loading sharply increases when porosity is incorporated to 40%. Xiang-Bin Xu and his group [26] developed a type of light-weight conductive MWCNT/rigid polyurethane composite by static casting. An amazingly low density with a desirable conductivity was successfully obtained. It was found that the conductivity of the foam depends on the CNTs that restricted in the cell walls and cell struts. With the decreasing of the foam density, the cell walls get thinner and transit from sphere to polyhedral, the conductivity will transit from three-dimensional to two-dimensional. The origin of the conductor-insulator transition is the break-up of the cell-strut network at the extremely low densities.

In this work, in order to investigate and optimize the enhancement of the sensitivity and the broadening of the measurable range of the changing resistance of the conductive nanocomposites, two types of foaming agents were used to add to the conductive nanocomposites. One is a new type of thermally expandable micro beads foaming agents. Novel high-sensitive piezoresistive foams with excellent elasticity were fabricated using MWCNT, 2-component silicone elastomer and the thermally expandable micro beads foaming agent. Effects of MWCNT and the foaming agent on the piezoresistivity were investigated. To verify the effect of the foaming process, the MWCNT/silicone nanocomposites without foaming agents were also prepared for comparison. The

conductive mechanism of the nanocomposite was discussed. The deformation of the cross section caused by external pressure was observed originally and its effect on the piezoresistivity was discussed in detail. The others are several normal types of foaming agents. These were used to fabricate a series of MWCNT/silicone conductive foamed nanocomposites were. The diverse porous structures, the distribution and orientation states of the MWCNTs in the silicone matrix were observed by a laser microscope and SEM with or without a compressive load. The influences of the porous structure and porosity on the foam density, elastic modulus, resistivity as well as piezoresistive property were studied. Calculated results of the resistive variations were used to compare to the measured values.

5.3 Investigation of MWCNT/Silicone Elastomeric Conductive Nanocomposites with Foaming Treatment with Thermally Expandable Beads and Their Piezoresistive Behaviors

5.3.1 Materials

MWCNT (VGCF-H, Showa Denko) with an average fiber length of 10~20μm and an average fiber diameter of 150nm was used as the conductive particles. 2-component silicone elastomer (CY52-276, part A and part B, Dow Corning Toray Co., Ltd.) and its cross-linking agent (RD-1, Dow Corning Toray Co., Ltd.) were used to synthesize the substrates. Thermally expandable micro beads DAIFOAM H750D and H850D (Dainichiseika Color & Chemicals Mfg. Co., Ltd.), with initial particle diagrams of 20μm and 35μm, respectively, were used as the foaming agent. The micro bead has a core-shell structure, with a core of low boiling point hydrocarbon compound and a shell of thermoplastic resins, which can expand about 4, 5 times in diagrams and 20-70 times in

volumes when heated.

5.3.2 Preparation of MWCNT/Silicone Elastomeric Conductive Nanocomposites with Foaming Treatment of Thermally Expandable Beads

Firstly, all the components of the silicone elastomer were mixed together according to the expected ratio (part A, part B and the cross-linking agent have a ratio by weight of 100:100:1), then the micro beads foaming agent and the MWCNT were added into the silicone mixture respectively (containing the formulas without foaming agent). The mixture was finely stirred using a planetary centrifugal vacuum mixer at a speed of 1000rpm under pressure of 0.6kPa for 10min, then immediately poured into a mold. After curing at 110˚C for 5min, the nanocomposite was obtained as a membrane shape with a thickness of 2mm. At last, the conductive MWCNT/silicone foam was obtained by free foaming for 10min at 170˚C in vacuum. For comparing, elastomers without foaming agent were also fabricated. The thicknesses of these foams or unfoamed membranes range from about 2mm to 4mm. A unique foam structure with closed cells was obtained, which is different from the common foams with closed pores. These cells can maintain the stiffness in some degree even after the foaming procedure, due to their cell walls. An industrial unit “phr”, namely “per hundred rubber” is used in this work, which represents the weights (gram) of added agents compared to per 100g of pure silicone substrate. The content of MWCNT was varied from 5phr to 20phr, while the content of the micro beads foaming agent was controlled to 5phr and 10phr. The weight fractions and volume fractions of MWCNT and foaming agent were listed in Table 5.1 and Table 5.2.

Table 5.1 Weight/volume fractions of MWCNT in MWCNT/silicone foams and unfoamed elastomers

MWCNT	Unfoamed (%)	H750D foamed (%)		H850D foamed (%)	
		5phr	10phr	5phr	10phr
5phr	4.76/2.28	4.55/2.18	4.35/2.1	4.55/2.18	4.35/2.1
10phr	9.09/4.46	8.7/4.27	8.33/4.11	8.7/4.27	8.33/4.11
15phr	13.04/6.54	12.5/6.28	12/6.04	12.5/6.28	12/6.04
20phr	16.67/8.53	16/8.2	15.38/7.89	16/8.2	15.38/7.89

Table 5.2 Weight/volume fractions of micro beads foaming agents in MWCNT/silicone foams and unfoamed elastomers

MWCNT	Unfoamed (%)	H750D foamed (%)		H850D foamed (%)	
		5phr	10phr	5phr	10phr
5phr	0/0	4.55/4.18	8.7/8.01	4.55/4.18	8.7/8.01
10phr	0/0	4.35/4.09	8.33/7.84	4.35/4.09	8.33/7.84
15phr	0/0	4.17/4	8/7.69	4.17/4	8/7.69
20phr	0/0	4/3.92	7.69/7.53	4/3.92	7.69/7.53

5.3.3 Characterizations

The CT photographs were taken by an SHIMADZU inspeXio SMX-90CT micro focus x-ray CT system. The volume resistivity was measured by an ADVANTEST R6243 DC voltage current source/monitor with a 4-wired method; the SEM observation was applied at an accelerating voltage of 15kV by a JEOL JSM-7600F field emission scanning electron microscope (The cross sections of the samples for these observations were

obtained by breaking them after freezing in liquid nitrogen. Each sample was loaded with a uniaxial pressure through the thickness direction by a pair of metallic plates set into the sample holder. The compressing strain was controlled to 0, 50% and 75%). The elastic modulus was measured by a SHIMADZU AGS-G Series Universal/Tensile Tester, with a compressing speed of 3mm/min.

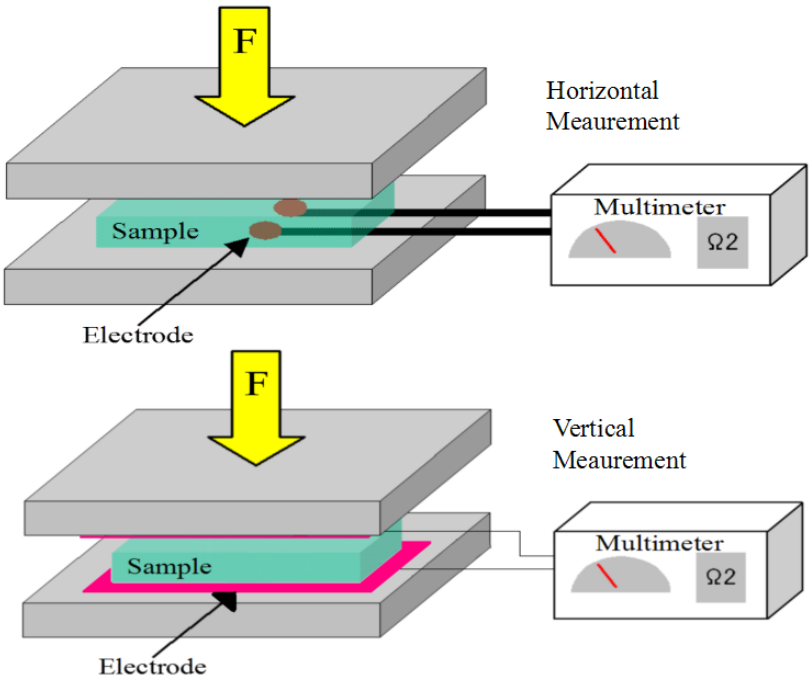

Fig. 5.1 Piezoresistivity measurements from the horizontal direction and the vertical direction

In the experiment, the sample membranes were cut to a sheet-like shape of 30mm×50mm for the measurement. Piezoresistivity was measured from both the horizontal direction and the vertical direction. The image of the horizontal measurement was shown in the upper part of the Fig. 5.1. The samples were put on a pair of round-shape copper electrodes with a same diagram of 12mm, the distance between the

centers of the two electrodes is 30mm. Then the electrodes were sandwiched between a pair of compressing plates to load an external pressure, which was controlled by the SHIMADZU AGS-G Series Universal/Tensile Tester. The electrodes were connected with a 2000 Series Digit Multimeter to measure the resistance using a 2-wire mode. For every sample, the resistance was measured under difference stress from 0 to 135kPa and listed as the form of common logarithms. The variation of the resistances was detected by the measuring system as the samples being compressed by an external pressure. The image of the vertical measurement was shown in the under part of Fig. 5.1, which is similar with the horizontal measurement, while the copper electrodes were placed between the samples and the compressing plates, each electrode has a square shape of 75mm×75mm for the vertical measurement. Silver paint was smeared to the sample surfaces to ensure a well surface contact with the electrodes in both the horizontal measurement and vertical measurement. Compared to the horizontal measurement, the vertical measurement can obtain more stable and precise results, because the parallel current paths within the sample are more uniform in the vertical measurement, while the current paths are more complex and related to the distances from the electrodes. However, the horizontal measuring system is far more appreciate for the applications in tactile sensors because of its simpler unidirectional wiring. The tiny resistance as well as inductance loss within the measuring system was neglected. It should be noted that the resistances of the samples with different MWCNT contents, or the resistances measured by the horizontal method and vertical method cannot be compared directly, because each sample has a different thickness. As important properties for the tactile sensor applications, the sensitivity of the variation of the resistance for the external pressure and the sensitive range for the external pressure are emphasized.

5.3.4 Results and Discussion

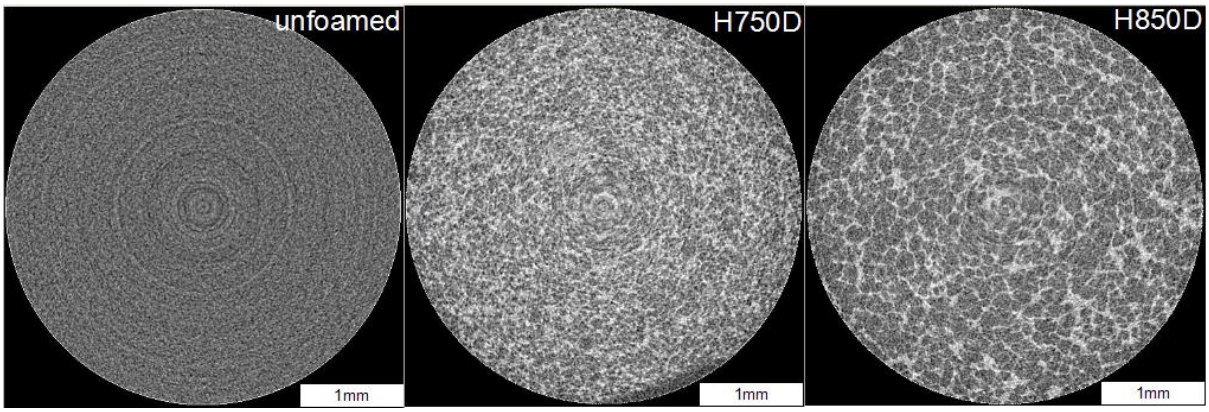

Fig. 5.2 CT photographs of the cross sections of unfoamed elastomer and MWCNT/silicone foams

The CT photographs of the cross sections of the MWCNT/silicone unfoamed elastomer, H750 foam and H850 foam with a MWCNT loading of 15phr were shown in the Fig. 5.2, a homogeneous content can be observed from the CT photo of the MWCNT/silicone unfoamed elastomer. Porous structures can be found in the CT photos of the foams. Concentrated tiny bubbles are observed in the H750D foam, while scattered large bubbles are observed in the H850D foam.

Table 5.3 Extrinsic densitise of MWCNT/silicone foams and unfoamed elastomers with different amount of additive agents

MWCNT	Unfoamed (g/cm^3)	H750D foamed (g/cm^3)		H850D foamed (g/cm^3)	
		5phr	10phr	5phr	10phr
5phr	1.04	0.55	0.36	0.48	0.30
10phr	1.04	0.59	0.37	0.60	0.32
15phr	1.05	0.68	0.40	0.65	0.35
20phr	1.10	0.72	0.66	0.72	0.36

The Extrinsic densities of MWCNT/silicone foams and unfoamed elastomers are listed in the Table 5.3. It can be found that the micro beads foaming agents have great weight-reducing effect on the MWCNT/silicone elastomers. Without the foaming agent, there are rarely variations in extrinsic densities for the composites even with different contents of MWCNT. The extrinsic density decreases as increasing of the added foaming agent. Meanwhile, micro beads H850D exhibits more weight saving effect than H750D especially for the composites with a high MWCNT added amount, which may be due to its larger particle sizes.

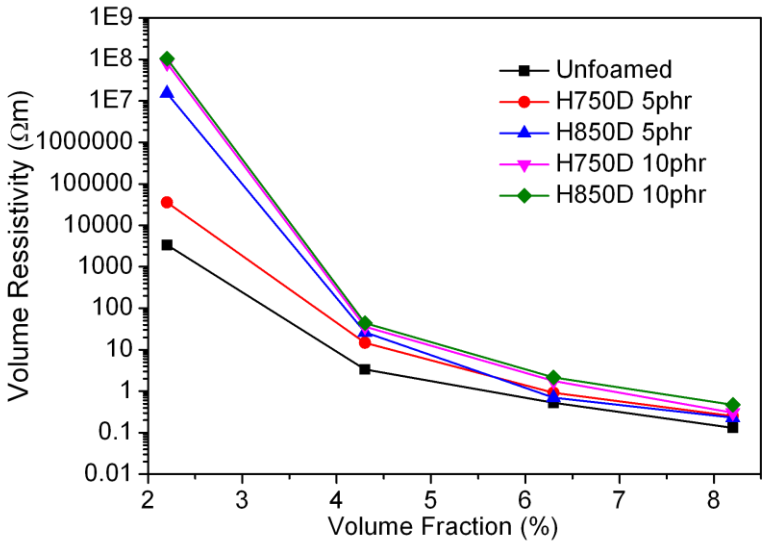

Fig. 5.3 Volume resistivity measured by 4-wire method (Van der Pauw Method)

The volume resistivity of the MWCNT/silicone unfoamed elastomers and the MWCNT/silicone foams are shown in the Fig. 5.3. It is apparent that the volume resistivity decreases rapidly as increasing of the added amount of MWCNT. The amount of the added micro beads foaming agents also have obvious effects on the volume resistivity of the MWCNT/silicone composites, among them, the H850D micro beads are more likely to be able to reduce the conductivity. It is noteworthy that the volume resistivity decreased dramatically when the added amount of the MWCNT varies from 5phr to 10phr (volume fraction of from 2% to 4%), no matter with a foamed or unfoamed structure. This boundary of the MWCNT content is equivalent to the percolation threshold of the composite. It is believed that above this range, an absolute electric conductive network can be built in the composite due to the contact or overlap between the MWCNT fibers.

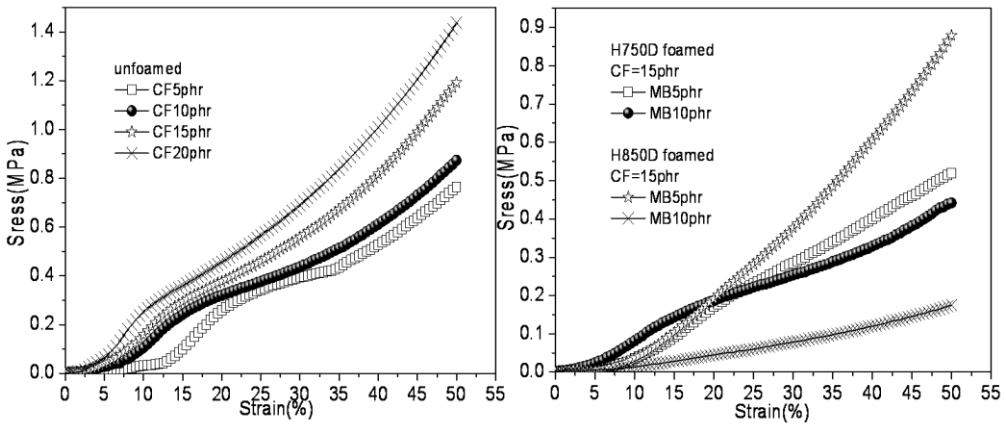

Fig. 5.4 Elastic modulus of MWCNT/silicone composites with different contents of MWCNT and foaming agents

Elastic modulus of MWCNT/silicone composites with different added amounts of MWCNT and foaming agents were tested to investigate the effect of additive agents on the elastic modulus of the MWCNT/silicone composites. The stresses at different strains for the unfoamed MWCNT/silicone elastomers with different contents of MWCNT are shown in the left part of the Fig. 5.4. It is apparent that the elastic modulus increases as increasing of the amount of the MWCNT, especially with a high MWCNT content. For instance, for the unfoamed elastomer with MWCNT additive amounts from 5phr to 20phr (the volume fraction varies from 2.28% to 8.53%), the elastic modulus at a strain of 50% are about 1.50MPa, 1.74MPa, 2.38MPa and 2.85MPa, respectively. It is considered that increasing of the elastic modulus is because that the configuration movement of the molecular chains are significantly restricted by the inorganic MWCNT fibers, which have a highly stiffness and a large specific surface area.

The right side of the Fig. 5.4 shows the stresses at different strains for the MWCNT/silicone foams using foaming agents H750D and H850D, both with a MWCNT

content of 15phr. The additive amount of the micro beads foaming agents leads to an apparent decreasing of elastic modulus. It is worth noting that the foaming efficiency of the H850D foaming agent seems to be more unstable and relevance to the additive amount. The expansion rate of the foaming agent is considered as an unstable factor here. The micro beads H750D foaming agent has smaller particle sizes and a lower expanding temperature, the majority of which can reach higher expansion rates as heated, making the sizes of obtained cells be more stable; the micro beads H850D foaming agent has bigger particle sizes and a higher expanding temperature, which can provide highly flexible cell walls. But the expansion of every particle is unstable, leading to a variable size of cells. The MWCNT/silicone foam with the H850D micro beads foaming agent at a content of 10phr exhibits the highest flexibility of about 0.32MPa at a strain of 50%.

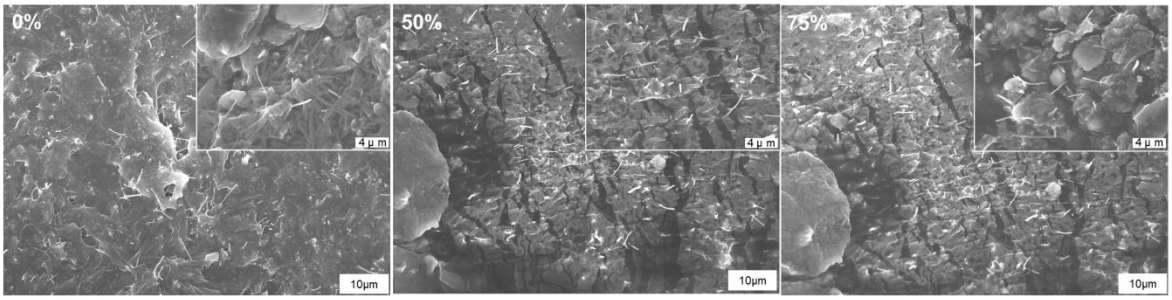

Fig. 5.5 SEM photographs of the unfoamed MWCNT/silicone elastomer with different strains

The cross sections of the unfoamed and micro beads foamed MWCNT/silicone composites were observed at an accelerating voltage of 15kV, under a changing external pressure. The cross sections were obtained by breaking the samples frozen by liquid nitrogen. Each sample was loaded an external pressure through the thickness direction by a pair of metallic plates that were set into the sample holder. Every sample was observed

under the compressing strains of 0, 50% and 75%. The SEM images of the unfoamed MWCNT/silicone elastomer with a MWCNT loading of 15phr at different strains are shown in the Fig. 5.5 It can be found that as the strain rises from low to high, there are many wrinkles appearing in the silicone substrate. A lot of carbon fibers can be found at the surface of the substrates but much more fibers are embedded in the substrate. At the strain of 0, the majority of the carbon fibers are found to be distributed randomly and isotropically in the substrate. Fibers are contacting and entangling with each other in many area. It is the overlap of carbon fibers that is considered the reason of the establishment of conductive paths. As increasing of the strain, the isotropic distribution is gradually changed and the carbon fibers are starting to rotate to the direction that perpendicular to the pressure. At the strain of 75%, the contacts of the MWCNT fibers can be found everywhere. The electrical conductive paths are strengthened by the external pressure. The image of the compressing procedure of the unfoamed elastomer is shown in the left part of the Fig. 4.4. The extending through the horizontal direction due to the Poisson's effect is apparent, which affects the piezoresistivity of the composites in some degree.

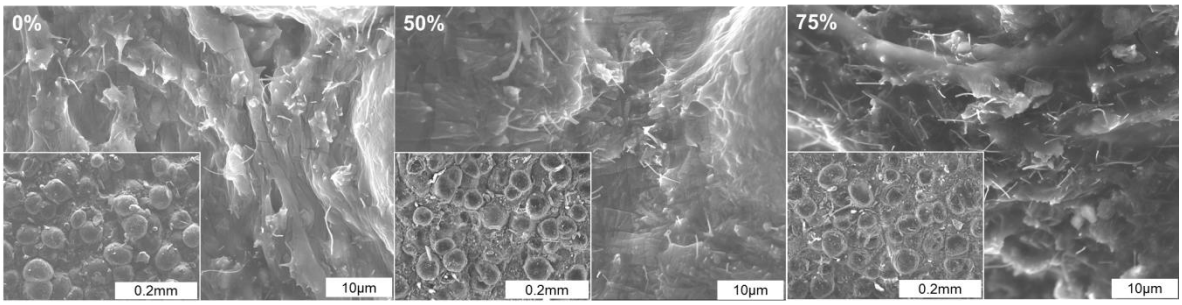

Fig. 5.6 SEM photographs of the MWCNT/silicone foam with H750D micro beads foaming agent at different strains

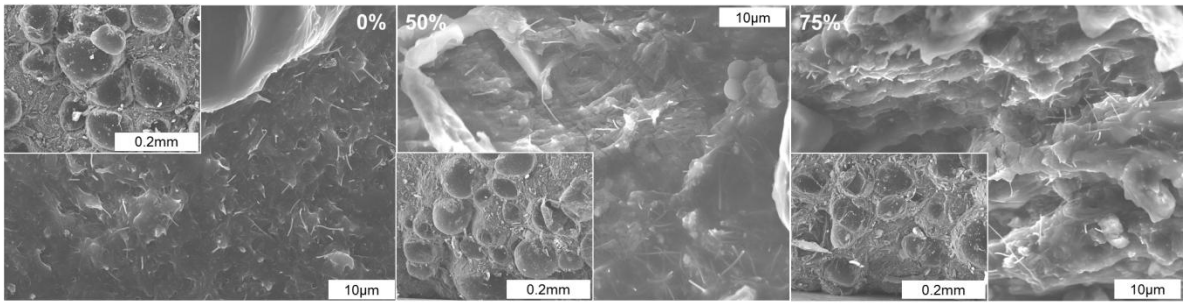

Fig. 5.7 SEM photographs of the MWCNT/silicone foam with H850D micro beads foaming agent at different strains

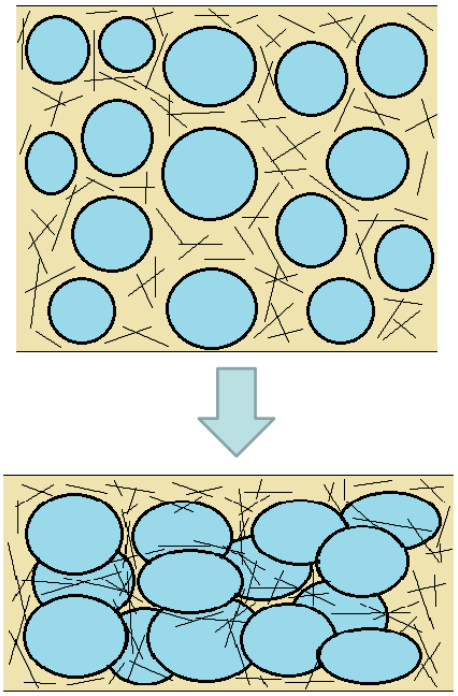

Fig. 5.8 A brief image of the compressing procedure of MWCNT/silicone foam under an external pressure

The SEM images of the MWCNT/silicone foam with a MWCNT loading of 15phr and a micro beads foaming agent loading of 10phr at different strains are shown in the Fig. 5.6 and Fig. 5.7, respectively. Unexpectedly, it is found that the deformation of the cells does not occupy the majority of the deformation of the foams, although it can be observed in

some degree. It is the compressing, twisting and folding of the areas between the cells that comprise the majority of the deformation. It is considered that the relatively tough shells of the cells are difficult to be compressed. At a low strain, the substrate between the cells seems flat, dispersion of the carbon fibers are isotropic and random. As increasing of the pressure, just like the unfoamed elastomer, there are much wrinkles appearing at the substrate, the distances between carbon fibers decrease and the fibers are beginning to rotate and point to the direction perpendicular to the external pressure. When the strain reaches 50%, the wrinkles become long and deep, folding of the substrate can be clearly observed. When the strain reaches as high as 75%, the majority of the substrate between the cells is found to be extruded out from the areas between the cells, especially for the foam with the H850D foaming agents. The majority of the MWCNT fibers are found to have the trend to point to the same direction at a high strain range. A brief image of the compressing procedure of the MWCNT/silicone foam is shown in the Fig. 5.8. As increasing of the external pressure, the conductive network of the MWCNT fibers is established gradually, because the carbon fibers are confined between the cells. It is considered that the restriction from the cells making the constructing of the conductive network be much more smooth and stable, unlike the rapidly and randomly establishing of the conductive paths in the unfoamed MWCNT/silicone elastomers.

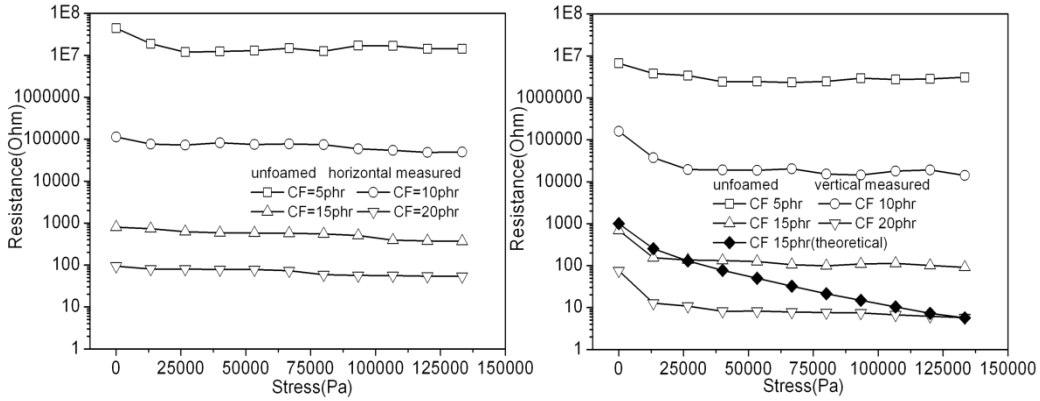

Fig. 5.9 Piezoresistivity of the unfoamed MWCNT/silicone elastomers

The piezoresistivity measurement of the MWCNT/silicone composites was conducted from both horizontal direction and vertical direction. Compared to the horizontal measurement, the vertical measurement can obtain stable and precise results due to the well contact and the uniform parallel current paths within the sample, compared to the complex current paths in the horizontal measurement, which are related to the distances from the electrodes. Nevertheless, the horizontal measuring system is more appreciate for the applications in tactile sensors because of its simpler unidirectional wiring. It should be noted that the resistances of the samples with different MWCNT contents could not be compared directly because each sample has a different thickness. As important parameters in the tactile sensor applications, the sensitivity of the variation of the resistance for the uniaxial pressure and the sensitive range for the uniaxial pressure are emphasized. In the figures of this thesis, CF is used as an abbreviation of the Vapor Grown Carbon Fiber (MWCNT), MB is used as an abbreviation of the micro beads foaming agent. The results of the piezoresistivity measurement for the unfoamed MWCNT/silicone elastomers are shown in the Fig. 5.9,

the left side of which shows the horizontal measurement. Without stress, the resistance decreases as increasing of the MWCNT content, this means that the internal conductive network of the MWCNT/silicone elastomer shifts from an incomplete structure to a complete one. These results show a similar variation trend with the volume resistivity results listed in the Fig. 5.3. For the elastomer with all MWCNT contents, decreasing of the resistance cannot be clearly observed under a growing stress. The reason for the lack of the resistance variation is that a stress of up to 135kPa is not large enough to produce an obvious deformation for the relatively high modulus of the elastomer without foaming, limiting the arraying and rotating of the carbon fibers. Furthermore, the Poisson's deformation of the matrix in the horizontal direction has the trend to widen the distances between the adjacent fibers and raise the resistance, which also explains the lack of resistance change.

This disadvantage from the horizontal deformation can be prevented by the vertical piezoresistivity measurement, as shown in the right side of the Fig. 5.9. The effect of the horizontal deformation can be ignored because all of the conductive paths can be covered by the electrodes with a large area. Elastomers with all contents of MWCNT show slight resistance decreasing at a low stress. It is considered that not all of the conductive paths have been completed at a low stress, creating a higher resistance; the conductive paths can be built gradually as the stress growing; a completed conductive network can be built everywhere in the elastomer, leading to a stable, lower resistance at a high stress. The theoretical values were calculated by Eq. (4-20) to compare with the results obtained from the piezoresistive measurement through vertical direction. A smoother and wider resistance variation was obtained from the theoretical calculation compared to the experimental value of the vertical measurement. It is believe that the

stress relaxation of the silicone molecule chains leads to less configurative changes of the carbon fibers in the silicone substrate, which reduces the variation of the resistance in the experimental result significantly.

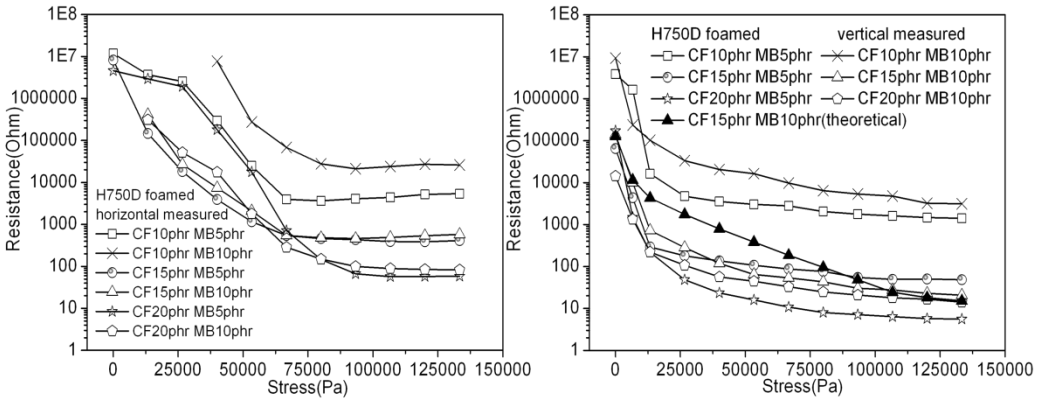

Fig. 5.10 Piezoresistivity of the MWCNT/silicone foams with the H750D micro beads foaming agent

The results of the piezoresistivity measurement for the MWCNT/silicone foams with the H750D micro beads foaming agent are shown in the Fig. 5.10. For the foams with a MWCNT loading of 5phr, the conductivity is so low that it could not be detected from the full stress range, from either the horizontal measurement or the vertical measurement. For the horizontal measurement, the conductivities of some samples at a low stress are too low to be detected out. It can be found that the foams with MWCNT loadings of from 10phr to 20phr show obvious piezoresistivities. Especially for the foam with a MWCNT loading of 20phr and a foaming agent loading of 5phr, the resistance decreases rapidly from about 5MΩ to less than 100Ω. Compared to the unfoamed elastomer, the H750D foam exhibits a wider variable resistance range, which shifts to a lower resistance range as increasing of the MWCNT loading. The reasons for

its piezoresistivity in the horizontal measurement are considered as below: (1) introducing of the foaming agent decreases the conductivity of the composite in some degree and reduces the stiffness of the composite; (2) the MWCNT fibers are confined and agglomerated at the matrix between the cells, promoting the building procedure of conductive networks and raising the sensitivity; (3) the horizontal deformation is reduced by the cells, which raises the decreasing speed of resistance; (4) during the compressing procedure, the resistance decreasing caused by vertical deformation is much greater than the resistance increasing caused by the horizontal deformation that limited by the cells.

It is found that the MWCNT/silicone foams with H750D foaming agents show stable piezoresistivities from the vertical measurement in the Fig. 5.10. The variation of the resistance occurs at the whole stress range. A resistance decrease from about over 4MΩ to lower than 4kΩ was detected for the foams with a MWCNT loading of 10phr; while resistance varies from a range of about 10kΩ to 200kΩ to a range of about 6Ω to 60Ω for the foams with MWCNT loadings of 15phr and 20phr. It is believed that reduction of the horizontal deformation leads to excellent results in the vertical piezoreistivity measurement. The theoretical values were calculated by Eq. (4-22). The results were used to be compared with the results obtained from the piezoresistance measurement through vertical direction. For the foam with a MWCNT loading of 15phr and a H750D micro beads loading of 10phr, similar variation ranges of resistance were obtained from both the theoretical calculation and the experimental result. The variation in the experimental result is more sensitive than in the theoretical result because of the real non-constant elastic modulus of the foam. It is believed that the cells in the foam reduce the stress relaxation and the Poisson's deformation of silicone, leading to the good

piezoresistivity results and a well fit between the theoretical and experimental values.

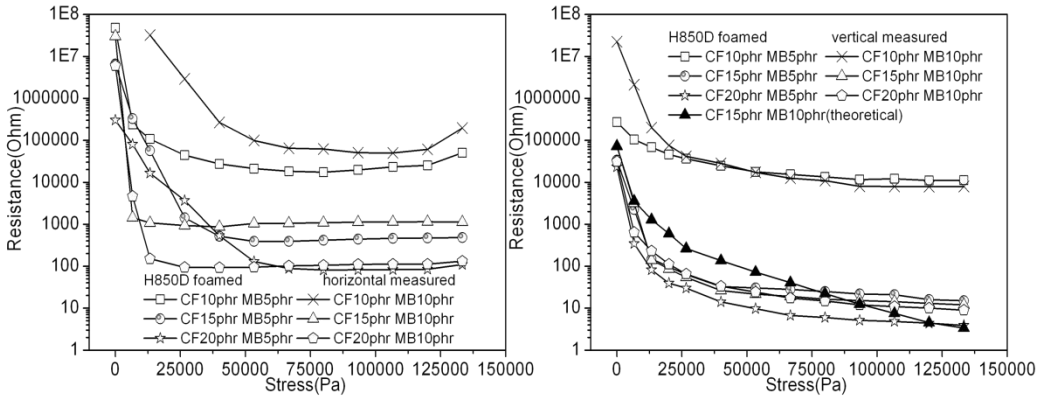

Fig. 5.11 Piezoresistivity of the MWCNT/silicone foams with the H850D micro beads foaming agent

The same piezoresistivity measurements from the horizontal direction and the vertical direction were conducted for the MWCNT/silicone foams with the H850D micro beads foaming agent. As it shows in the Fig. 5.11, the low conductivities of the foams with a MWCNT loading of 5phr cannot be detected out from either the horizontal measurement or the vertical measurement. The piezoresistivities of all the foams can be found to have relatively wide stress ranges in the vertical measurement. For the 10phr MWCNT loaded foams, the resistance can be found at a high range. For the foams with MWCNT contents of 15phr and 20phr, the highly sensitivity towards a low stress was observed. It is believed that the H850D micro beads can also reduce the elastic modulus of the composites, limit the Poisson's deformation and broaden the sensitive range. The theoretical values calculated by Eq. (4-20) were also used here. A well-fit but little uniformly-varied theoretical result was also obtained compared to the experimental result from the vertical measurement of the foam with a MWCNT content of 15phr and

a H850D micro beads content of 10phr.

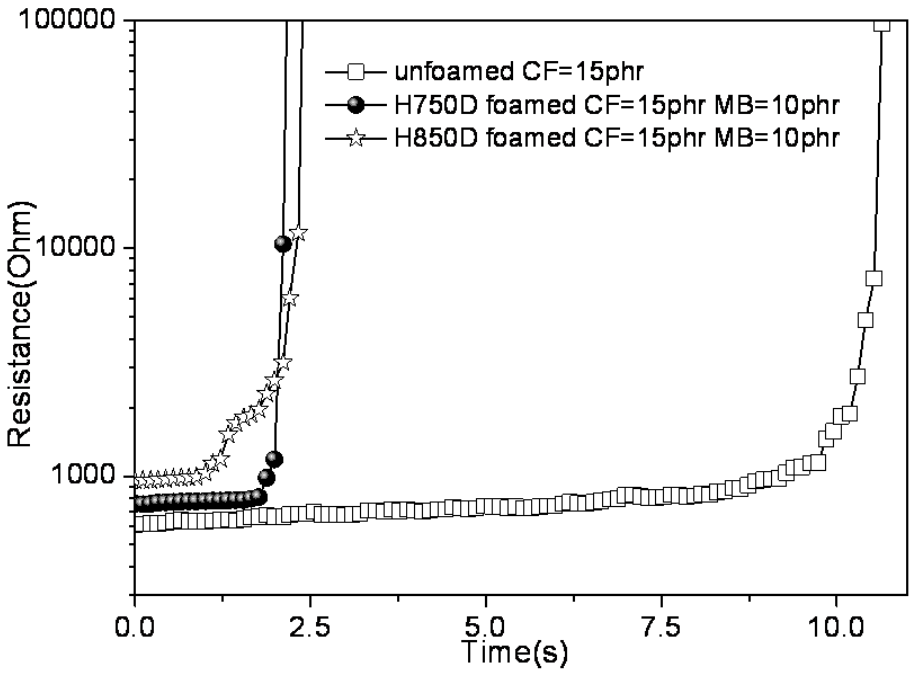

Fig. 5.12 The recovery times of MWCNT/silicone elatomer and MWCNT/silicone foams

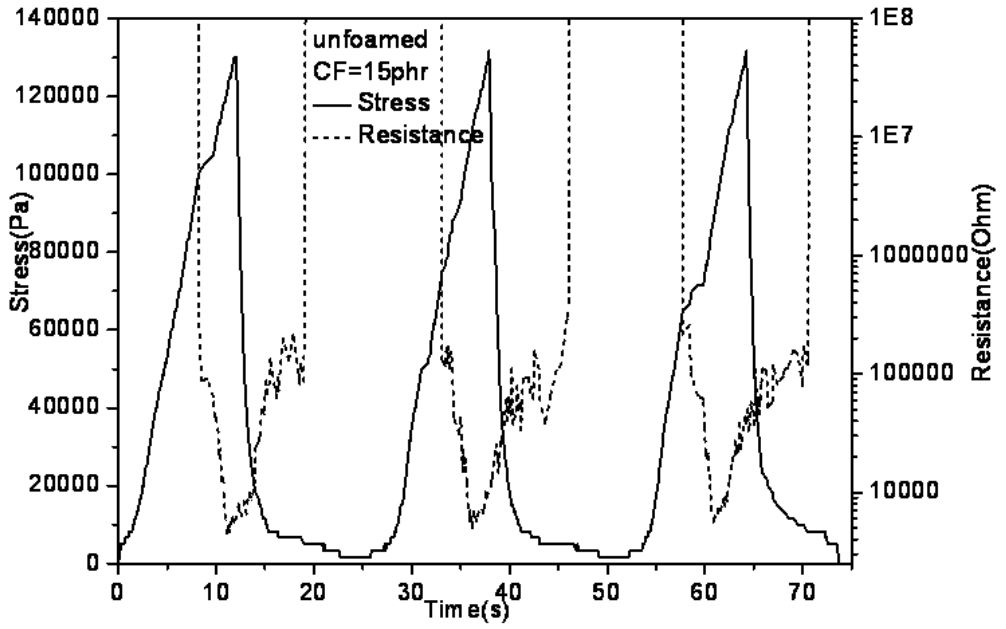

Fig. 5.13 Piezoresistivity of the unfoamed MWCNT/silicone elatomers under a periodic pressure

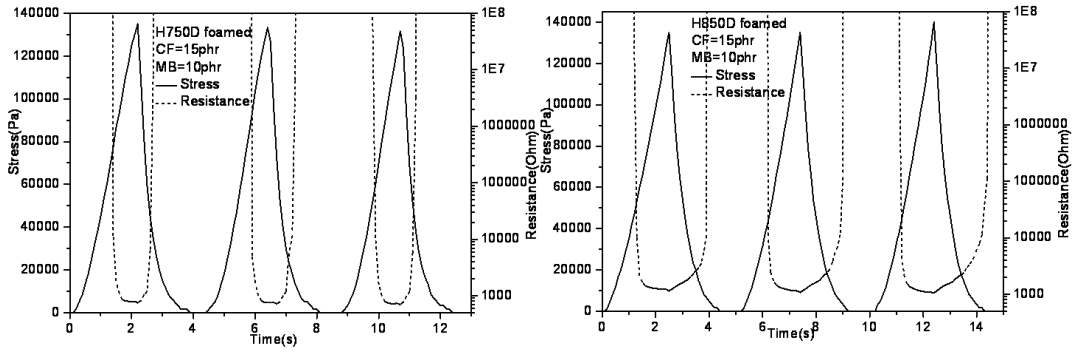

Fig. 5.14 Piezoresistivity of the MWCNT/silicone foams with micro beads foaming agents under periodic pressures

Tactile sensors made by polymeric piezoresistive materials face the disadvantage of their viscoelasticity which can prolong the recovery time and reduce the sensitivity. The foaming procedure is expected to be able to reduce the viscoelasticity of the material. To

test the sensitivities of all types of the piezoresistive materials, the recovery times and piezoresistivities under periodic pressures were measured.

The recovery times and the periodic piezoresistivity of the MWCNT/silicone unfoamed elastomers with a MWCNT content of 15phr and the MWCNT/silicone foams with a MWCNT content of 15phr and the micro beads content of 10phr were measured with the aforementioned horizontal method. The recovery time were measured after loading them with a pressure of 135kPa and releasing the pressure suddenly. The time from releasing to the point which the resistance recovers to 100kPa is regarded as the recovery time of the piezoresistive material. A shorter recovery time means a more sensitive piezoresistivity. As it shows in the Fig. 5.12, the unfoamed MWCNT/silicone has a recovery time longer than 10 seconds. While the H750D foamed and H850D foamed MWCNT/silicone foams have similar recovery times of lower than 2.5 seconds. This shows that the sensitivity can be improved dramatically by the foaming procedure, whose reason is considered that the porous structure of the composite apparently increases its elasticity.

Because of the different thickness of every sample, the periodic piezoresistivity was measured with different compressing speeds which are set to match its recovery time. The unfoamed elastomer, H750D foam and H850D foam were compressed by a plate with speeds of 3mm/min, 20mm/min and 30mm/min respectivily, by which their periods can be controlled at about 20 seconds for the unfoamed elastomer and about 4 seconds for the foams. The pressure was loaded until the stress reaching 135kPa, then the plate was stopped and returned oppositely immediately at the same speed until the stress decreasing to 0. This procedure was repeated 3 times for each sample.

The piezoresistivity measurement of the unfoamed MWCNT/silicone elatomer with a MWCNT loading of 15phr under a periodic pressure is shown in the Fig. 5.13. 3 peaks of

the stress curve have almost the same shape. The apparent reduction of the resistance occurred in all of the periods. It is believed that the conductive paths can be established quickly as the compressing of the MWCNT/silicone elastomer, but the viscosity of the molecular chains of its silicone matrix is very high that it takes a long time for the elastomer to recover to its initial shape and disassemble the conductive paths. The long-time recovery procedure of the composites limits the application in the tactile sensors. It is of great significant to reduce the viscosity and shorten the recovery time,

The piezoresistivity measurements of the MWCNT/silicone foams with micro beads foaming agents under periodic pressures are shown in the Fig. 5.14. The measurements for the foams fabricated with H750D foaming agent and H850D foaming agent with a MWCNT loading of 15phr and a micro beads loading of 10phr are shown in the left part and right part of the Fig. 5.14, respectively. Unlike the unfoamed elastomer, the piezoresistive curves of the foams show much shorter periods. The peaks of these curves are synchronous well with their peaks in stress curves, apparent and rapid recovering of the resistances can be clearly observed. This is because the introduction of the foaming agents can shift the compression type of the composites. H750D and H850D foaming agents are micro beads which can maintain their stiffness in some degree even after expanding. The compression mode conversed from simply compressing of the elastomer to a mixing deformation of compressing, twisting and folding of the areas between the cells and the compressing of the gas confined within the cells, which can drastically reduce the viscosity movement of the silicone substrates. It is proved that addition of the micro beads foaming agents can effectively improve the sensitiveness and repeatability of the MWCNT/silicone composites.

5.4 Investigation of MWCNT/silicone Elastomeric Conductive Nanocomposites Foamed by Normal Foaming Agents and Their Piezoresistive Behaviors

5.4.1 Materials

A type of multi-walled carbon nanotube (VGCF-H, Showa Denko) with an average fiber length of 10~20μm and an average fiber diameter of 150nm was used as the conductive filler. The polymer matrix was synthesized by 2-component silicone elastomer, including the main component (KE-1308, Shin-Etsu Chemical Co., Ltd.) and the curing agent (CAT-1300L-4, Shin-Etsu Chemical Co., Ltd.). 3 types of foaming agents were used, including an OBSH type with a main component of 4,4'-Oxybis (benzenesulfonylhydrazide) (CELMIC S, SANKYO KASEI CO., LTD.), an ADCA type with a main component of Azodicarbonamide (M-35, Otsuka Chemical Co., Ltd.) and a inorganic carbonate type with a main component of Sodium Hydrogen Carbonate (P-5, Otsuka Chemical Co., Ltd.).

5.4.2 Preparation of MWCNT/silicone Elastomeric Conductive Nanocomposites Foamed by Normal Foaming Agents

Firstly, all the components of the silicone elastomer were added to a PTFE container according to an expected ratio (the curing agent was added at an amount of 6% of the main component by mass). Then the foaming agent and the MWCNT were also added. The mixture was finely stirred using a planetary centrifugal vacuum mixer at a speed of 1000rpm at a pressure of 0.6kPa for 10min and then poured into a mold immediately, the nanocomposite membrane before foaming was obtained after curing at 110˚C for 5min. Finally, the conductive MWCNT/silicone foam was obtained by free foaming for 10min

at 170˚C in vacuum. The thicknesses of these foams were controlled approximately to 4mm. Foam structures with closed voids were obtained, the shapes of the voids vary with the types of the foaming agents. The volume fractions of MWCNT and foaming agent (before foaming) were listed in Table 5.4. In order to investigate the the effect of the porosity on the piezoresistive properties, the volume fraction of MWCNT of all samples were controlled to around 4%, at which an obvious piezoresistivity would be obtained according to the result in Section 5.3. Each type of foaming agent was added to the silicone matrix with two different volume fractions.

Table 5.4 Volume fractions of the MWCNT and foaming agents in the MWCNT/silicone conductive foams

Component \ Series Number		O1	A1	S1	O2	A2	S2
MWCNT		4.16%	4.19%	4.13%	4.21%	4.25%	4.16%
Foaming Agents	OBSH	5.95%	-	-	9.05%	-	-
	ADCA	-	5.33%	-	-	8.16%	-
	$NaHCO_3$	-	-	6.69%	-	-	10.11%

5.4.3 Characterizations

The volume resistivity was measured by an ADVANTEST R6243 DC voltage current source/monitor with a 4-wired method; the laser microscope observation was conducted by an OLYMPUS LEXT OLS4000 3D measuring laser microscope; the SEM observation was applied at an accelerating voltage of 15kV by a JEOL JSM-7600F field emission scanning electron microscope (The cross sections of the samples for these observations were obtained by breaking them after freezing in liquid nitrogen. Each sample was loaded

with a uniaxial pressure through the thickness direction by a pair of metallic plates set into the sample holder, the compressing strain was controlled to 0 and 75%). The elastic modulus was measured by a SHIMADZU AGS-G Series Universal/Tensile Tester, with a compressing speed of 3mm/min.

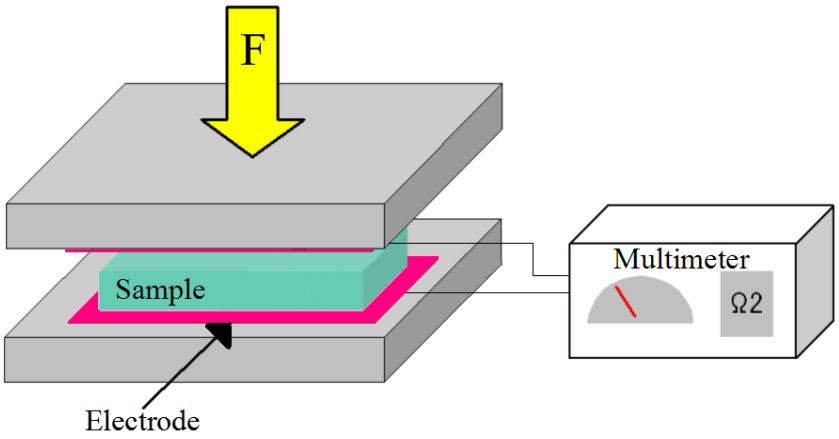

Fig. 5.15 Piezoresistivity measurements through the vertical direction

The piezoresistive properties were measured though the direction parallel to the external pressure. Each sample was cut to a square-shape sheet of 30mm×30mm. The measurement was shown in the Fig. 5.15. Every sample was sandwiched between a pair of 75mm×75mm square-shape copper electrodes. A linear-increasing uniaxial pressure was loaded by a compressing plate, which was controlled by the SHIMADZU AGS-G Series Universal/Tensile Tester. Silver paint was smeared to the sample surfaces to ensure a well surface contact with the electrodes. The electrodes were connected to a 2000 Series Digit Multimeter to measure the resistance with a 2-wire mode. The tiny resistance as well as inductance loss within the measuring system was neglected. For every sample, the resistance was measured under difference stress from 0 to 112kPa and listed as the

form of common logarithms.

5.4.4 Results and Discussion

Table 5.5 Density and resistivity of MWCNT/silicone conductive foams

Series Number	O1	A1	S1	O2	A2	S2
Density ($g \cdot cm^{-3}$)	0.55	0.93	0.89	0.41	0.84	0.88
Resistivity ($\Omega \cdot m$)	5267.8	5.79	6.59	21922.8	9.62	13.74

The density and resistivity of MWCNT/silicone conductive foams (4-wired method) were listed in the Table 5.5. It can be found that the O1 and O2 samples have the lowest densities and the highest resistivity, which means that the OBSH foaming agent has the highest foaming efficiency. With increasing of the foaming agents, the density decreases and the resistivity increases obviously for all samples. It is believed that a lower density, namely, a highly porous structure leads to a higher resistivity. It is also found that the OBSH foaming agent effectively increased the percolation threshold of the MWCNT/silicone composites, making the resistivity increase significantly. For the A1 and A2 samples, with increasing of the foaming agent, the density decreases but the resistivity keeps at a same level. For the S1 and S2 samples, an obvious change can be observed from neither the density nor the resistivity with increasing of the foaming agent. Only relatively low foaming efficiencies and weak conductivity-reducing effects could be brought by the ADCA and $NaHCO_3$ foaming agents.

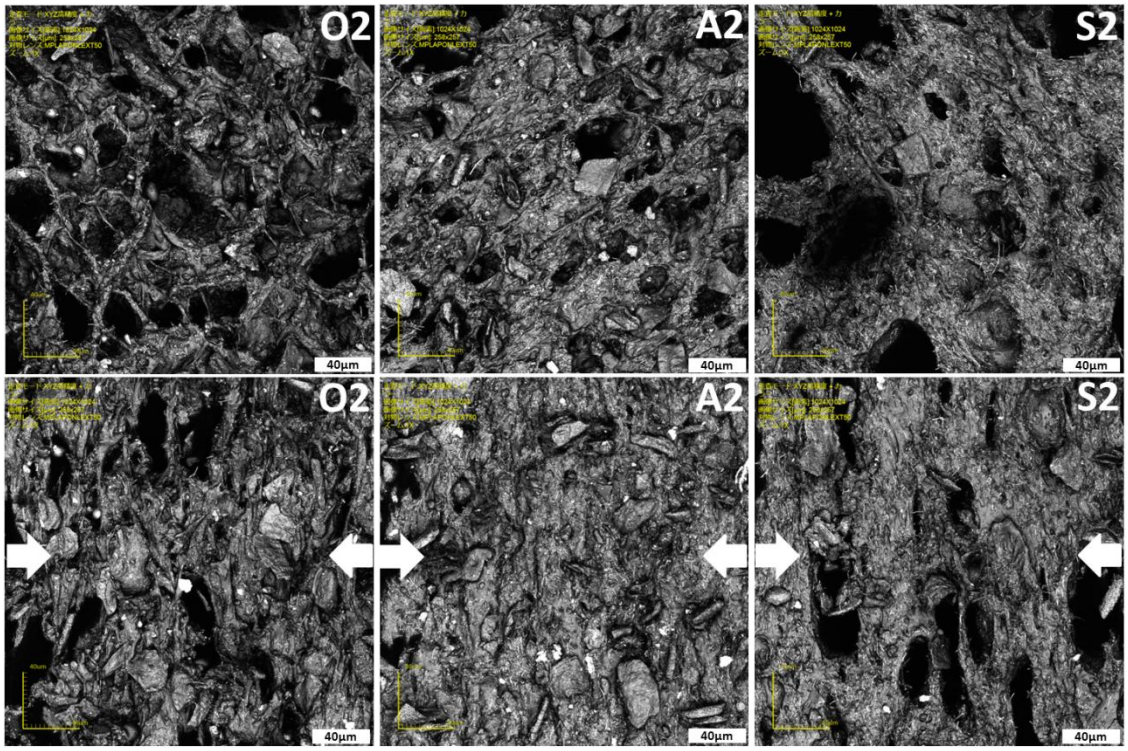

Fig. 5.16 Laser microscope images of the porous structures in MWCNT/silicone conductive foams with and without a uniaxial load

The cross-sectional area of the conductive foam samples of O2, A2 and S2 series were observed by the laser microscope. The porous structures with many closed-cell pores can be clearly observed from all samples. The images of the MWCNT/silicone conductive foams without a compressing strain were shown in the upper parts of the Fig. 5.16. Small voids can be found from the O2 and A2 samples, which were found to be crowded in the former one and loose in the latter one, meanwhile large voids with a small amount were found in the S2 samples. The reason of the diverse porous structures was considered as follows: (1) the OBSH foaming agent has a relatively lower molecular polarity and has been surface treated previously to gain a well affinity with the non-polar silicone matrix. After a high shearing mixing procedure, the clusters of the OBSH particles maintained

relatively small sizes until absolutely curing. Furthermore, the OBSH is a type of compound with rather low decomposing temperature accompanied with a high decomposing speed and a relatively low gas releasing amount. Thus during the free foaming procedure, a dense and fine porous structure could be obtained with a short heating time; (2) the $NaHCO_3$ foaming agent has a relatively higher molecular polarity, which leads to a poor affinity with the silicone matrix. The clusters of the foaming agents would begin to agglomerate bigger and bigger after the high shearing mixing procedure. These big clusters would release a large amount of gas and create big pores in the S2 sample; (3) although the ADCA foaming agent has a large gas releasing amount as twice as the OBSH and the $NaHCO_3$ foaming agent, the amino groups contained in its molecules are easy to react with the platinum catalyst of the 2-component silicone matrix, which would obstruct the curing of the silicone matrix and disturb the foaming procedure, resulting in a lower porosity and a smaller average pore diameter.

The images of the MWCNT/silicone conductive foams under a compressing strain of 75% were shown at the bottoms of the Fig. 5.16. For all samples, most of the voids were found crushed severely by the external pressures. Because the voids can be easily squashed, the elastic modulus was reduced greatly, making the compressive deformation much more obvious compared to the pure silicone matrix. At the same time, the variation range of the resistivity of the conductive composites was thought to be enlarged significantly due to the smaller elastic modulus.

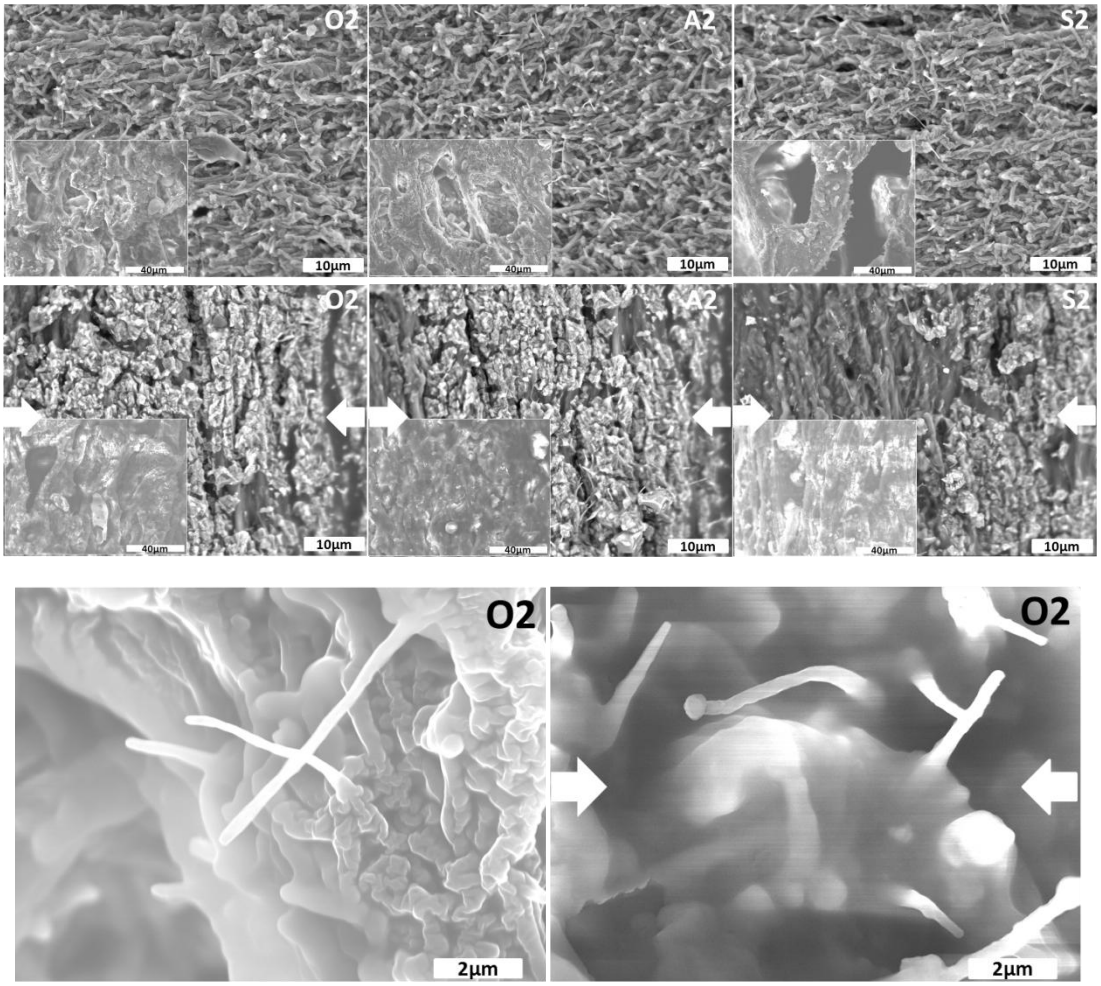

Fig. 5.17 SEM images of the MWCNT/silicone conductive foams with and without a uniaxial load

The backscattered electron images of the MWCNT were taken at a high magnification while normal SEM images of the voids structures were taken with a low magnification. The images of the porous structures from all the foams were found similar with those obtained from the laser microscope observation, which convinced the observations of the laser microscope. The images of the MWCNT/silicone conductive foams without/with a compressing strain of 75% were shown in the top and middle of the Fig. 5.17, respectively. It can be found that all the MWCNT fibers were distributed in the silicone

matrix homogeneously with random orientations before compression. For the composite under a stress, the majority of MWCNT fibers were found being oriented to the direction perpendicular to the compressive strain. In the bottom of the Fig. 5.17, the high resolution SEM images of the OBSH foamed composite without/with a compressing strain of 75% were shown to illustrate the states of MWCNT fibers. The majority of the fibers were found to be covered tightly with silicone elastomer. Several half-naked particles distributed in the cross-section surface can be found, which were pulled up during the sample preparation. Although a small part of MWCNT fibers were found contacted, overlapped directly with each other, forming conductive networks partially, the majority of MWCNTs would not probably contact each other due to the covered layer. It is believed that the tunnel effect dominates the conductive mechanism. As illustrated in the Fig. 4.4, when the nanocomposite deforms under the pressure, the average angle between the shortest connecting line of two adjacent fibers and the pressure direction would be reduced, the average minimum distance between adjacent fibers would be shortened. According to the calculation from the Eq. (4-22), the average resistance of the nanocomposite through the pressure direction would be reduced. It is also believed that the coated silicone layers hindered the direct contact between the MWCNT fibers, preventing the construction of the short circuit and making the resistivity of the conductive foams become much more changeable.

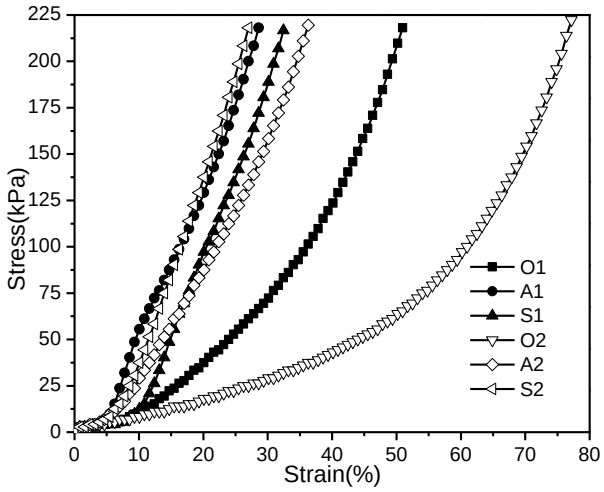

Fig. 5.18 Compressive stress-strain curves of the MWCNT/silicone conductive foams

The compressive stress-strain curves were shown in the Fig. 5.18. The slope of every point in a curve represents the elastic modulus of the conductive foam at that strain. In order to make the elastic results simple and quantitative, the average compressive elastic modulus during the whole strain range for one sample was calculated by the equation below. The results were listed in the Table 5.6.

$$\bar{E} = \frac{2\int_0^{\varepsilon max}\sigma(\varepsilon)d\varepsilon}{(\Delta\varepsilon)^2} \quad (5\text{-}1)$$

Table 5.6 Average compressive elastic modulus of the MWCNT/silicone conductive foams

Series Number	O1	A1	S1	O2	A2	S2
Elastic Modulus (kPa)	278.4	621.2	471	154.8	463.4	608.6

Evidently the O2 and O1 samples showed the lowest elastic modulus, which proved

that the OBSH foaming agent has the best affinity with the silicone elastomer and the highest foaming efficiency. Relatively higher elastic modulus was found from the samples foamed with the ADCA and $NaHCO_3$ foaming agents, proving their lower foaming efficiencies. These results were found well matched with those from the density measurement. In addition, the stress-strain curves of the A series and S series samples were found to be almost linear. The reason was considered that the A or S series samples have a similar compressive procedure with solid conductive composites due to the low porosity, a procedure which obeys the Hook' law. Oppositely, highly porous structures found in the O series samples lead to a nonlinear, complicated compressive mode. It was thought that the elastic modulus would decrease as the increase of all types of foaming agents. Unexpectedly, the elastic modulus of the conductive foam increased obviously as increasing of the $NaHCO_3$ foaming agent. The reason for which was considered that the $NaHCO_3$ foaming agent has a relatively low reaction rate, the unreacted foaming agent granules partially hindered the polymer chain movements of the silicone matrix and increased the elastic modulus.

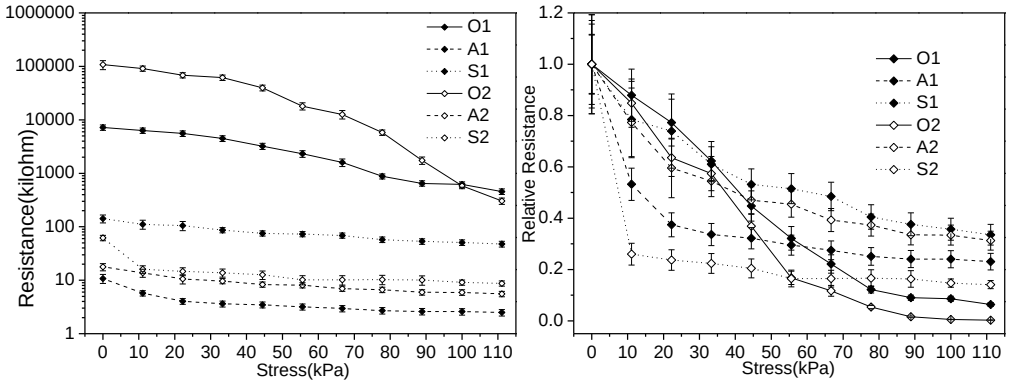

Fig. 5.19 Piezoresistive properties of the MWCNT/silicone conductive foams

The piezoresistive properties of the MWCNT/silicone conductive foams with all types of foaming agents were shown in the Fig. 5.19, the left-hand part of which illustrates the resistance-stress connections while the right-hand part of which shows the relative resistance-stress connections. Error bars have been included in the figure according to the measurement errors. The error range became narrower as the decrease of resistance due to the measurement property of the instrument. The resistance decrease can be found from all samples as the increase of the stress, almost all of the resistance-stress curves and relative resistance-stress curves were found to be nonlinear, which could be caused by their complex foam compression modes. Obvious deceases can only be found from the O1 and O2 samples especially from the latter one. This demonstrates that a lower elastic modulus brought by the foaming agent with a high foaming efficiency leads to a higher piezoresistive sensitivity, which can be enhanced simply by increasing the loading of the foaming agent. The relative resistances of the O1 and O2 samples dropped obviously when loaded with a uniaxial stress of about 110kPa. It is believed that the voids in the foams occupied much space of the silicone matrix, enlarged the distances between the MWCNT particles. Therefore the resistivity was increased significantly. The resistance changes of the O1 and O2 samples are precise and rapid enough to be utilized within a piezoresistive tactile sensor. Oppositely, only slight resistance decreases were obtained from A series and S series samples due to the relatively lower foaming efficiencies of the ACDA and the $NaHCO_3$ foaming agents. It is also noteworthy that the resistances maintained in higher ranges for samples O1 and O2 and in lower ranges for other samples. Within the normal foaming agents OBSH, ADCA and $NaHCO_3$, only OBSH can bring an obvious piezoresistivity to the silicone matrix.

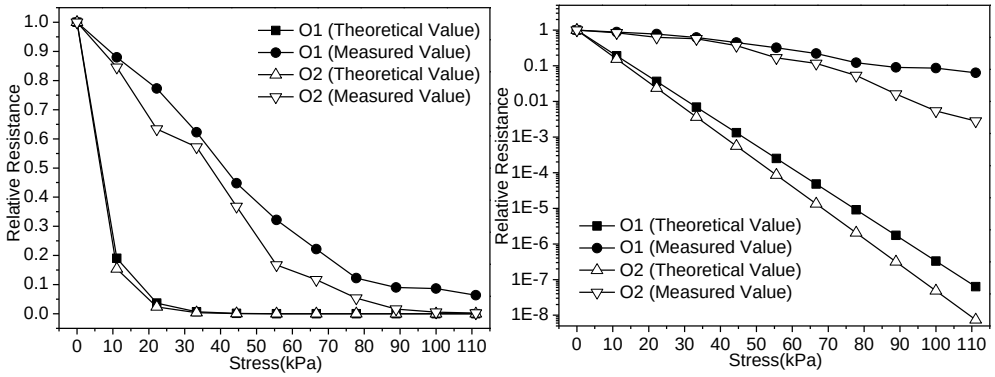

Fig. 5.20 Comparison of the theoretical and measured piezoresistive properties of the MWCNT/silicone conductive foams

To verify the practicality of the piezoresistive model developed in this work, the theoretical variations of relative resistance of the O1 and O2 samples were calculated by the Eq. (4-14) accompanied with Eq. (4-11) and Eq. (4-13). The results were illustrated in the Fig. 5.20 to compare to the measured relative resistance variations. The relative resistance-stress curves with a normal linear form were shown in the left part while those with a common logarithmic form were shown in the right part. Although the overall trends of the resistance changes matched, notable separations could be found between the theoretical values and the measured values no matter for the O1 or the O2 samples. The theoretically calculated relative resistances of both samples drop significantly under even a low stress and almost keep decreasing exponentially about 10^7 to 10^8 times under a stress of about 110kPa; on the contrary, the measured relative resistances dropped of less than 1000 times at the same stress. The resistance change was much less sensitive than the theoretical calculation, the main reason of which was thought as the viscoelasticity of the silicone matrix, which could severely weaken the interior deformation of the matrix and

delay the approaching speeds of the adjacent MWCNT particles. The factor of the viscoelasticity will be considered to improve the accuracy of the piezoresistive model in our future works.

5.5 Conclusion

Novel highly-sensitive piezoresistive MWCNT/silicone elastomeric nanocomposites were fabricated and foamed with two types of foaming strategy. One of them is foamed with thermal expanding microbeads. The other is foamed with normal foaming agents.

Firstly, nanocomposites with MWCNTs, silicone elastomer and micro beads foaming agent were fabricated, which are expected for the utilization in tactile sensors. Effects of the MWCNT and the foaming agents on the piezoresistivitiy were investigated. It is found that the percolation threshold of the composite is within a volume fraction from 2% to 4%. Compared to the H850D foaming agent, the H750D foaming agent has a more stable extending procedure, which can lead to a stable piezoresistivity. Deformations of the composites caused by external pressures were observed by SEM from the cross sections. It is found that the compressing, twisting and folding of the areas between the cells comprise the majority of the deformation and lead to the establishment and breaking of the conductive network. It is proved that the addition of the micro beads foaming agents can not only improve the piezoresistivities of the composites, but also improve the sensitiveness and repeatability of the MWCNT/silicone composites. It was found that the H750D foaming agent has a slightly better piezoresistive enhancing performance than that of H850D foaming agent. The nanocomposite with the highest sensitivity, the widest measurable stress range and the best repeatability is the MWCNT/silicone composite with a MWCNT content of 20phr (8.2vol%), foamed by H750D microbeads

with a loading of 5phr (3.9vol%).

Next, a series of novel MWCNT/silicone conductive foamed nanocomposites were fabricated with an OBSH, an ADCA and a $NaHCO_3$ type foaming agents. The porous structures of the foams, the distribution and orientation state of the MWCNTs in the silicone matrix were both observed with a laser microscope and SEM with or without a compressive load. It was found that the majority of the voids in the matrix crashed by the external pressure, which leaded to a reducing modulus and improved the piezoresistance of the composites. A dense and fine porous structure was obtained by using the OBSH foaming agent which has the best affinity with the silicone elastomer and a highest foaming efficiency. Within the normal foaming agents foamed composites, the most sensitive piezoresistive property was obtained by the OBSH foamed one with a MWCNT content of 4.2vol% and a OBSH loading of 9.1vol%. Both of the two types of foaming method were found to be able to enhance the sensitivity and measurable ranges of the conductive nanocomposites and broaden the scope of applications, however, the porous structure brought by the microbeads foaming agents is proved to be far more efficient in piezoresistivity enhancement. The overall trends of the resistance changes between the theoretical values and the measured values matched, however notable separations were found in their resistance-stress curves, which are thought to be caused by the viscoelasticity of the silicone matrix. In the future works, the factor of the viscoelasticity will be considered to improve the accuracy of the piezoresistive model, meanwhile the temperature dependent piezoresistivity of foamed MWCNT/silicone nanocomposites will be studied.

References

[1] Nayak, S., Rahaman, M., Pandey, A. K., Setua, D. K., Chaki, T. K., & Khastgir, D. (2013). Development of poly (dimethylsiloxane)–titania nanocomposites with controlled dielectric properties: Effect of heat treatment of titania on electrical properties. Journal of Applied Polymer Science, 127(1), 784-796.

[2] Liou, J. W., & Chiou, B. S. (1998). Dielectric tunability of barium strontium titanate/silicone-rubber composite. Journal of Physics: Condensed Matter, 10(12), 2773.

[3] Cherney, E. A. (2005, October). Silicone rubber dielectrics modified by inorganic fillers for outdoor high voltage insulation applications. In Electrical Insulation and Dielectric Phenomena, 2005. CEIDP'05. 2005 Annual Report Conference on (pp. 1-9). IEEE.

[4] Kerpa, O., Weiss, K., & Worn, H. (2003, October). Development of a flexible tactile sensor system for a humanoid robot. In Intelligent Robots and Systems, 2003.(IROS 2003). Proceedings. 2003 IEEE/RSJ International Conference on (Vol. 1, pp. 1-6). IEEE.

[5] Carpi, F., & Rossi, D. D. (2005). Improvement of electromechanical actuating performances of a silicone dielectric elastomer by dispersion of titanium dioxide powder. IEEE Transactions on Dielectrics and Electrical Insulation, 12(4), 835-843.

[6] Varga, Z., Filipcsei, G., & Zrínyi, M. (2006). Magnetic field sensitive functional elastomers with tuneable elastic modulus. Polymer, 47(1), 227-233.

[7] Ansari, S., & Giannelis, E. P. (2009). Functionalized graphene sheet—Poly (vinylidene fluoride) conductive nanocomposites. Journal of Polymer Science Part B: Polymer Physics, 47(9), 888-897.

[8] Grossiord, N., Loos, J., Regev, O., & Koning, C. E. (2006). Toolbox for dispersing carbon nanotubes into polymers to get conductive nanocomposites. Chemistry of

materials, 18(5), 1089-1099.

[9] Loos, J., Alexeev, A., Grossiord, N., Koning, C. E., & Regev, O. (2005). Visualization of single-wall carbon nanotube (SWNT) networks in conductive polystyrene nanocomposites by charge contrast imaging. Ultramicroscopy, 104(2), 160-167.

[10] Chen, X. M., Shen, J. W., & Huang, W. Y. (2002). Novel electrically conductive polypropylene/graphite nanocomposites. Journal of materials science letters, 21(3), 213-214.

[11] Wang, Wei, KA Shiral Fernando, Yi Lin, Mohammed J. Meziani, L. Monica Veca, Li Cao, Puyu Zhang, Martin M. Kimani, and Ya-Ping Sun. "Metallic single-walled carbon nanotubes for conductive nanocomposites." Journal of the American Chemical Society 130, no. 4 (2008): 1415-1419.

[12] Tkalya, E. E., Ghislandi, M., de With, G., & Koning, C. E. (2012). The use of surfactants for dispersing carbon nanotubes and graphene to make conductive nanocomposites. Current Opinion in Colloid & Interface Science, 17(4), 225-232.

[13] Shang, S., Zeng, W., & Tao, X. M. (2011). High stretchable MWNTs/polyurethane conductive nanocomposites. Journal of Materials Chemistry, 21(20), 7274-7280.

[14] Wu, C., Huang, X., Wang, G., Lv, L., Chen, G., Li, G., & Jiang, P. (2013). Highly Conductive Nanocomposites with Three‐Dimensional, Compactly Interconnected Graphene Networks via a Self‐Assembly Process. Advanced Functional Materials, 23(4), 506-513.

[15] Song, L. N., Xiao, M., & Meng, Y. Z. (2006). Electrically conductive nanocomposites of aromatic polydisulfide/expanded graphite. Composites science and technology, 66(13), 2156-2162.

[16] Mattoso, L. H. C., Medeiros, E. S., Baker, D. A., Avloni, J., Wood, D. F., & Orts, W. J. (2009). Electrically conductive nanocomposites made from cellulose nanofibrils and polyaniline. Journal of Nanoscience and nanotechnology, 9(5), 2917-2922.

[17] Xu, J., & Wong, C. P. (2004). Effects of the low loss polymers on the dielectric behavior of novel aluminum-filled high-k nano-composites. In Advanced Packaging Materials: Processes, Properties and Interfaces, 2004. Proceedings. 9th International Symposium on (pp. 158-170). IEEE.

[18] Newnham, R. E., Skinner, D. P., & Cross, L. E. (1978). Connectivity and piezoelectric-pyroelectric composites. Materials Research Bulletin, 13(5), 525-536.

[19] Newnham, R. E., & Ruschau, G. R. (1993). Electromechanical properties of smart materials. Journal of Intelligent Material Systems and Structures, 4(3), 289-294.

[20] Tressler, J. F., Alkoy, S., Dogan, A., & Newnham, R. E. (1999). Functional composites for sensors, actuators and transducers. Composites Part A: Applied Science and Manufacturing, 30(4), 477-482.

[21] Michel, S., Zhang, X. Q., Wissler, M., Löwe, C., & Kovacs, G. (2010). A comparison between silicone and acrylic elastomers as dielectric materials in electroactive polymer actuators. Polymer international, 59(3), 391-399.

[22] Yang, Y., Gupta, M. C., Dudley, K. L., & Lawrence, R. W. (2005). Conductive carbon nanofiber–polymer foam structures. Advanced materials, 17(16), 1999-2003.

[23] Shafieizadegan-Esfahani, A. R., Katbab, A. A., Pakdaman, A. R., Dehkhoda, P., Shams, M. H., & Ghorbani, A. (2012). Electrically conductive foamed polyurethane/silicone rubber/graphite nanocomposites as radio frequency wave absorbing material: The role of foam structure. Polymer Composites, 33(3), 397-403.

[24] Kanaun, S., & Kochekseraii, S. B. (2012). Conductive properties of foam materials

with open or closed cells. International Journal of Engineering Science, 50(1), 124-131.

[25] Klicker, K. A., Schulze, W. A., & Biggers, J. V. (1982). Piezoelectric composites with 3–1 connectivity and a foamed polyurethane matrix. Journal of the American Ceramic Society, 65(12).

[26] Xu, X. B., Li, Z. M., Shi, L., Bian, X. C., & Xiang, Z. D. (2007). Ultralight Conductive Carbon-Nanotube–Polymer Composite. Small, 3(3), 408-411.

[27] Bowden, N., Brittain, S., Evans, A. G., Hutchinson, J. W., & Whitesides, G. M. (1998). Spontaneous formation of ordered structures in thin films of metals supported on an elastomeric polymer. Nature, 393(6681), 146-149.

Chapter6 General Conclusion

In order to meet the demand for a variety of flexible mechanical sensors, this thesis conducted the study of capacitive and piezoresistive properties of functional silicone elastomeric nanocomposites, investigated the possibility and potential of incorporating the functional silicone elastomeric nanocomposites in a mechanical system to detect a mechanical stimulus by transferring it into an electrical signal, evaluated the sensitivity and preciseness of the mechanical systems.

In Chapter 2 and 3, the theoretical calculation from extreme cases proves that agglomeration of BT fillers in vertical direction could seriously reduce the dielectric constants of composites membranes, the dielectric constant can be raised by improving the dispersion of BT particles. To improve the dispersity of BT particles, a novel silicone coupling agent was utilized to modify the surface of particles. TG and FTIR results show that coupling agent was successfully connected to the surface. Raw BT and BT modified by silicone coupling agent were incorporated in the silicone elastomer to fabricate the BT/silicone membranes. Particle size distribution measurement and SEM observation show that surface modified BT particles can get higher compatibility with silicone matrix. Their dispersity in silicone substrate was considerably improved after surface modification. Dielectric properties were evaluated by a LCR meter accompanied with a Multimeter, results show that dielectric constants of composites membranes were increased after improving of dispersion states of BT particles by surface modification. For the BT/silicone nanocomposites, the dielectric constant can reach the value as high as around 35. The obvious effect from the particle size on the dielectric constant of the nanocomposite has not been observed. The capacitance measuring system containing BT/silicone membrane is expected to have several applications such as mechanical

sensors. The current related to the deformation of BT/silicone membrane was detected, which is expected to have the applications in mechanical sensors due to its rapid response of instantaneous electric signals, simple structures and low costs.

In Chapter 4 and 5, in order to clarify and predict the piezoresistive behavior of conductive particles incorporated nanocomposite, 3 types of theoretic piezoresistive models for the conductive particles reinforced elastomeric nanocomposites were introduced from different prospects. Each model was built considering both the solid and foamed conductive nanocomposite. These piezoresistive models were deduced based on the percolation threshold and the tunnel conductive theory of conductive elastomeric nanocomposites, the situations both considering and ignoring the spherical/fiber-like shapes of the conductive particles were discussed in detail. Based on the theoretic analysis, a series of novel multi-walled carbon nanotubes/silicone conductive foamed nanocomposites were fabricated. The experimental results proves that multi-walled carbon nanotubes/silicone conductive nanocomposites are of great significance because of their unique electrical and mechanical properties and are expected to open up a new field of applications as smart functional materials. Especially, their noticeable piezoresistive behaviors can be utilized to produce flexible tactile sensors with large sizes but low costs. To enhance the sensitivity of the piezoresistive property, foaming procedures were introduced to the conductive polymeric composites with different types of foaming agents: a thermal expanding microbeads type and normal types, to obtain a diverse porous structure. The porous structures of the foams, the distribution and orientation state of the multi-walled carbon nanotubes in the silicone matrix were both observed using a laser microscope, CT, and SEM with or without a compressive load. The influences of the porous structure and porosity on the

foam were studied. It was found that a different porosity and different voids structure affected the density, elastic modulus, resistivity as well as piezoresistive property significantly. For the microbeads foamed nanocomposites, it is found that the percolation threshold of the composite is within a volume fraction from 2% to 4%. Compared to the H850D foaming agent, the H750D foaming agent has a more stable extending procedure, which can lead to a stable piezoresistivity. Deformations of the composites caused by external pressures were observed by SEM from the cross sections. It is found that the compressing, twisting and folding of the areas between the cells comprise the majority of the deformation and lead to the establishment and breaking of the conductive network. It is proved that the addition of the micro beads foaming agents can not only improve the piezoresistivities of the composites, but also improve the sensitiveness and repeatability of the MWCNT/silicone composites. For the nanocomposites foamed by normal foaming agents, it was found that the majority of the voids in the matrix crashed by the external pressure, which leaded to a reducing modulus and improved the piezoresistance of the composites. A dense and fine porous structure was obtained by using the OBSH foaming agent which has the best affinity with the silicone elastomer and a highest foaming efficiency. A sensitive piezoresistive property was obtained by the OBSH foamed MWCNT/silicone conductive nanocomposite. The overall trends of the resistance changes between the theoretical values and the measured values matched, however notable separations were found in their resistance-stress curves, which are thought to be caused by the viscoelasticity of the silicone matrix. The factor of the viscoelasticity, much more efficient foaming methods will be studied to further improve the piezoresistive property. Among all of the MWCNT/silicone foamed nanocomposite, the highest sensitivity, the widest measurable

stress range and the best repeatability was obtained from the MWCNT/silicone composite with a MWCNT content of 20phr (8.2vol%), foamed by H750D microbeads with a loading of 5phr (3.9vol%).

Based on the above mentioned studies, it can be concluded that a relatively precise and sensitive mechanical sensor can be easily developed from different prospects, by utilizing the capacitive, or the piezoresistive properties of functional silicone elastomeric nanocomposites. This work provides a variety of simple, low cost and practical potential solutions for the increasing recent demands for mechanical sensing systems. It is difficult to decide which one is better, because these two types do have their own advantages and disadvantages. For the BT/silicone nanocomposite, in order to achieve a sensitive, accurate measuring performance, it should be fabricated to a membrane with a small thickness, with which the effect of viscoelasticity can be neglected. A system containing a BT/silicone membrane and a Multimeter is appropriate for detection of a short-time mechanical stimulus, like an instantaneous impact or a vibration with a short period, within the time as short as around 0.1s; a system containing a BT/silicone membrane and a LCR meter is able to measure a constant pressure. Due to the large elastic modulus of BT/silicone membrane, it is suitable for a large pressure rather than a small one. For the MWCNT/silicone foamed nanocomposite, a highly adjustable resistivity and elastic modulus can be easily obtained. A small pressure (as low as 5kPa or less) can be easily detected with a high accuracy with a system containing such a MWCNT/silicone foamed nanocomposite, which is within the same pressure range exerted by human fingers. The measuring accuracy is higher than those of many other studies [1,2]. There is still much work to do to improve this study in the future works. 3 main development directions were considered: (1) Investigating

the temperature dependent conductive property of MWCNT/silicone nanocomposites. (2) Enhancing the capacitive and piezoresistive property of the silicone elastomeric nanocomposites. For example, enhancing the dielectric property by doping BT with other rare earth elements; improving the conductivity of MWCNT by surface metal grafted, etc. (3) Expanding the versatility of the silicone elastomeric nanocomposite. For instance, investigate the sensing features of a MWCNT/silicone elastomeric nanocomposite to a rapidly changing stress, i.e., a mechanical impact, etc. (4) Conducting the research of some practical applications using silicone elastomeric nanocomposites, for example, an artificial skin of a civil robot, or a component of a smart fabric fabricated by silicone elastomeric nanocomposites, etc [3-8].

References

[1] Zhang, X. W., Pan, Y., Zheng, Q., & Yi, X. S. (2000). Time dependence of piezoresistance for the conductor-filled polymer composites. Journal of Polymer Science part B: polymer physics, 38(21), 2739-2749.

[2] Chen, L., Chen, G. H., & Lu, L. (2007). Piezoresistive Behavior Study on Finger-Sensing Silicone Rubber/Graphite Nanosheet Nanocomposites. Advanced Functional Materials, 17(6), 898-904.

[3] Park, Y. L., Chen, B. R., & Wood, R. J. (2012). Design and fabrication of soft artificial skin using embedded microchannels and liquid conductors. IEEE Sensors Journal, 12(8), 2711-2718.

[4] Ulmen, J., & Cutkosky, M. (2010, May). A robust, low-cost and low-noise artificial skin for human-friendly robots. In Robotics and Automation (ICRA), 2010 IEEE International Conference on (pp. 4836-4841). IEEE.

[5] Fritzsche, M., Elkmann, N., & Schulenburg, E. (2011, March). Tactile sensing: A key technology for safe physical human robot interaction. In Proceedings of the 6th International Conference on Human-robot Interaction (pp. 139-140). ACM.

[6] Parkova, I., Vališevskis, A., Ziemele, I., Briedis, U., & Vilumsone, A. (2013). Improvements of smart garment electronic contact system. In Advances in Science and Technology (Vol. 80, pp. 90-95). Trans Tech Publications.

[7] Stoppa, M., & Chiolerio, A. (2014). Wearable electronics and smart textiles: a critical review. Sensors, 14(7), 11957-11992.

[8] Dunne, L. E., Brady, S., Smyth, B., & Diamond, D. (2005). Initial development and testing of a novel foam-based pressure sensor for wearable sensing. Journal of NeuroEngineering and Rehabilitation, 2(1), 4.

Research Activities

(Oral presentation) **Chen Guo**, Yasuo Kondo, Dianming Sun, Chika Takai, Razavi Hadi, Masayoshi Fuji. *Piezoresistive Phenomenon of MWCNT/Silicone Elastomeric Composite and Its Application in Mechanical Sensors.*The 7th Asian Partical Technology Symposium (APT 2017), Taoyuan, Taiwan, Jul. 2017.

(Poster presentation) **Chen Guo**, Yasuo Kondo, Chika Takai, Masayoshi Fuji. *Piezoresistive Phenomenon of MWCNT/Silicone Elastomeric Composite and Its Application in Mechanical Sensors.*The 9th Integrated Molecular/Materials Science & Engineering (IMSE-9), Qingdao, China, Oct. 2016.

(Oral presentation) **Chen Guo**, Chika Takai, Takashi Shirai, Masayoshi Fuji. *Barium Titanate/Silicone Composites for Mechanical Sensor.*The Tech-connection of Advanced Materials 2016 (TAM 2016) jointed with The 4th International Symposium on Rare Earth Resource Utilization & the 7th International Symposium on Functional Materials (ISRERU-4 & ISFM-7), Changchun, China, Aug. 2016.

(Oral presentation) **Chen Guo,** *Dielectric Properties of $BaTiO_3$/Silicone Composites and its Applicatoins.*The First Joint Seminar for Students between BUCT and NIT, Beijing, China, Oct. 2015.

List of Publications

1. **Chen Guo**, Yasuo Kondo, Chika Takai, and Masayoshi Fuji. *Multi-walled carbon nanotubes/silicone conductive foams and their piezoresistive behaviors.* Journal of Materials Science: Materials in Electronics 28, no. 11 (2017): 7633-7642.
2. **Chen Guo**, Yasuo Kondo, Chika Takai, and Masayoshi Fuji. *Piezoresistivities of vapor‐grown carbon fiber/silicone foams for tactile sensor applications.* Polymer International 66, no. 3 (2017): 418-427.
3. **Chen Guo**, and Masayoshi Fuji. *Effect of silicone coupling agent on dielectric properties of barium titanate/silicone elastomer composites.* Advanced Powder Technology 27, no. 4 (2016): 1162-1172.

Acknowledgement

I would like to thank my supervisor Prof. Masayoshi Fuji gratefully for his selfless, kind, and patient supervision and suggestions of not only the professional knowledge and academic experience, but also the way of thinking about and solving problems. I would also like to thank Prof. Takashi Shirai, Dr. Chika Takai, Dr. Razavi Hadi, other professors and members of the Advanced Ceramics Research Center, for their kind guidance and helps. I would also like to express my gratitude to my family for their years of support. Additionally, I acknowledge the support from Kitagawa Industries Co., Ltd. I also acknowledge the support from Advanced Low Carbon Technology Research and Development Program (ALCA) of Japan Science and Technology Agency (JST)-Japan.